4th Stanford-Berkeley Summer School on
"Applications of Synchrotron Radiation"
Stanford, CA, June 17, 2005

Interfaces, Heavy Metals, Microbes, and Plants: Shedding New Light on Environmental Science at the Molecular Level

Gordon E. Brown, Jr.
Stanford University and Stanford Synchrotron Radiation Laboratory

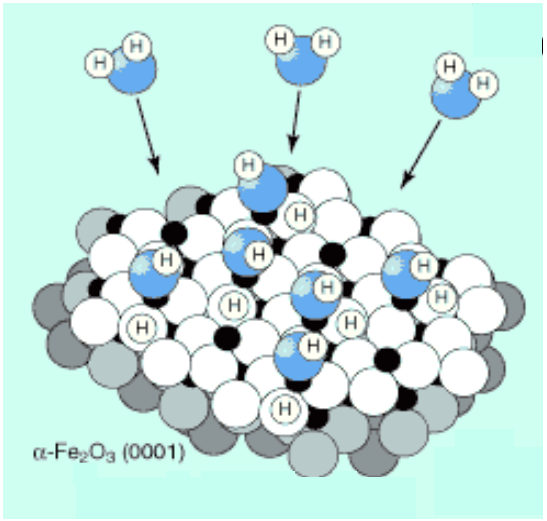

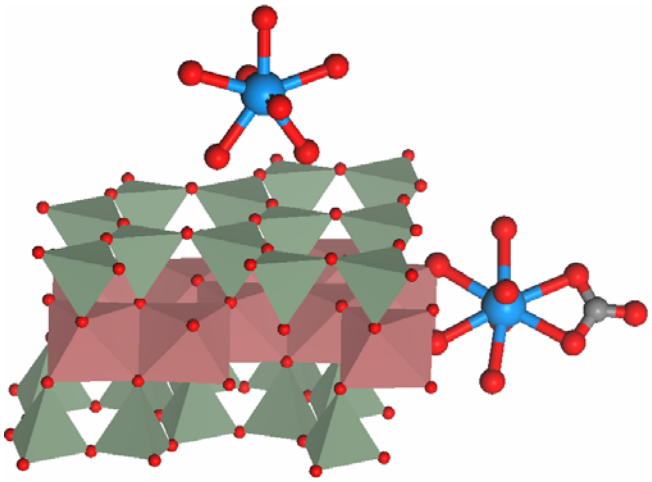

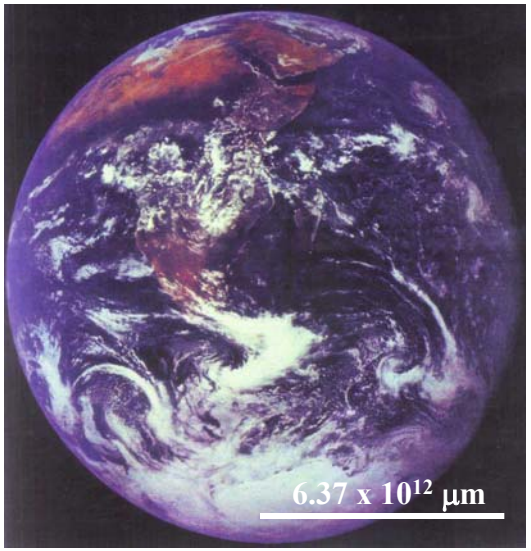

Presentation Outline

- **Synchrotron Radiation and U.S. Synchrotron Radiation Sources**
- **Important Issues in Molecular Environmental Science (MES)**
- **Some Key Environmental Problems**
- **Reaction of Water Vapor with Metal Oxide Surfaces: Example of Application of Photoemission Spectroscopy to Interfacial Reactions**
- **X-ray Absorption Fine Structure (XAFS) Spectroscopy**
- **Sorption Processes at Solid/Aqueous Solution Interfaces**
- **XAFS and X-ray Standing Wave (XSW) Spectroscopy Applications in MES**
- **Crystal Truncation Rod (CTR) Diffraction Studies of Surface Structure under Hydrous Conditions**
- **Applications of Microbeam and Spectromicroscopy SR Methods to MES**
- **Applications of STXM to MES: Bioweathering and Biomineralization**
- **Applications of Photoemission and Soft X-ray XAFS Spectroscopy to Acid Mine Drainage**
- **Applications of XAFS Spectroscopy to Zn, As, and Se Pollution Problems**
- **Applications of XAFS Spectroscopy to Pu, Cr, and U Speciation at DOE Sites**
- **Future Developments and Conclusions**

Collaborators

John R. Bargar (Stanford Synchrotron Radiation Laboratory)
Karim Benzerara (now at the University of Paris VII)
Benjamin C. Bostick (now at Dartmouth College)
Georges Calas (LMPC, University of Paris VI)
Jeffrey G. Catalano (now at Argonne National Laboratory)
Francois Farges (University of Marne-la-Vallée, France)
Farid Juillot (LMPC, University of Paris VII)
Tom Kendelewicz (Stanford University)
Ping Liu (Stanford Synchrotron Radiation Laboratory)
Guillaume Morin (LMCP, University of Paris VI-VII)
Alfred M. Spormann (Stanford University)
Alexis S. Templeton (now at Scripps Institution of Oceanography)
Thomas P. Trainor (now at University of Alaska, Fairbanks)
Tolek Tylizsczak (Lawrence Berkeley National Laboratory)
Tae Hyun Yoon (Stanford University)
John M. Zachara (Pacific Northwest National Laboratory)

Financial Support

DOE-BES DE-FG03-93ER14347-A010
NSF-Collaborative Research Activity in Environmental Molecular Science (CHE-0089215)
NSF-Environmental Molecular Science Institute (CHE-0431425)

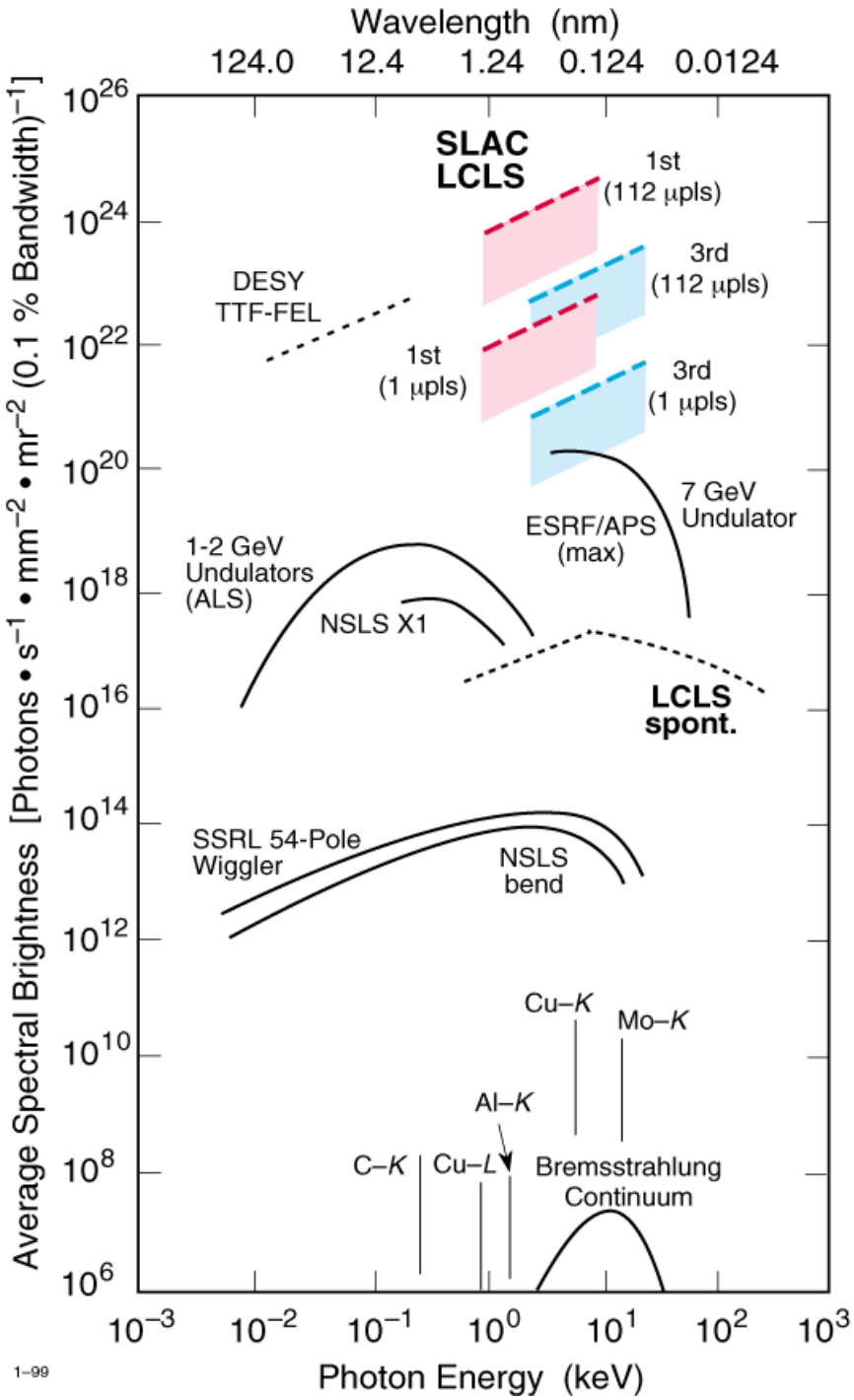

Attributes of Synchrotron Radiation

- **Brightnesses 10^5 to 10^{10} greater than standard sealed X-ray tube**
- **Broad spectral range continuously tunable from the IR to hard X-rays**
- **High degree of polarization in the plane of the storage ring**
- **Natural collimation and small source size**
- **Pulsed time structure**
- **High vacuum environment**
- **High stability**

U.S. Synchrotron Light Sources I (DOE User Facilities)

(Total of 166 beam line stations - 62 beam line stations currently used or available for Earth and Environmental Science research)

Advanced Light Source

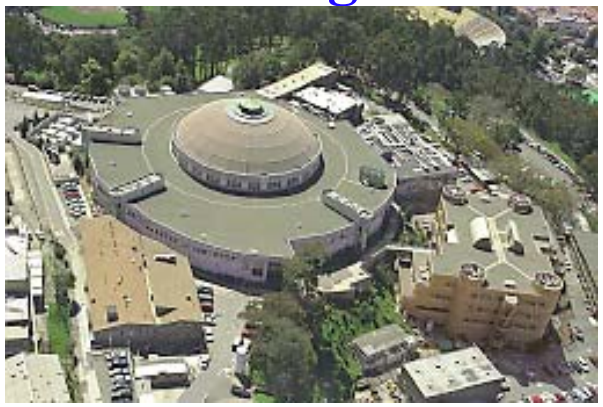

1993 12 BL Stations

Advanced Photon Source

1995 15 BL Stations

NSLS

NATIONAL SYNCHROTRON LIGHT SOURCE

1982 14 BL Stations

STANFORD SYNCHROTRON RADIATION LABORATORY

SSRL

1974 15 BL Stations

U.S. Synchrotron Light Sources II (non-DOE User Facilities)

(Total of 50 beam line stations - 19 beam line stations currently used or available for Earth and Environmental Science research)

CAMD

1990 4 BL Stations

CHESS

Cornell High Energy Synchrotron Source

1979 8 BL Stations

SRC

Home of Aladdin

1987 7 BL Stations

Some Key Issues in Molecular Environmental Science

Water and Interfaces

Complexity

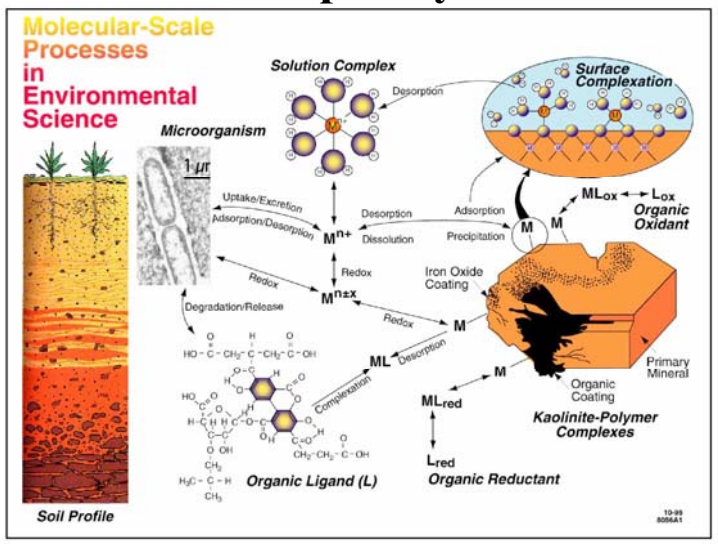

Speciation

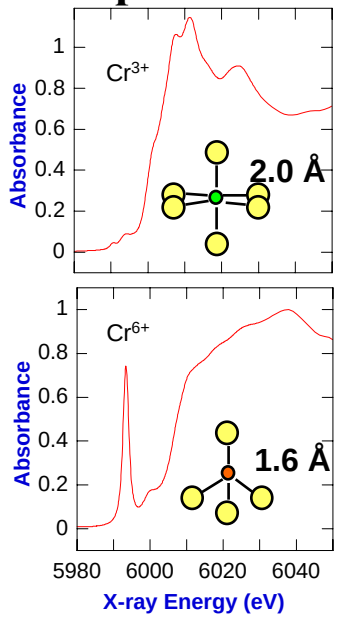

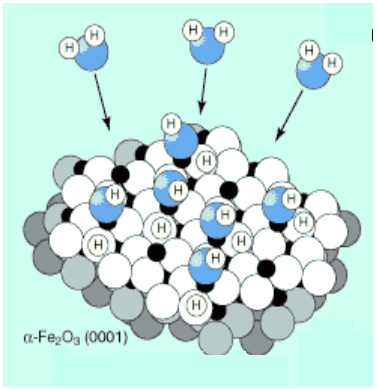

Surface Reactions

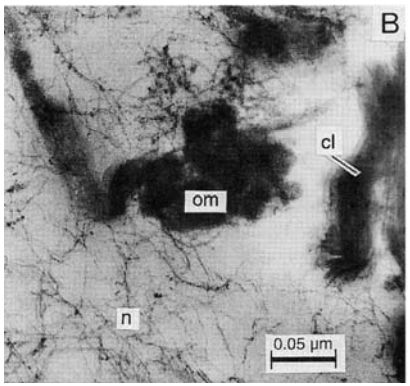

Natural Organic Matter

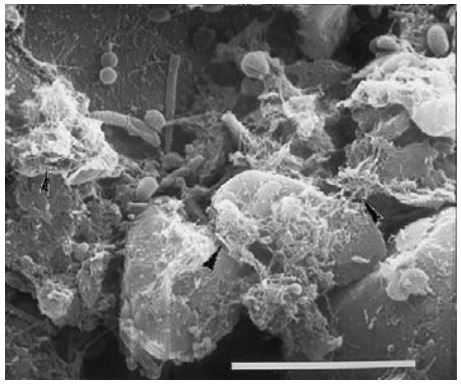

Microorganisms & Biofilms

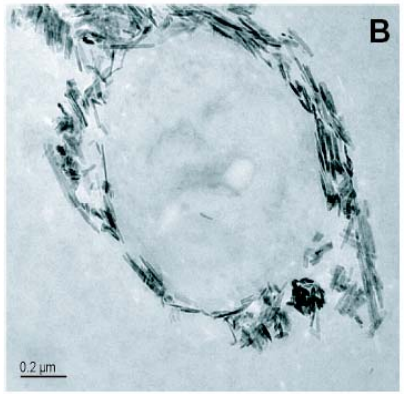

Nanoparticles

Examples of Heavy Metal and Actinide Pollution in Different Environmental Settings

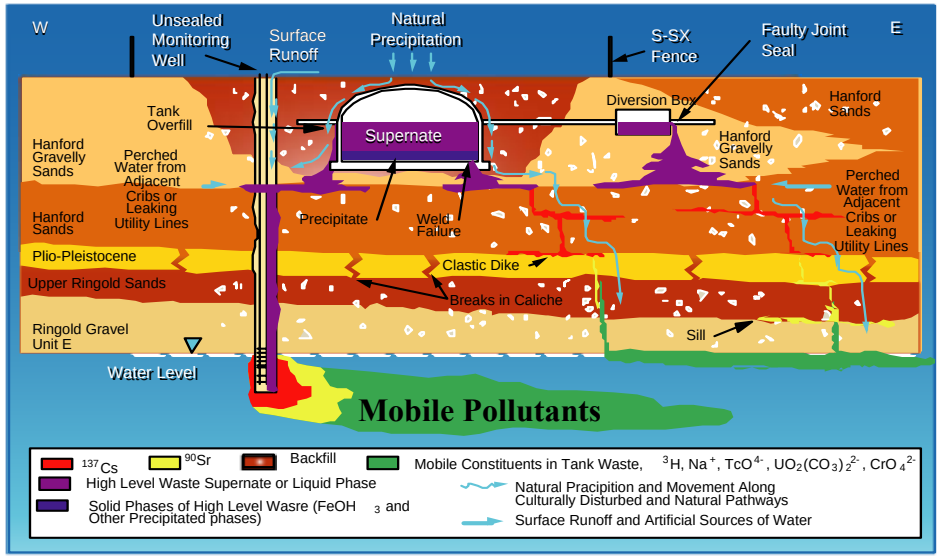

Heavy Metal and Radionuclide Contamination in the Hanford Vadose Zone

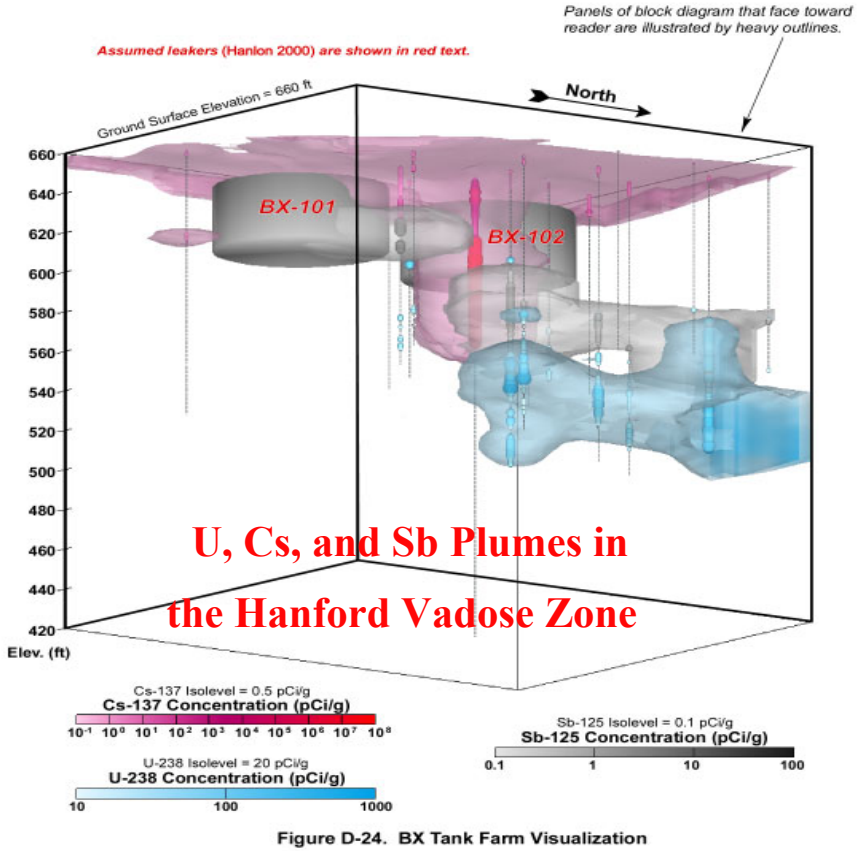

Figure D-24. BX Tank Farm Visualization

A.W. Pearsons (2000) *Hanford Tank Farms Vadose Zone Monitoring Project, BX Tank Farm Addendum.* U.S. Department of Energy GJO-98-40-TARA, GJO-HAN-19

Uranium-Contaminated Sites at Oak Ridge National Laboratory

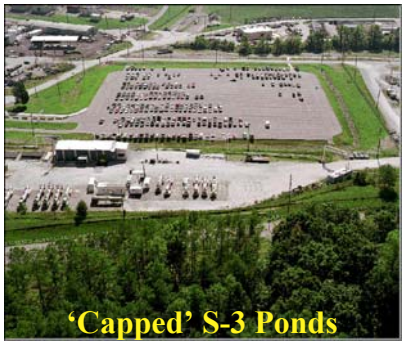

Mercury-Contaminated Sites in California

Arsenic Contamination in Bangladesh

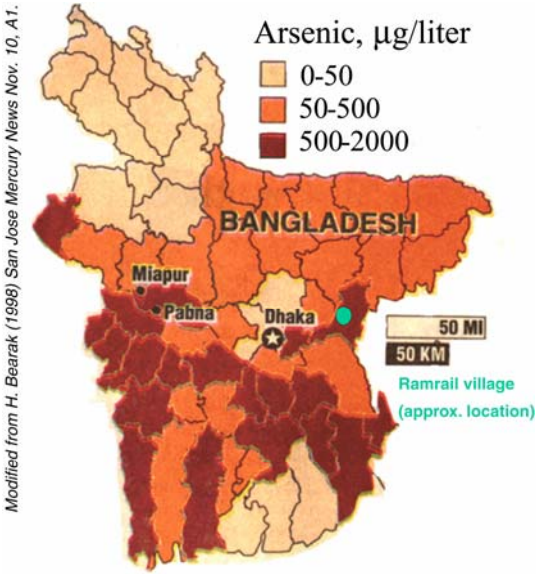

the southeastern part of the country (unaffected by As) is not shown in this graphic

Reaction of Water Vapor with Metal Oxide Surfaces: An Example of the Application of Photoemission Spectroscopy to Interfacial Reactions

AFM Image of Air-Cleaved MgO(100)

***(Liu et al. Surf. Sci. 412/413*, 287, 1998)**

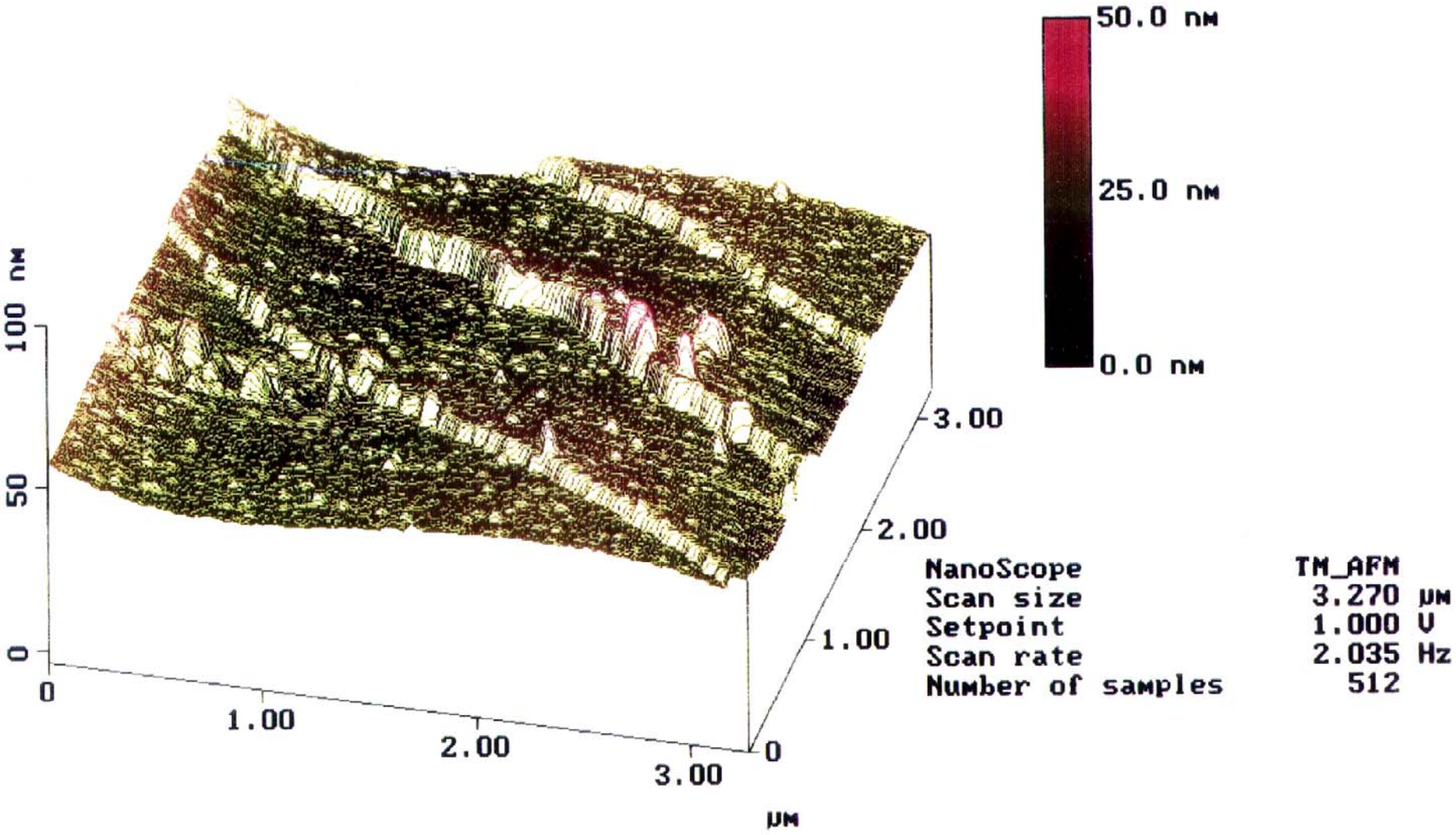

AFM Image of Air-Cleaved MgO(100) after Two Weeks of Air Exposure in Dessicator

***(Liu et al. Surf. Sci. 412/413*, 287, 1998)**

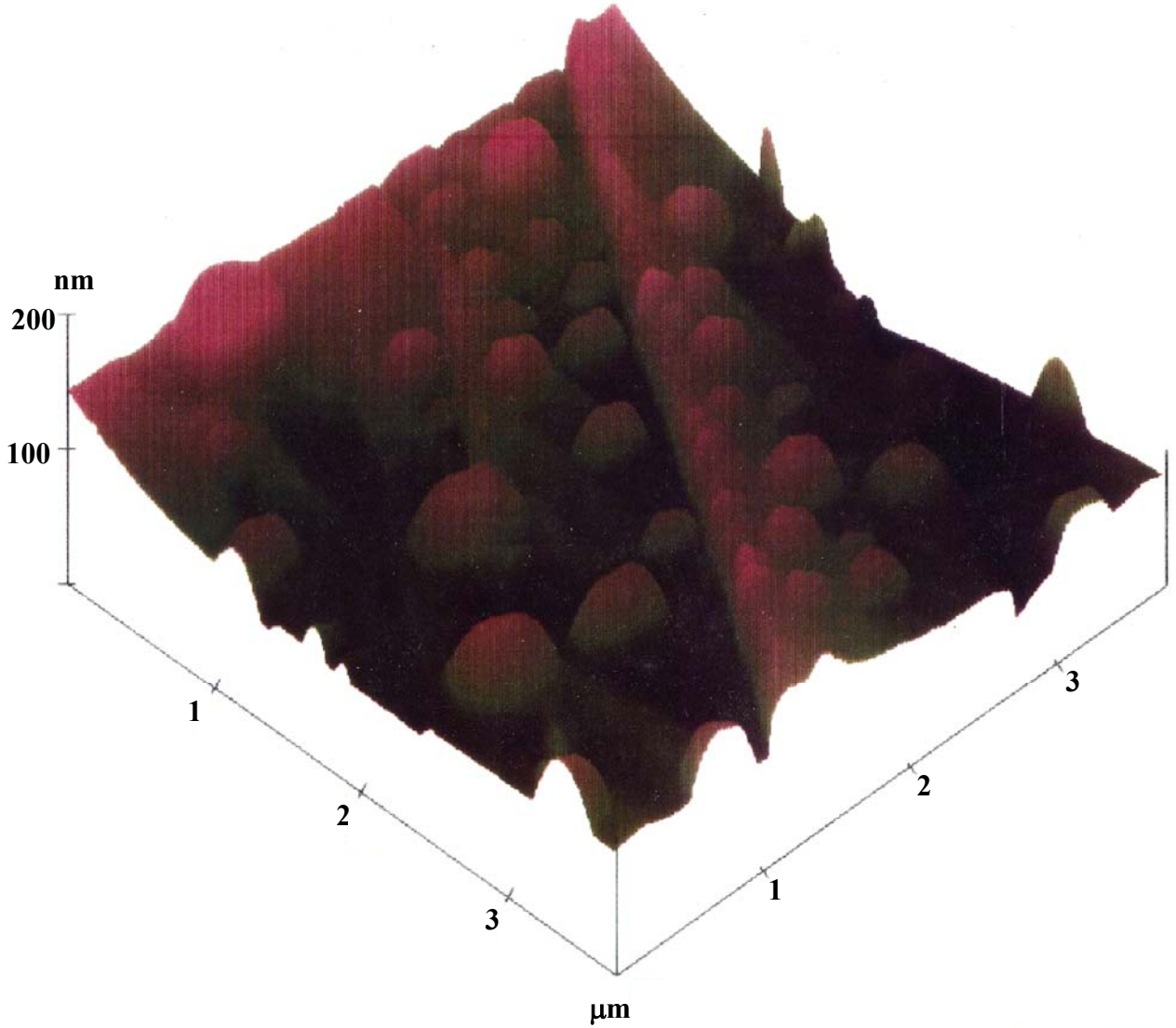

Surface Sensitivity of X-ray Photoemission Spectroscopy

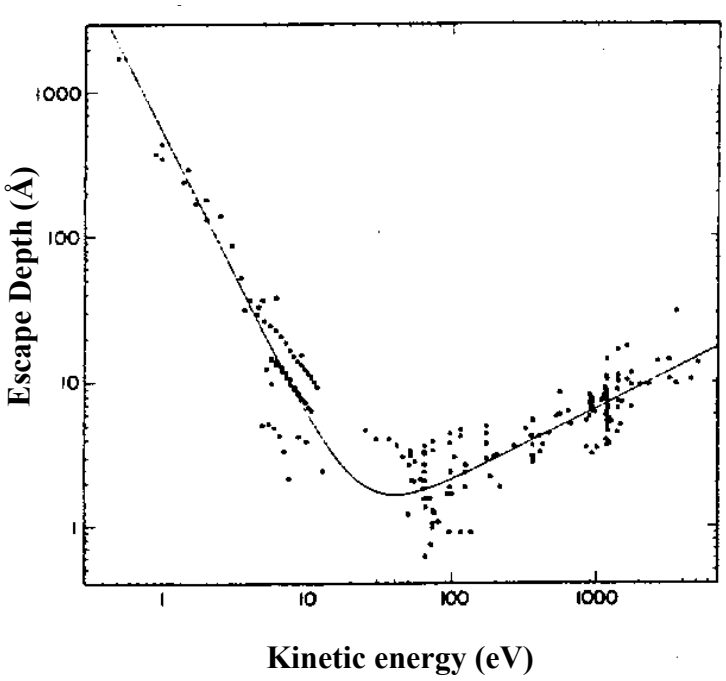

Universal Curve

(Seah and Dench, *Surf. Interface Anal.* 1, *2* 1979)

(Lindau and Spicer, *J. Electron Spec. Rel. Phenom. 3*, 409, 1974)

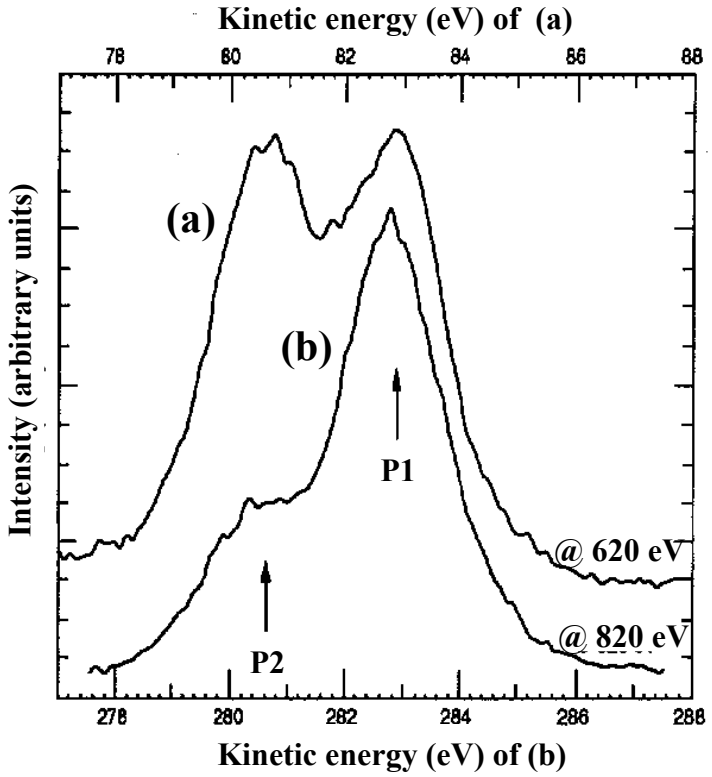

Oxygen 1s spectra of MgO(100)/H_2O

(Liu *et al., Surf. Sci. 412/413*, 287, 1998)

(SSRL)

Reaction of Water with Low Defect MgO (100) Surfaces

***(Liu et al. Surf. Sci. 412/413*, 287, 1998)**

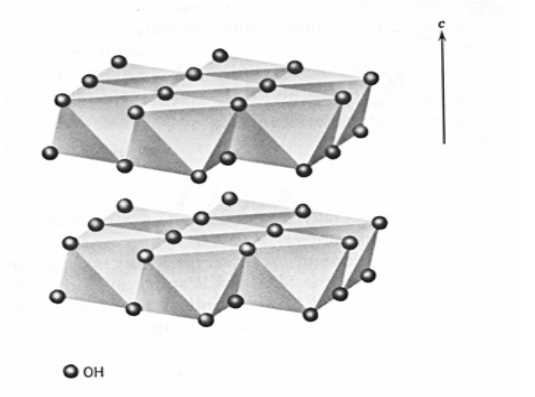

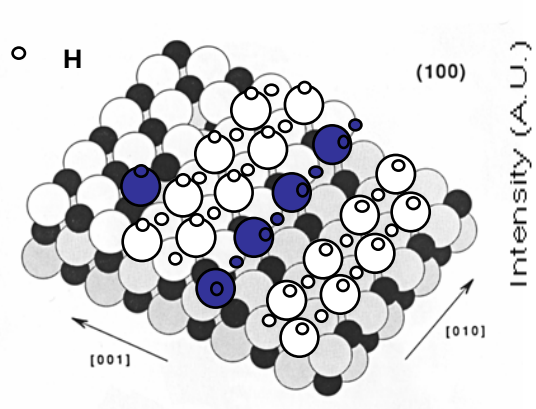

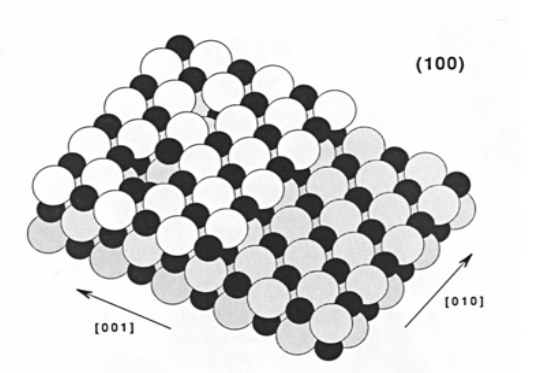

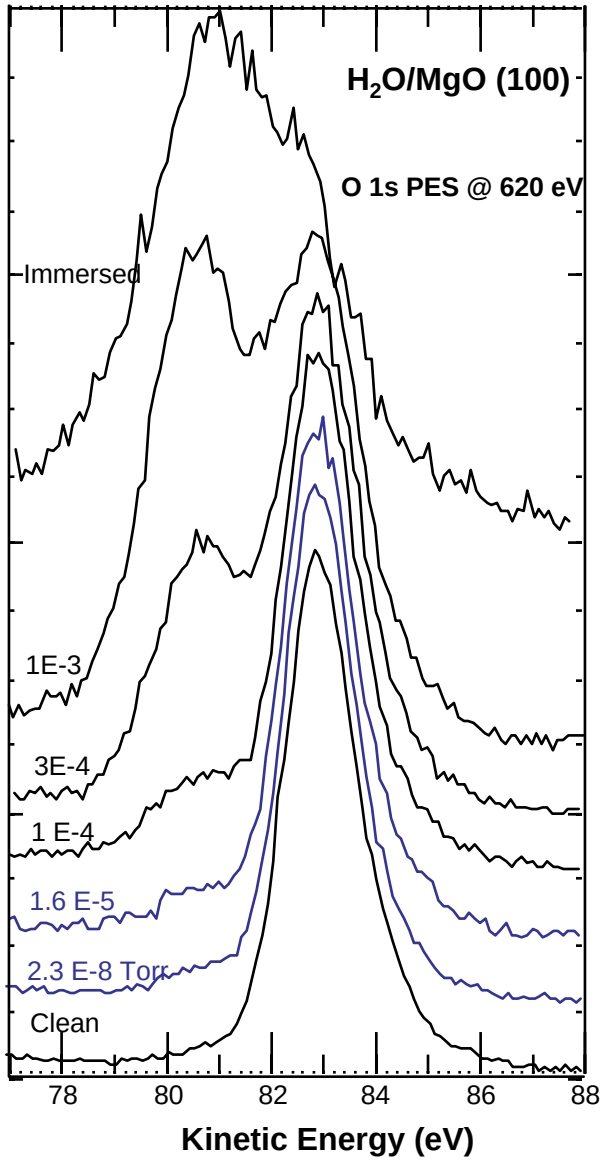

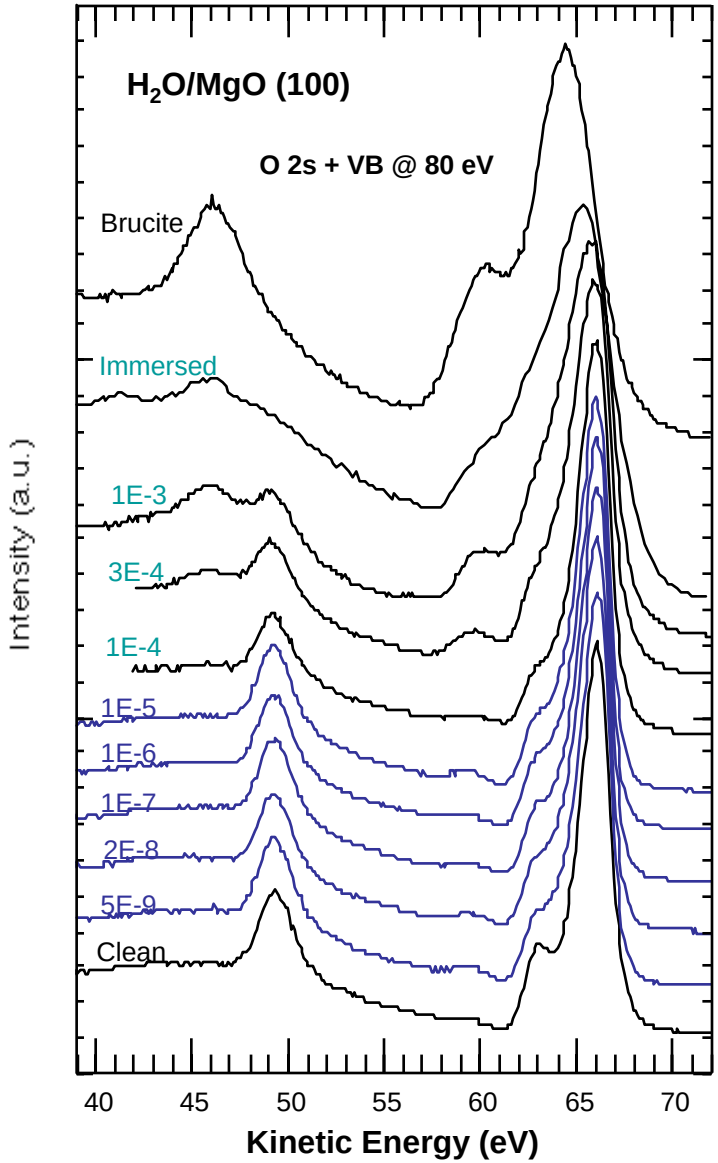

Reaction of Water with the Low Defect α-Al_2O_3 (0001) (1x1) Surface

(Liu *et al.*, *Surf. Sci. 417*, 53, 1998)

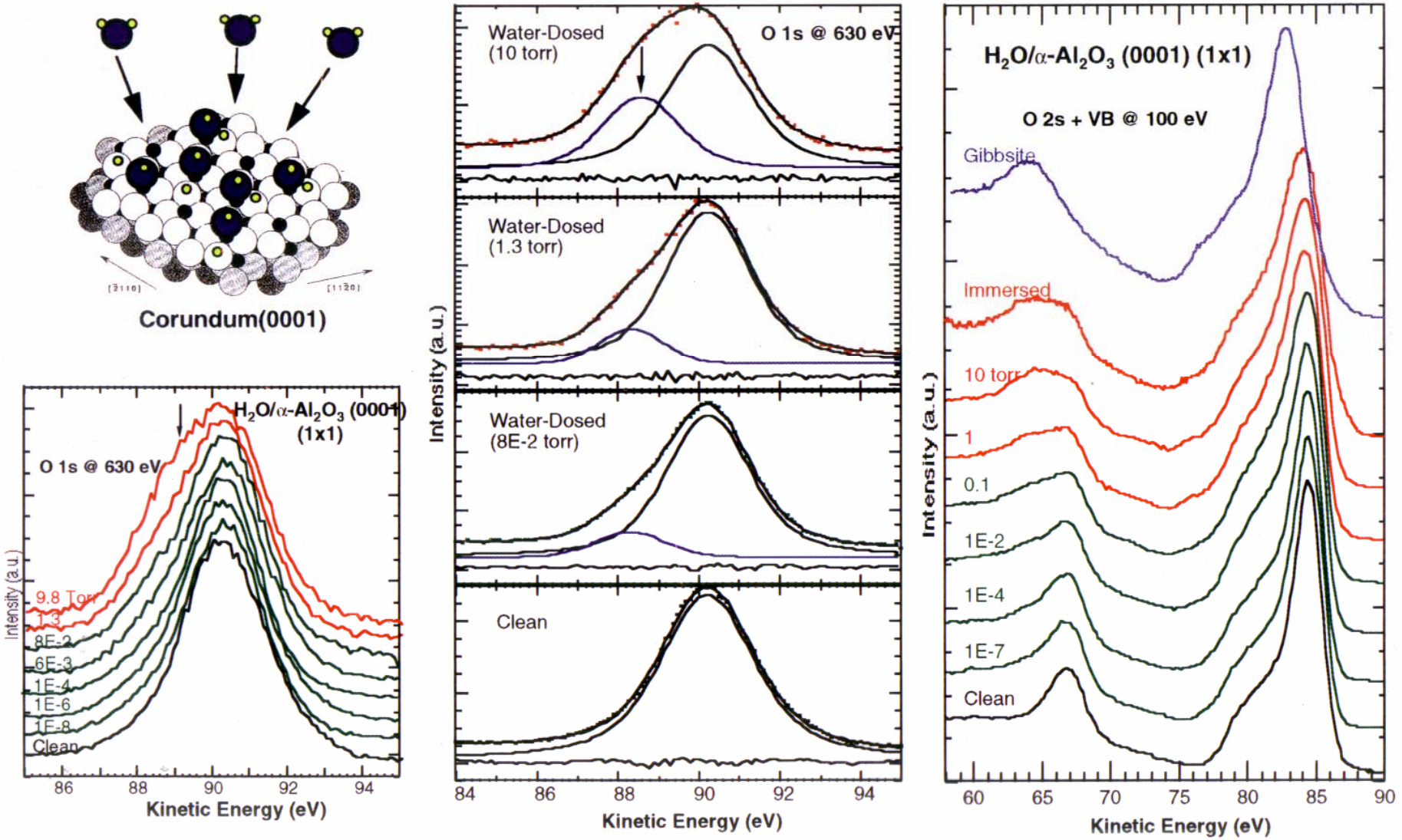

(SSRL)

Comparison of Initial Reaction of H_2O Vapor with Clean, Low Defect α-Al_2O_3 (0001) and α-Fe_2O_3 (0001) Surfaces

(Liu *et al.*, *Surf. Sci. 417*, 53, 1998)

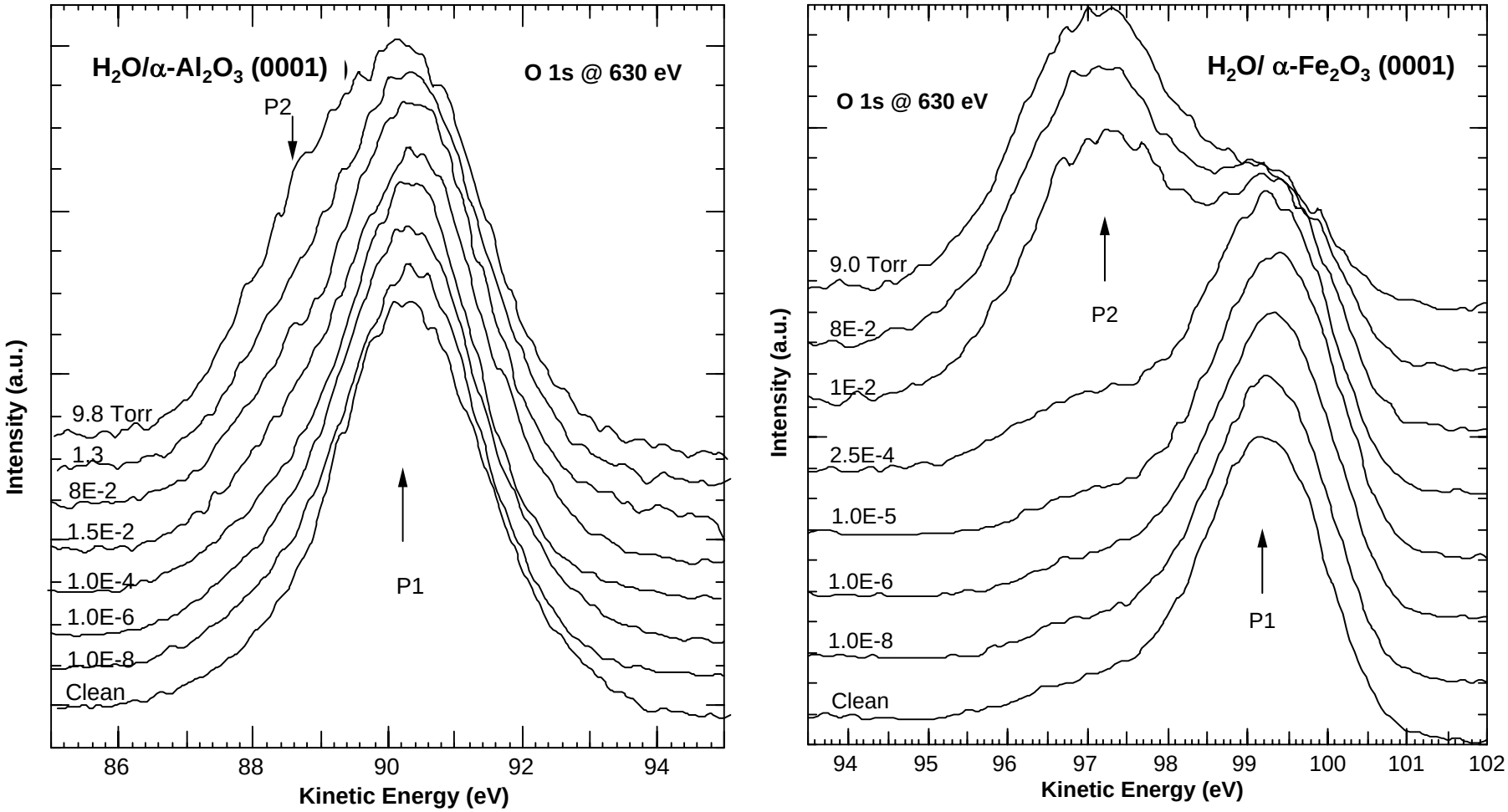

Conclusion: α-Fe_2O_3(0001) significantly more reactive to H_2O vapor than α-Al_2O_3(0001)

(SSRL)

X-ray Absorption Fine Structure Spectroscopy

X-ray Absorption K-edges of Some First-Row Transition Metal Foils

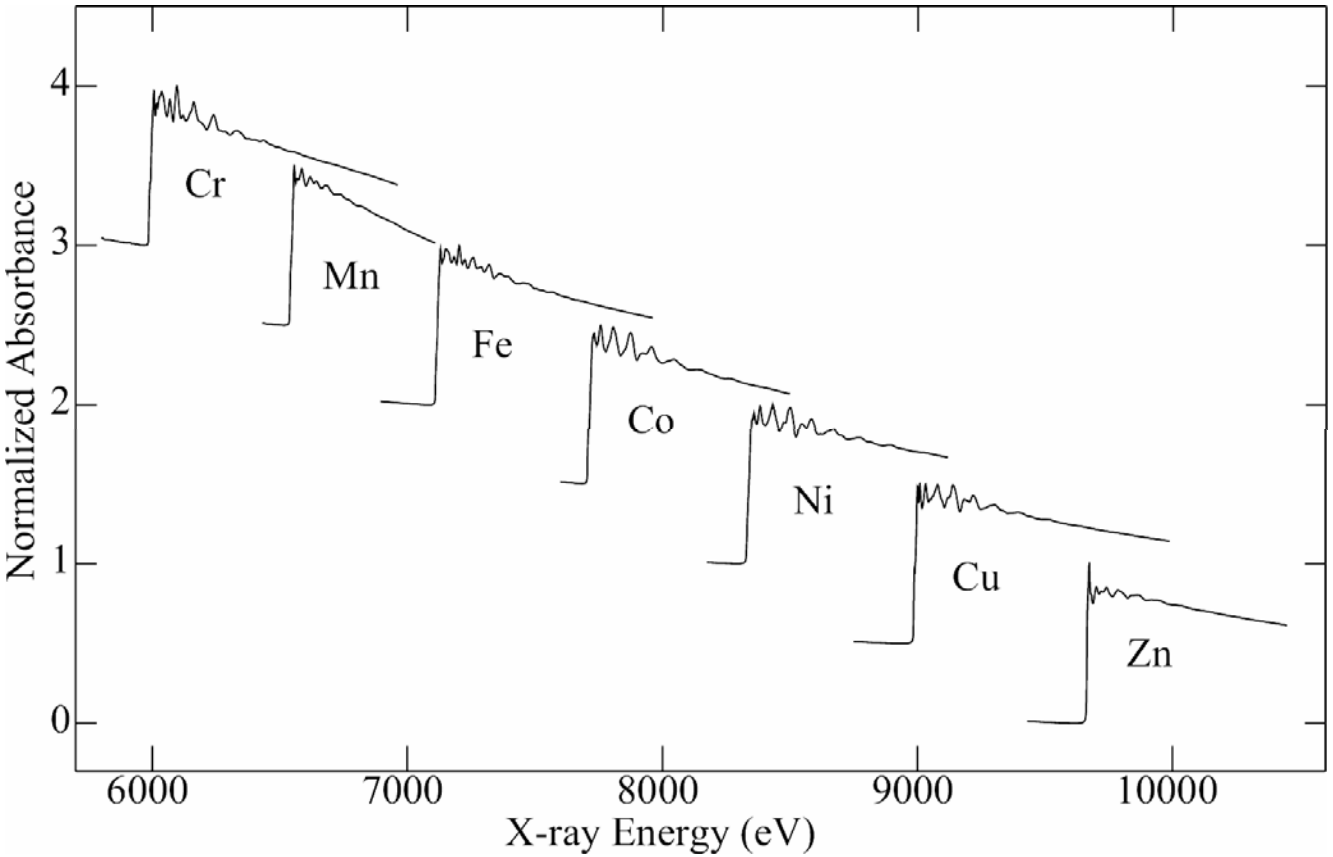

XAS is Element Specific

X-ray Absorption Near Edge Spectrum

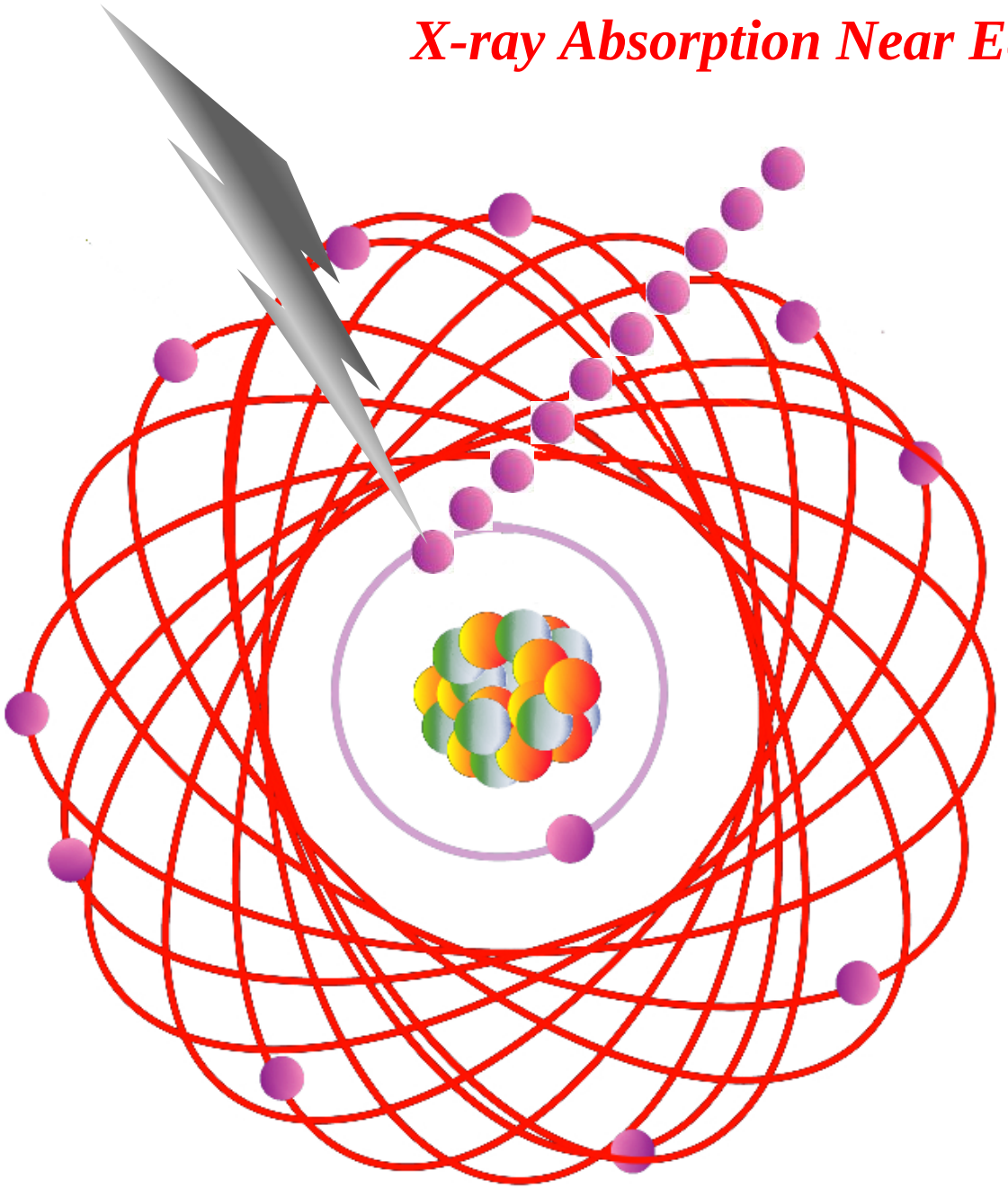

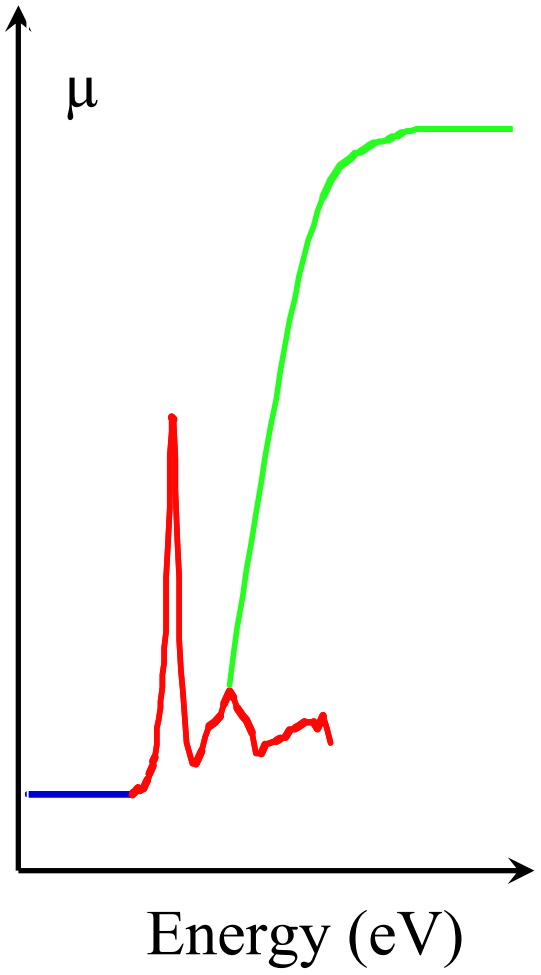

X-ray Absorption Fine Structure Spectrum

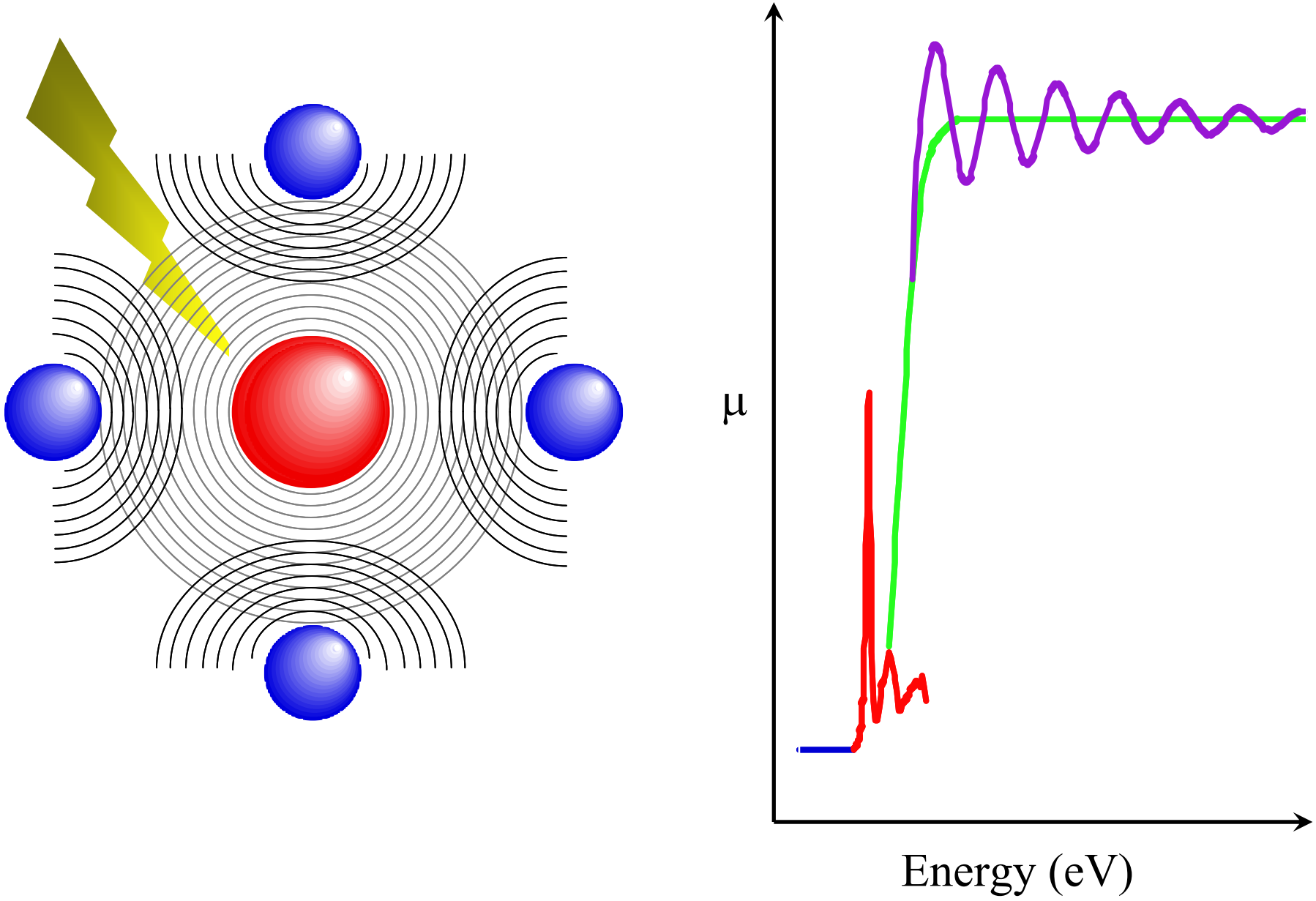

Generation of XAFS in Transmission & Fluorescence

- **transmission**

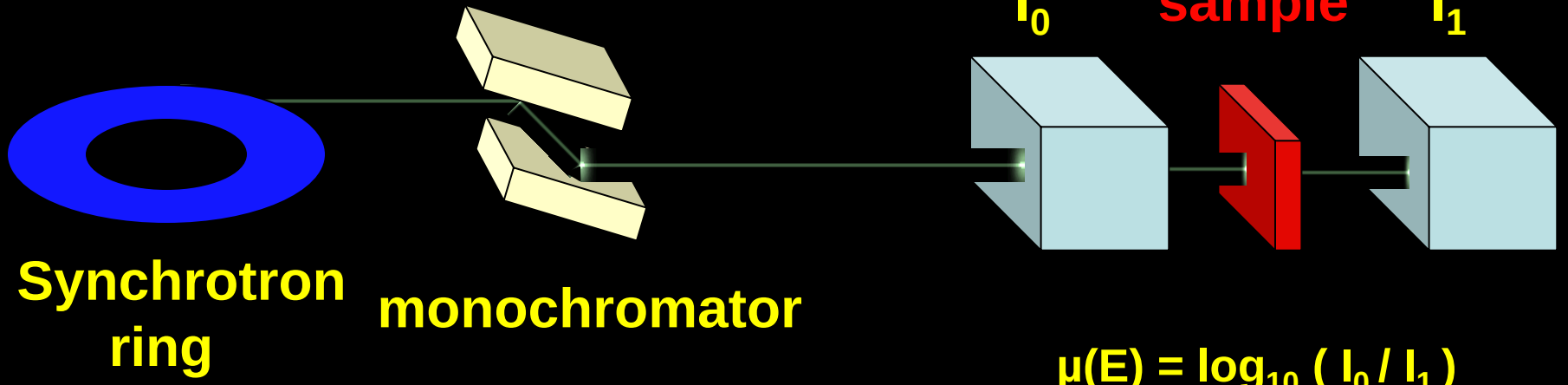

$$\mu(E) = \log_{10} (I_0 / I_1)$$

- **"fluorescence"**

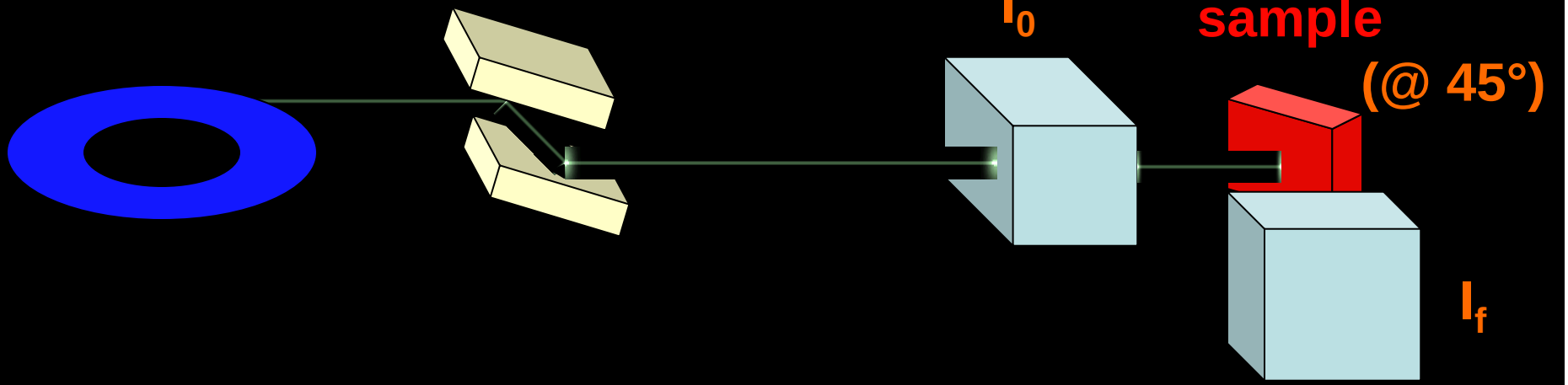

$$\mu(E) \sim I_f / I_0$$

Mn XANES K-edge Spectra

(Bargar *et al.*, *Geochim. Cosmochim Acta 64*, 2775, 2000)

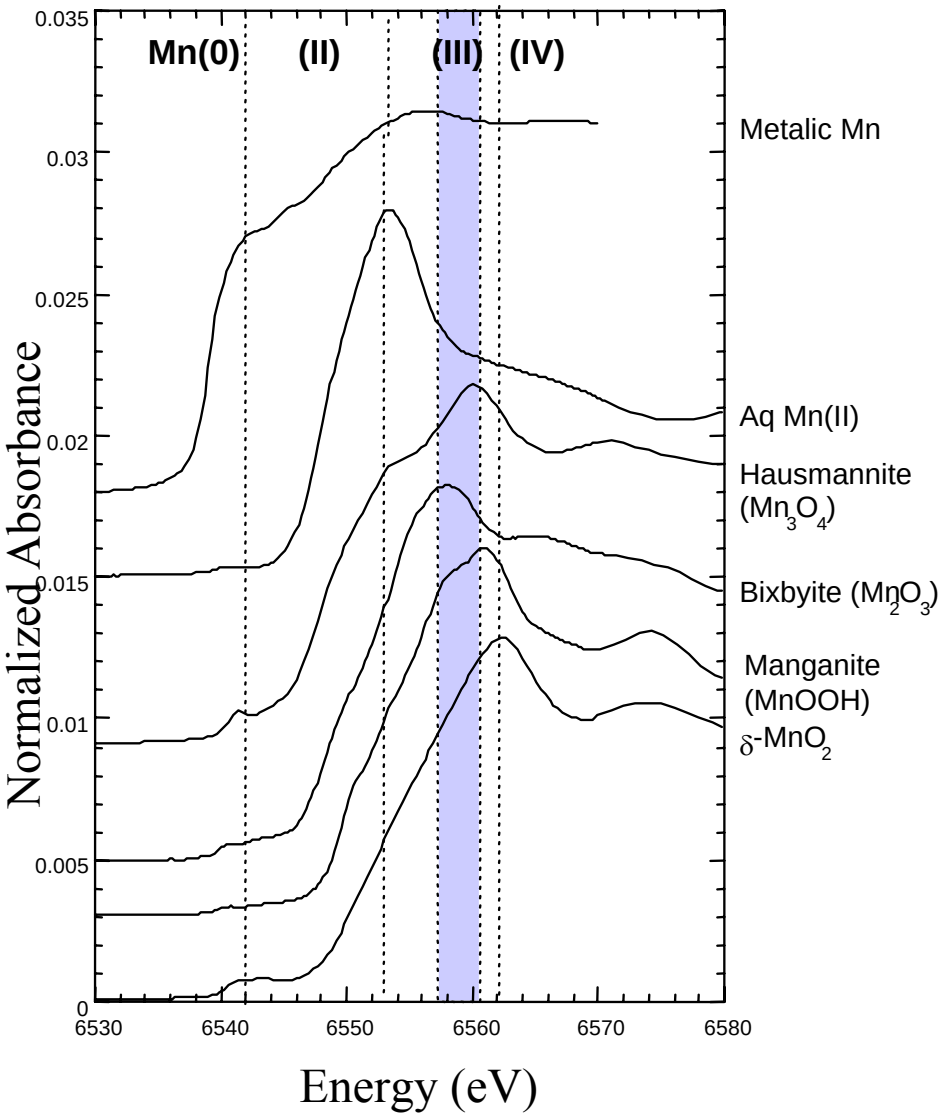

- Edge position is sensitive to oxidation state
- Edge shape is sensitive to host phase (local coordination environment)

EXAFS Data Analysis

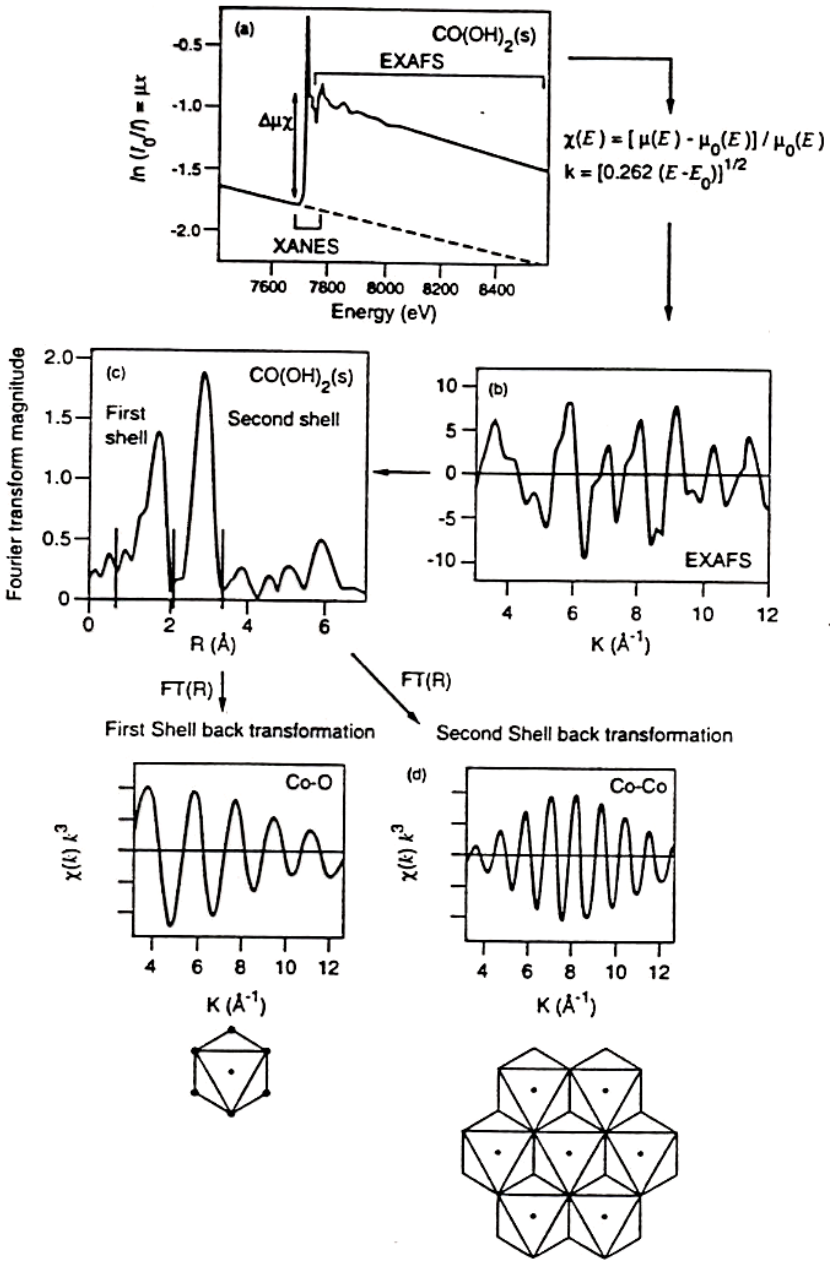

Sorption Processes at Solid/Aqueous Solution Interfaces

(after Manceau *et al.*, *Rev. Mineral.* 49, 341, 2002)

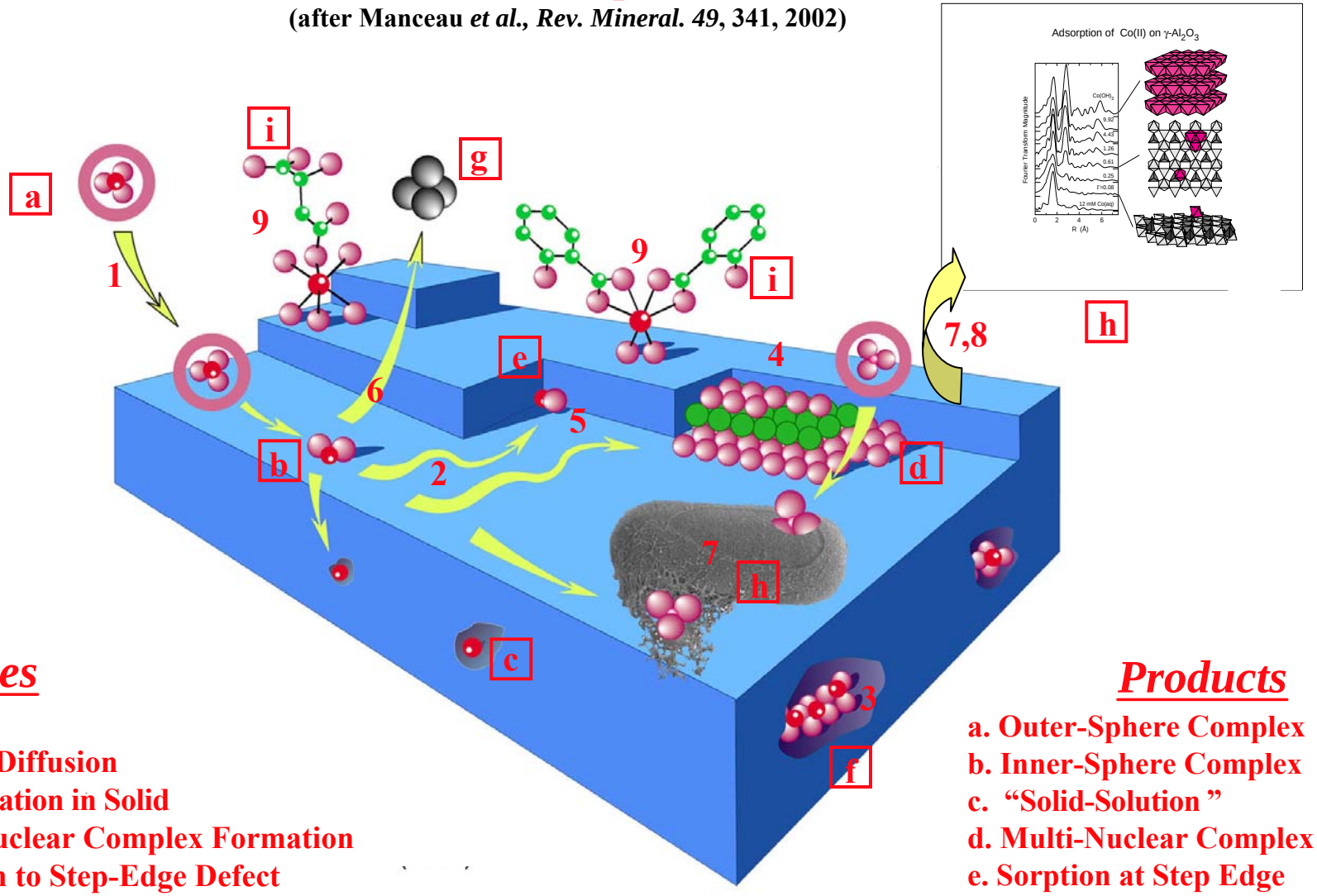

Processes

1. Sorption
2. Surface Diffusion
3. Incorporation in Solid
4. Multi-Nuclear Complex Formation
5. Diffusion to Step-Edge Defect
6. Desorption
7. Dissolution
8. Reprecipitation
9. Ternary Complex Formation

Products

a. Outer-Sphere Complex
b. Inner-Sphere Complex
c. "Solid-Solution"
d. Multi-Nuclear Complex
e. Sorption at Step Edge
f. "Solid Solution"
g. Solution Complex
h. Precipitates
i. Ternary Complexes

Intrinsic Properties of Metal Oxides: Dielectric Constants and pH_{ppzc} Values

(after Sverjensky, *Geochim. Cosmochim. Acta 58*, 3123, 1994)

□□□□□	**Dielectric Constant**	**$s/r_{M\text{-}OH}$***	**Experim. pH_{ppzc}**	**Calculated pH_{ppzc}****
α-SiO_2	4.578	0.3818	2.9	3.02
$Al_2Si_2O_5(OH)_4$	11.8	0.2754	4.5	4.66
α-TiO_2	120.91	0.2248	5.8	5.16
Fe_3O_4	20,000	0.1768	6.6	7.07
α-Fe_2O_3	25.0	0.1645	8.5	8.51
α̃□□□□□	11.7	0.165	9.0-9.7	9.4
α-Al_2O_3	10.43	0.1711	9.1	9.48
α-$Al(OH)_3$	8.4	0.1716	10.0	9.98
MgO	9.83	0.1070	12.4	12.42
CaO	11.95	0.0976	--	12.4
β-MnO_2	10,000	0.2301	4.6-7.3	4.8

*$s = z_i/CN_i$ ** $pH_{ppzc} = -0.5(\Delta\Omega_r/2.303RT)(1/\varepsilon_k) - B(s/r_{M\text{-}OH}) + \log K''_{H^+}$

The Electrical Double Layer and Sorption Behavior of Cations and Anions on Hydrous Ferric Oxide as a Function of pH

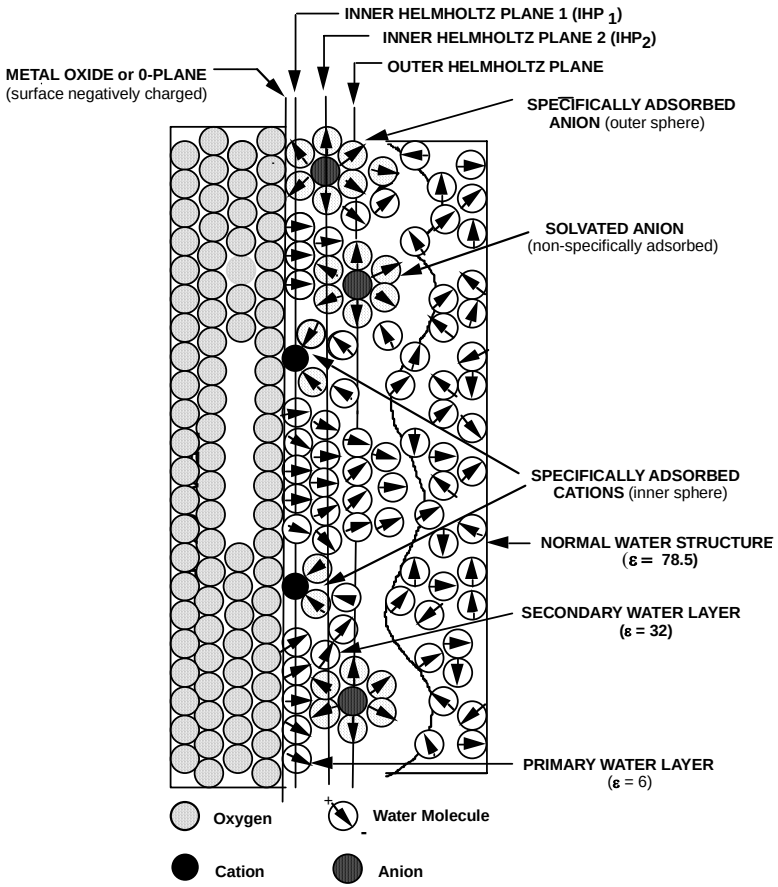

Point of Zero Charge = pH at which the surface charge is neutral

(Brown and Parks, *Int. Geol. Rev. 43*, 963-1073, 2001)

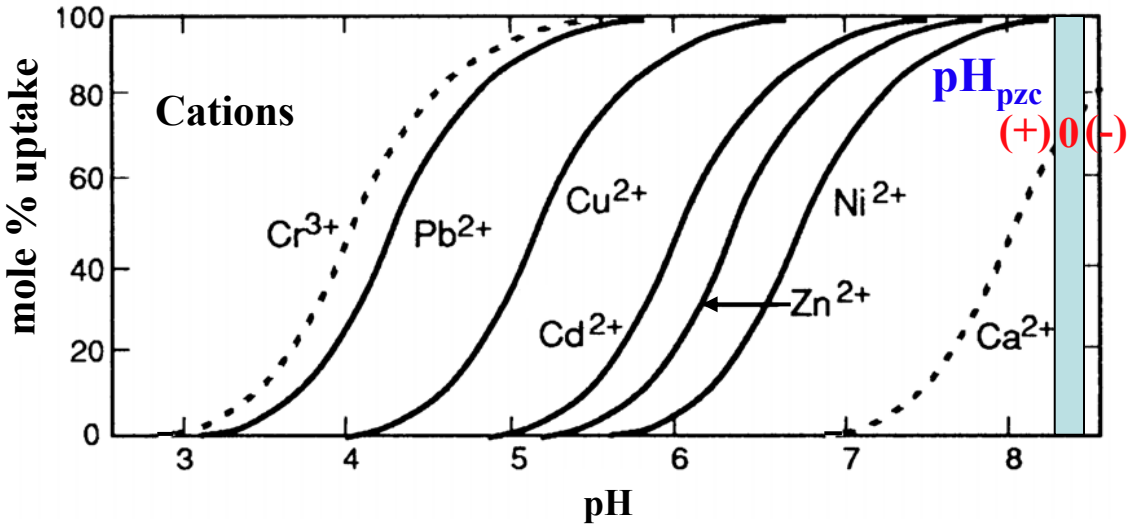

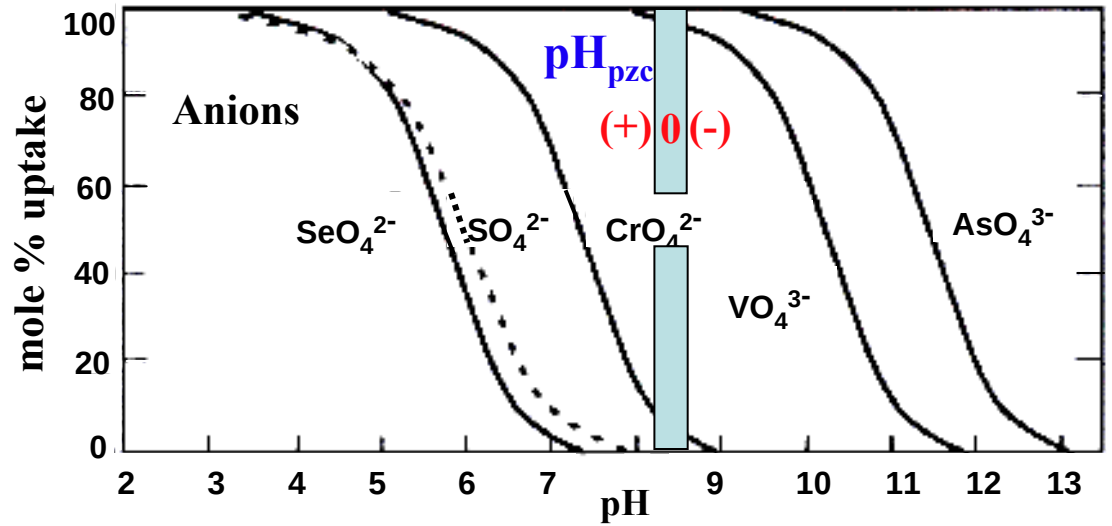

(after Stumm, *Chemistry of the Solid-Water Interface,* Wiley, 1992)

Effect of Ionic Strength on Uptake of Metal Ions on α-FeOOH

(after Hayes and Leckie, *J. Colloid Interface Sci. 115*, 564, 1987)

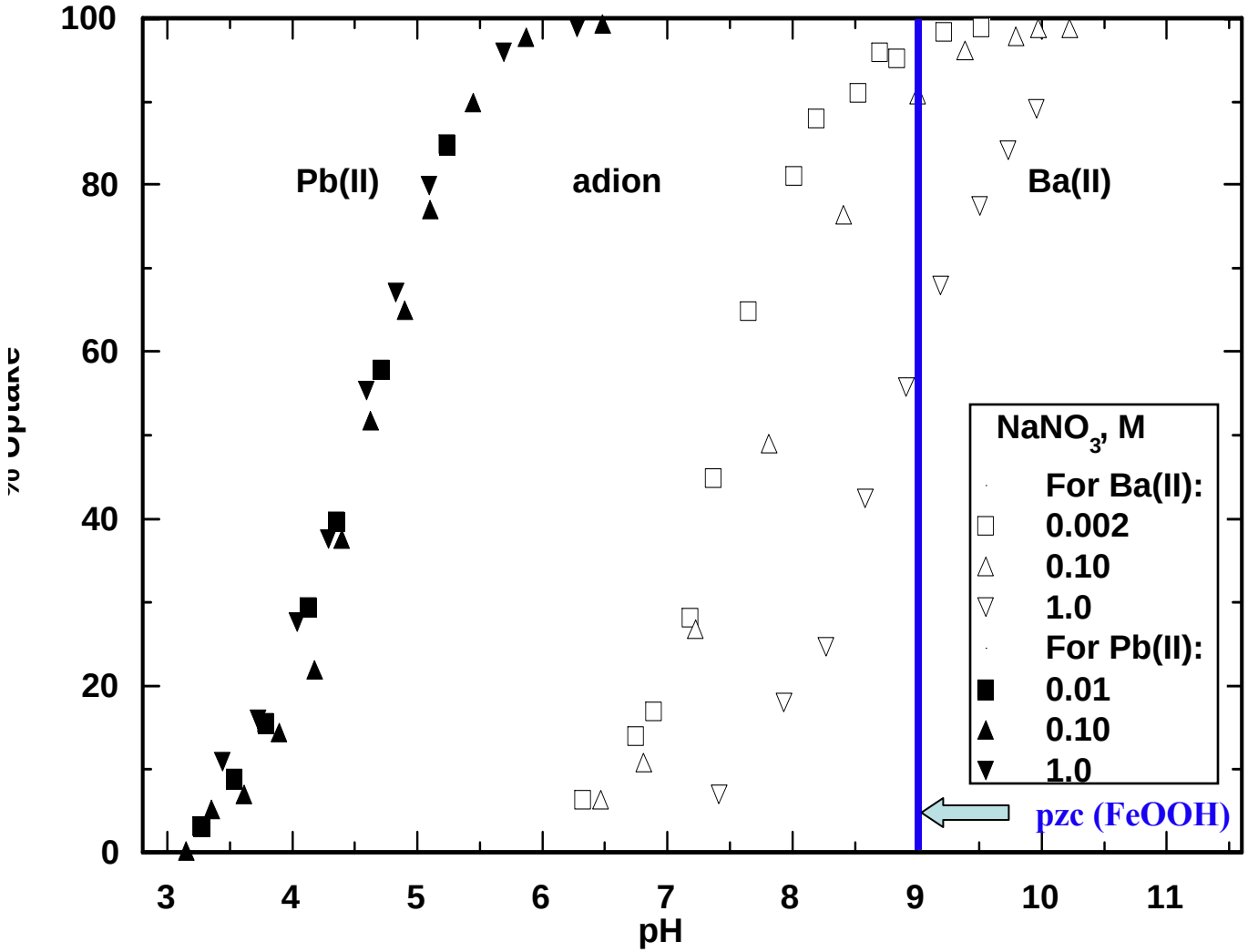

Lack of ionic strength dependence of Pb(II) uptake and complete uptake well below the pzc of FeOOH suggests more strongly bonded surface complex than for Ba(II)

Comparison of Binding Site Densities and Pb(II) Binding Affinities for Al- and Fe(III)-Oxide Surfaces

Mineral substrates	Type of binding site	Site density (log n)	Binding affinities (log K_{app})
α-Al_2O_3 (0001)	M_1	-6.25	5.35
	M_2	-5.05	2.7
α-Al_2O_3 (1-102)	M_1	-6.25	6.0
	M_2	-5.15	3.55
α-Fe_2O_3 (0001)	M_1	-5.85	6.65
	M_2	-5.1	3.5

(Yoon *et al.*, *Langmuir 21*, 4503, 2005)

Experimental Methods in Metal Ion Sorption Studies on Solids

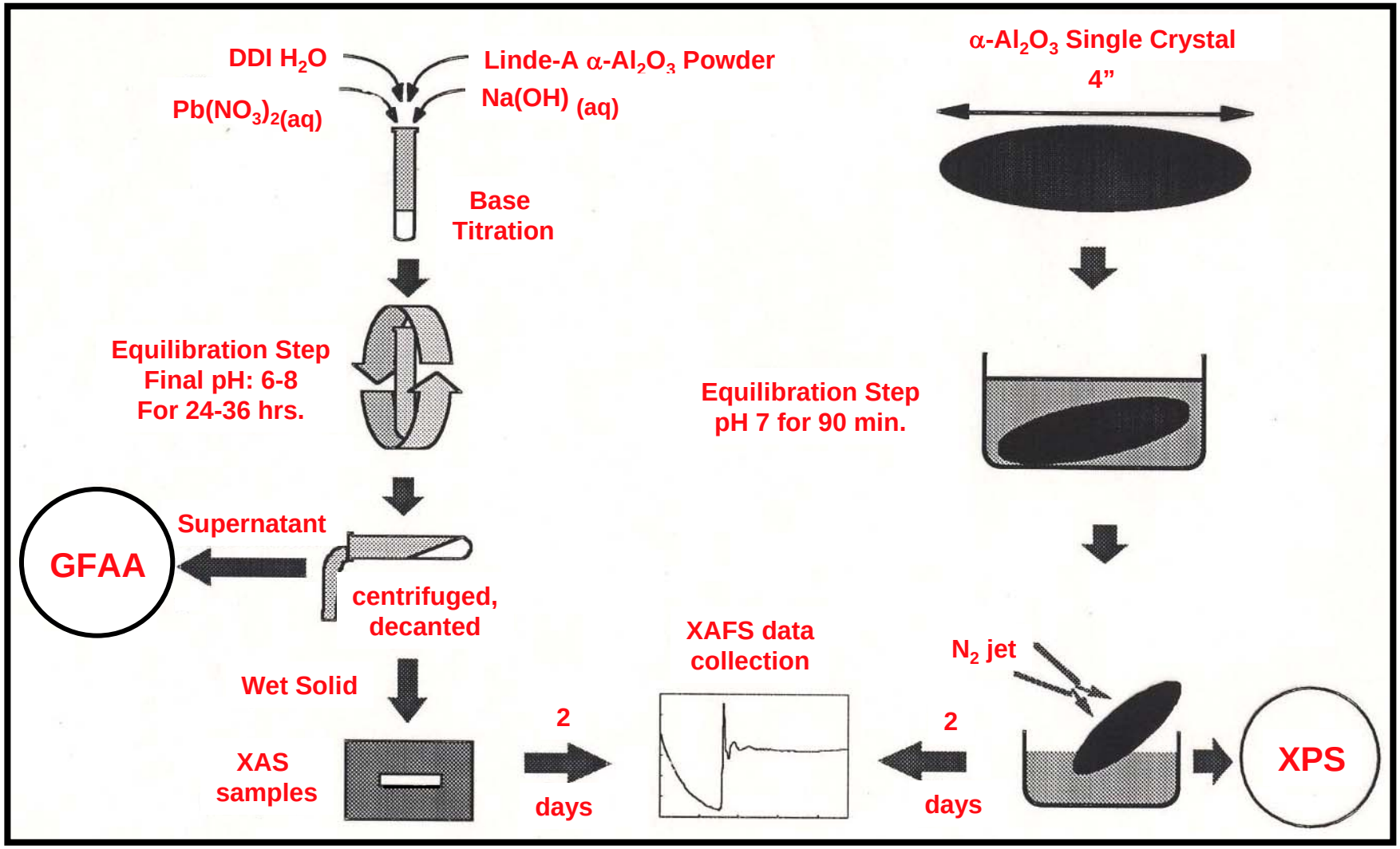

Zn(II) and Pb(II) Sorption on Al- and Fe-(oxyhydr)oxide Surfaces (XAFS Studies of Model Systems)

Zn K-EXAFS Spectra and Fourier Transforms for Zn(II) sorbed on α-Al_2O_3 as a Function of Zn Surface Coverage (Trainor et al., 2000)

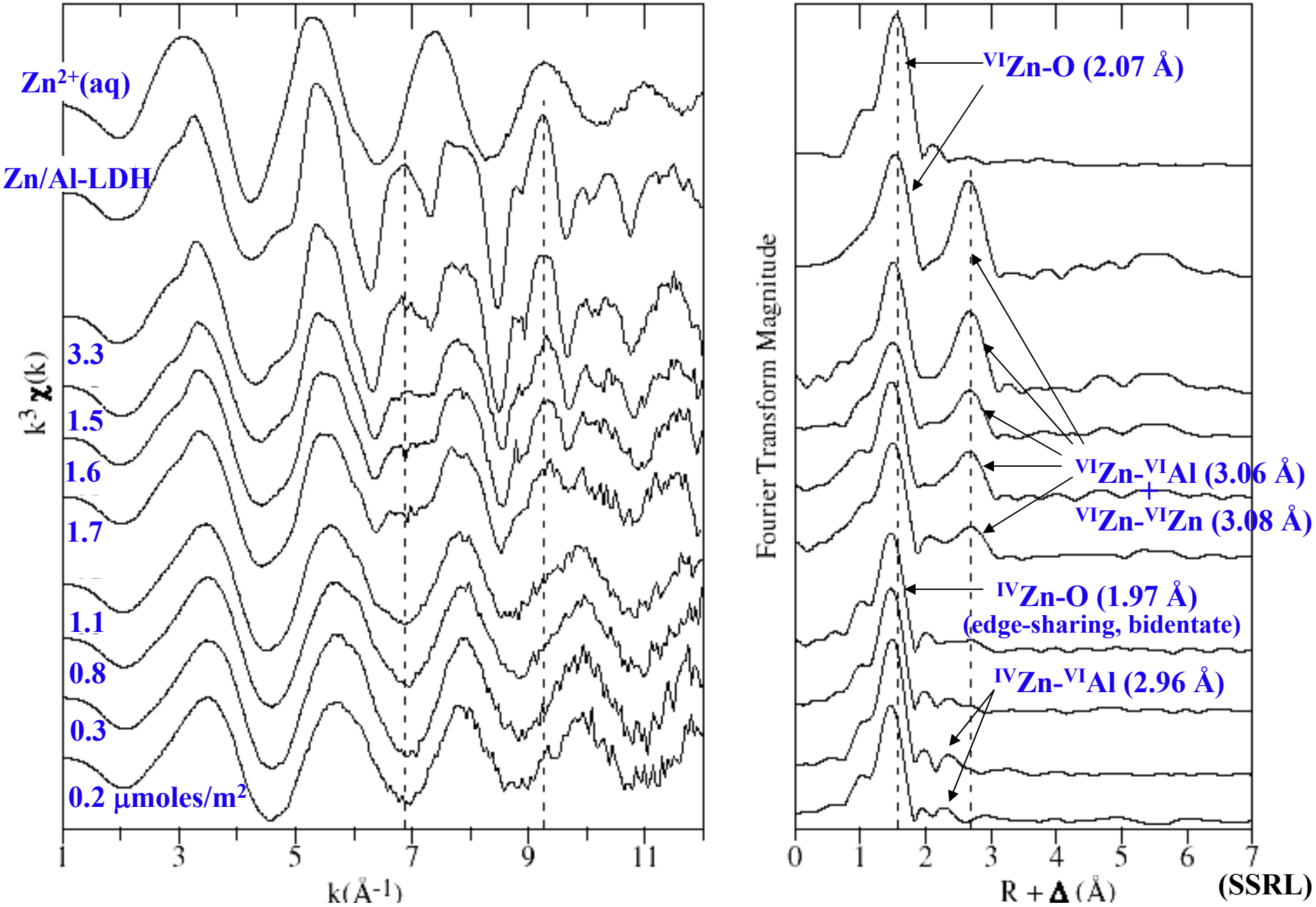

(SSRL)

What are these precipitates?

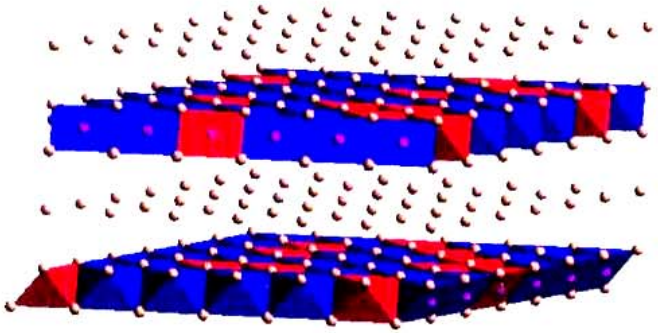

Zn^{2+} , Al^{3+}

A^{n-}, H_2O

Zn^{2+} , Al^{3+}

Layered Double Hydroxides

$$[M^{2+}_{1-x}M^{3+}_{x}(OH)_2]^{x+}(A^{n-}_{x/n}) \cdot mH_2O \quad 0.2<x<0.33$$

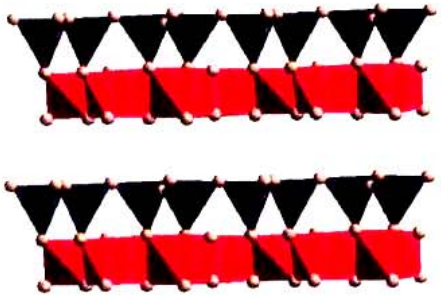

Kaolinite (Al, Si)
Nepouite (Ni, Si)

Pyrophyllite (Al, Si)
Talc (Mg, Si)

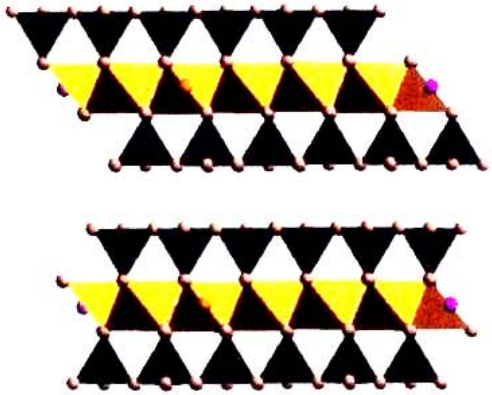

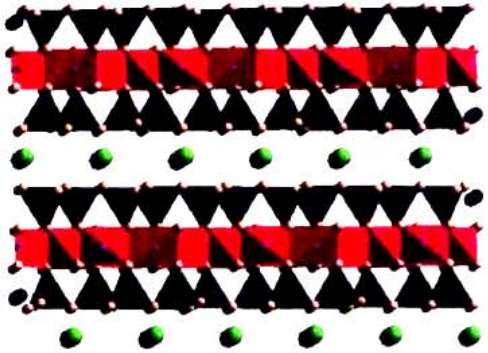

Smectites
Micas

X-RAY STANDING WAVES

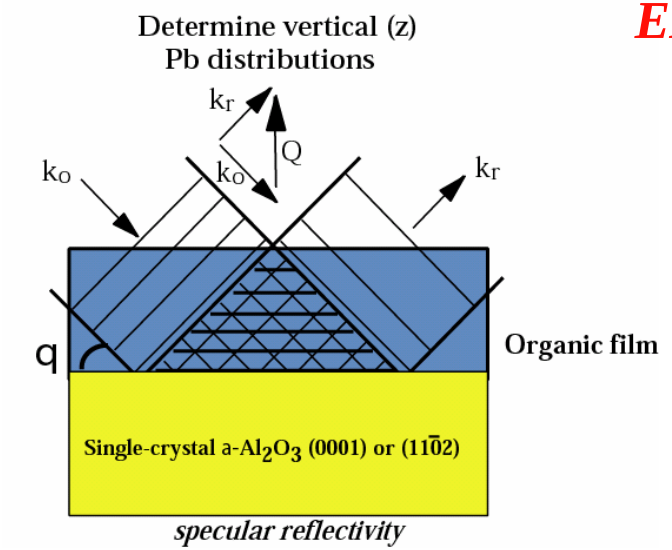

Instrumental Setup for Grazing-Incidence EXAFS, XSW-FY, and Reflectivity Measurements

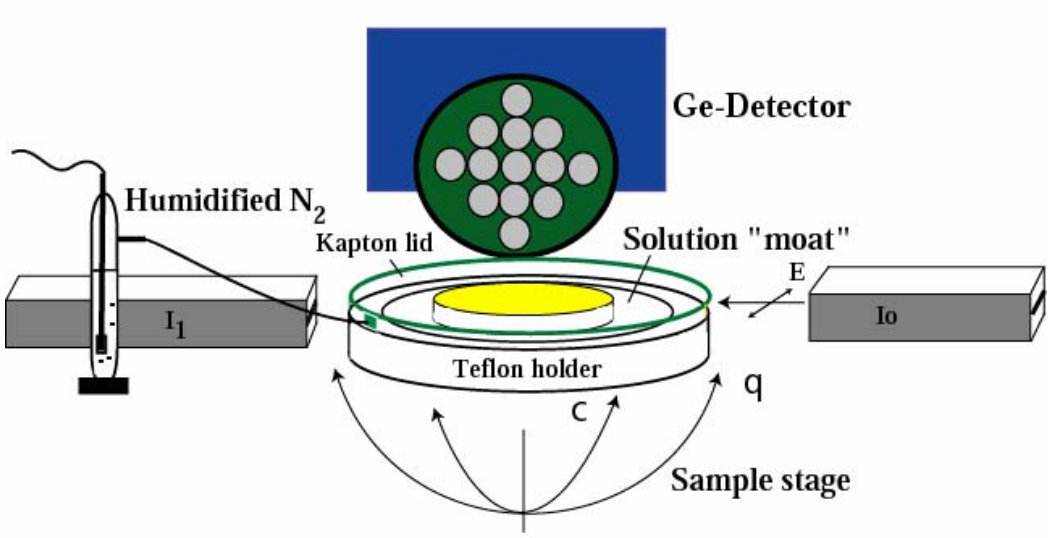

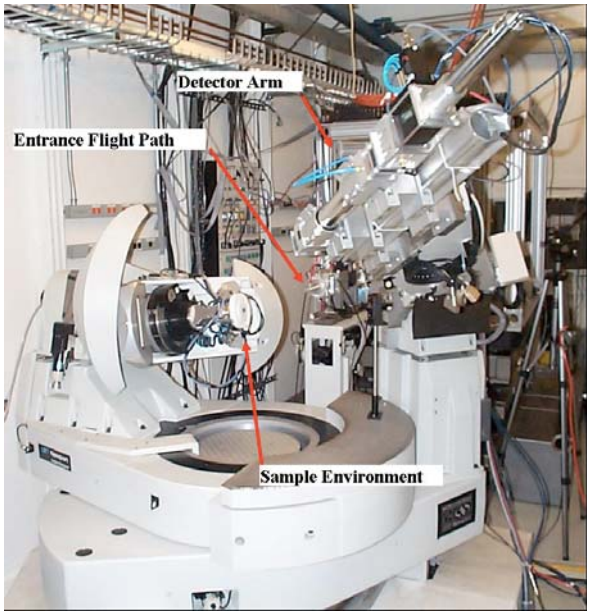

Kappa Diffractometer at GSECARS
APS Sector 13-ID-C

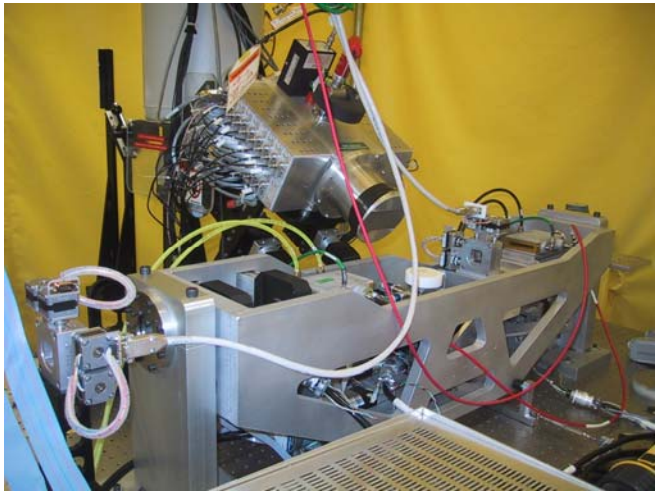

Grazing-Incidence Spectrometer
at SSRL BL 11-2

EXAFS Results for Pb^{2+} Adsorbed at the α-Al_2O_3 (1-102)/Water Interface

(Bargar, Brown, Parks, *Geochim Cosmochim Acta 61*, 2617, 1997)

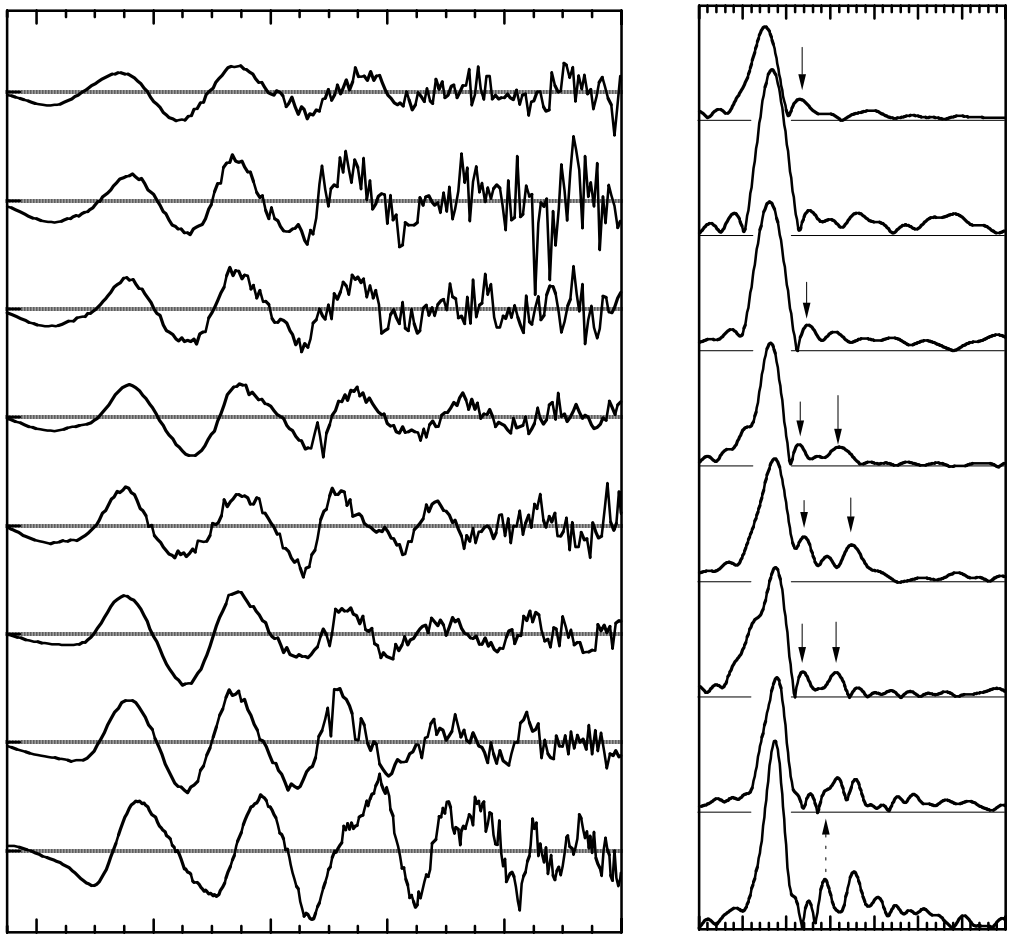

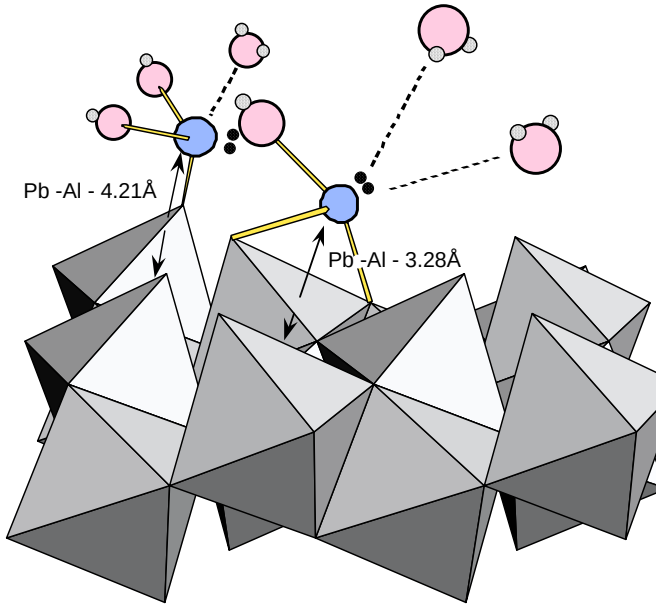

Pb^{2+} forms dominantly inner-sphere complexes at α-Al_2O_3(1-102)/H_2O and α-Fe_2O_3(0001)/H_2O interfaces.

(SSRL)

Outer-Sphere Adsorption of Pb^{2+} on α-Al_2O_3(0001)

(Bargar *et al.*, *J. Colloid Interface Sci. 85*, 473, 1997)

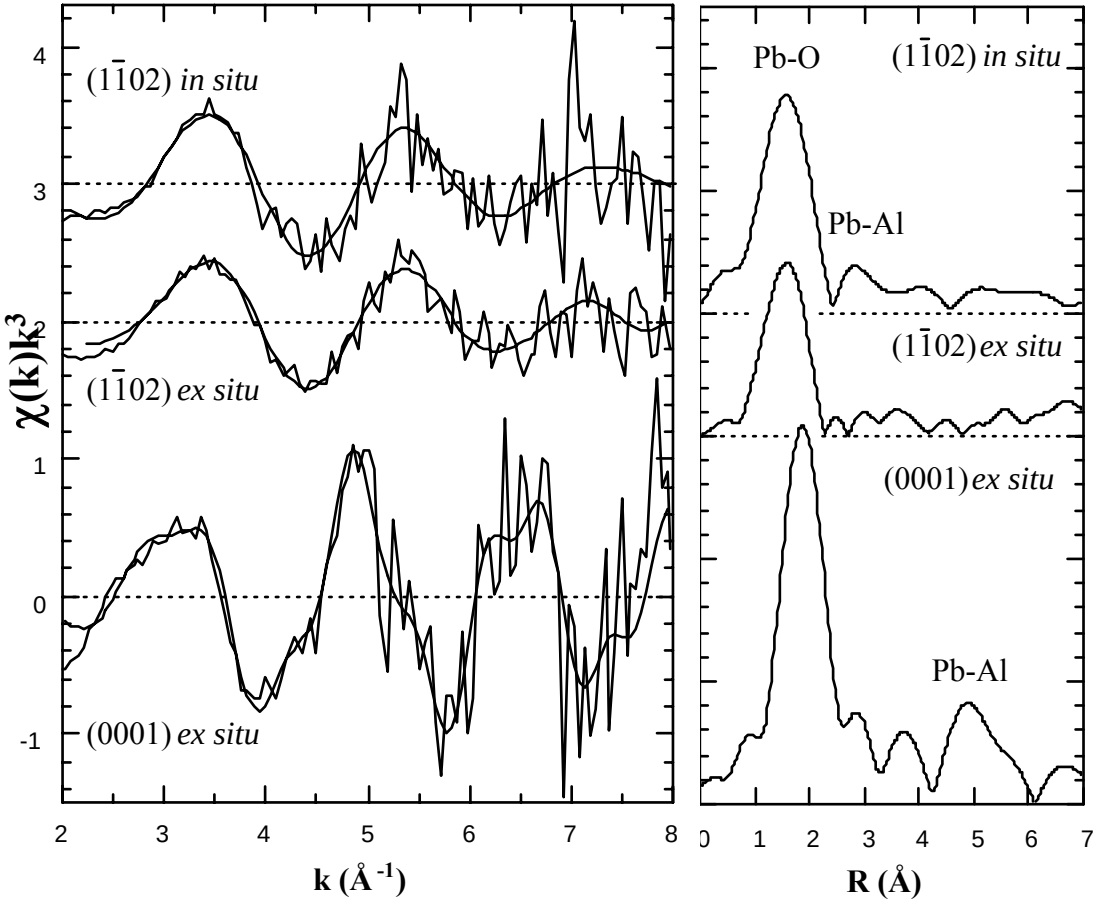

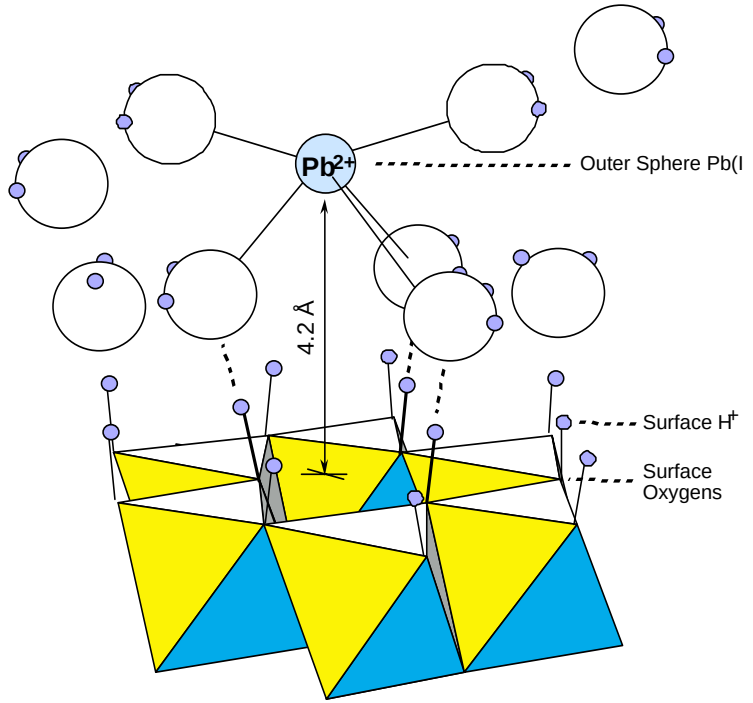

Pb^{2+} forms dominantly outer-sphere complexes at α-Al_2O_3(0001)/H_2O interfaces.

(SSRL)

Grazing-Incidence XAFS Study of Pb(II) Sorption on α-Fe_2O_3

(Bargar *et al.*, *Langmuir 20*, 166, 2004)

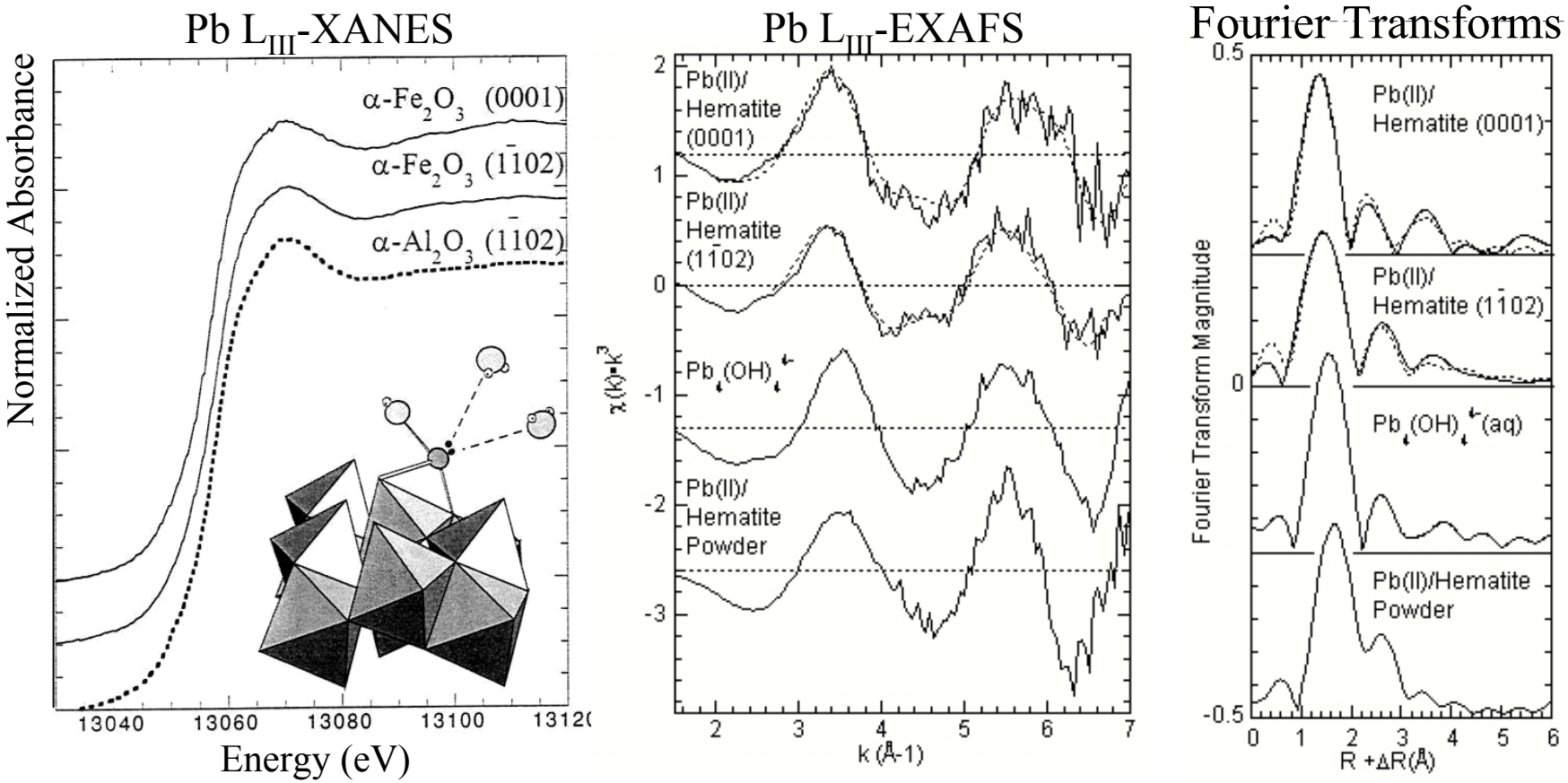

In contrast with Pb(II) sorption on α-Al_2O_3 (0001), where dominantly outer-sphere complexes are found, Pb(II) forms dominantly inner-sphere, bidentate complexes on α-Fe_2O_3 (0001).

These and other XAFS studies, coupled with XPS studies of Pb^{2+} uptake, indicate the following order of reactivity:

α-Fe_2O_3(0001) > α-Al_2O_3(1-102) >> α-Al_2O_3(0001)

(SSRL)

Sorption of Pb(II) on α-Al_2O_3 and α-Fe_2O_3

- Sorbate binding mode

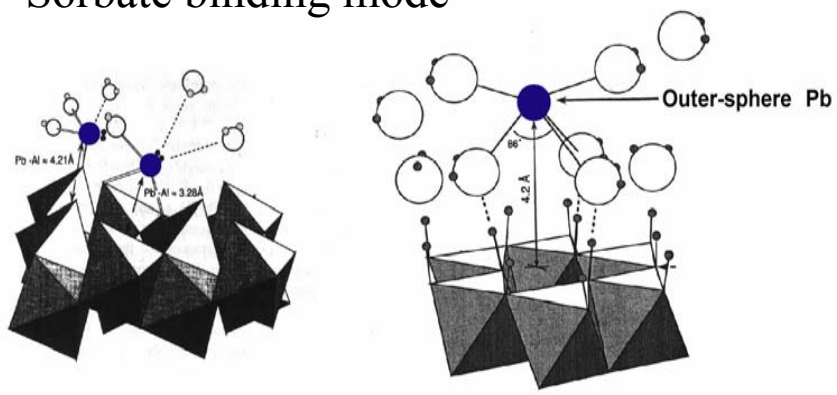

Pb(II) inner sphere:
α-Fe_2O_3 (0001), (1-102)
α-Al_2O_3 (1-102)

Pb(II) outer sphere:
α-Al_2O_3 (0001)

Bargar *et al., J. Colloid Interface Sci.* ***185***, 473-492 (1997)
Bargar *et al., Langmuir* ***20***, 1667-1673 (2004)

- Crystal face-specific reactivity

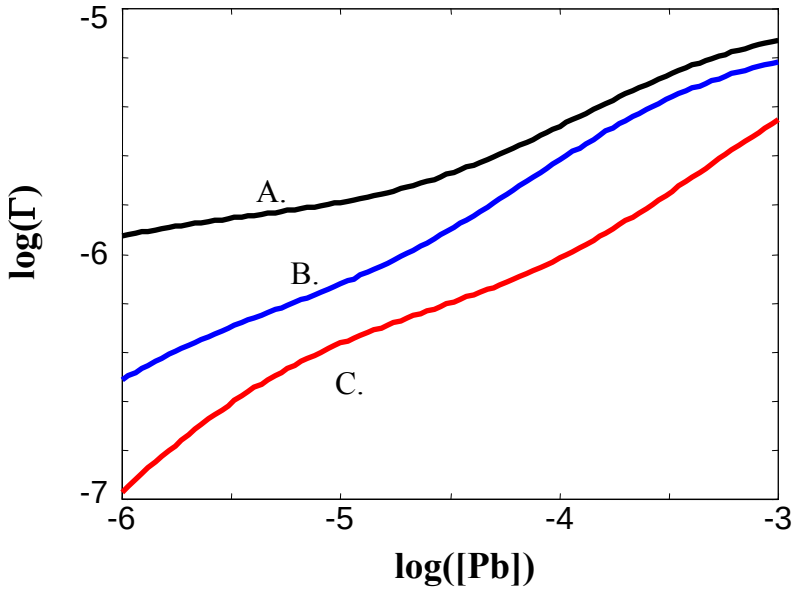

Pb(II) adsorption isotherms:

A. α-Fe_2O_3 (0001)
B. α-Al_2O_3 (1-102)
C. α-Al_2O_3 (0001)

After: Templeton *et al., Proc. Nat. Acad. Sci. USA* ***98***, 11897-11902 (2001)

Mineral surface reactivity is determined by structure and composition

Natural Organic Matter and the Effective Monolayer Hypothesis

Most particles in marine environments are coated by thin films (effective monolayer) of organic matter

- **However, TEM study of continental shelf sediments found no evidence for organic thin films on sediment particles. (Ransom *et al.*, *Marine Geol. 138*, 1, 1997)**

- **Also, enthalpies of gas adsorption have shown that no more than 15% of particle surfaces in marine sediments are covered by organic matter. (Mayer, *GCA 63*, 207 1999)**

- **However, comparison of BET specific surface area of heated and untreated soils suggests that most soil minerals are covered by organic matter. (Mayer and Xing, *Soil Sci. Soc. Am. J. 65*, 250, 2001)**

- **A relevant question is what effect do organic coatings, including microbial biofilms, have on the reactivity of metal oxide surfaces.**

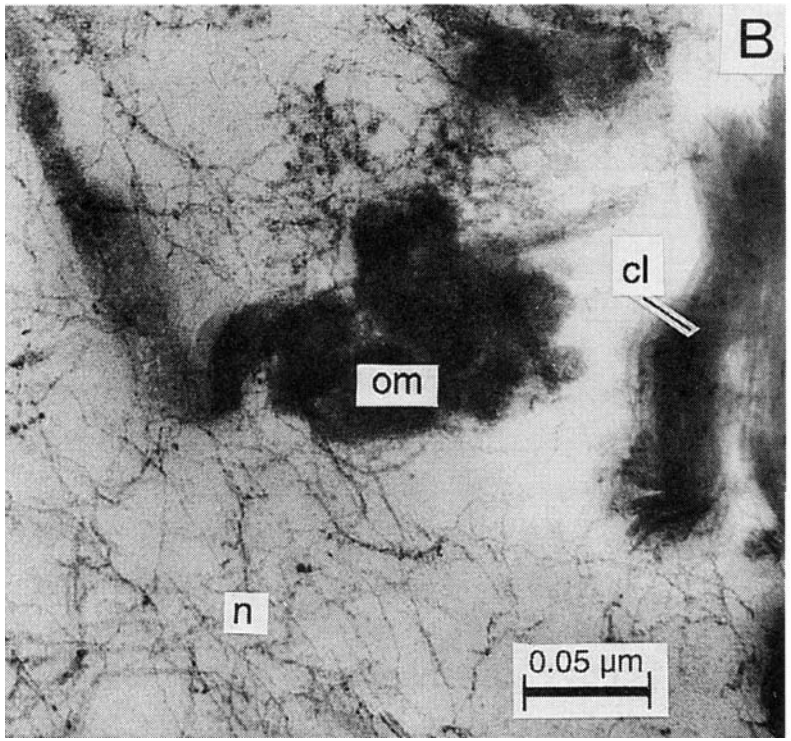

(Ransom *et al.*, *Marine Geol. 138*, 1, 1997)

Do they block reactive surface sites?

Do they preferentially adsorb aqueous metal ions?

XSW-FY Simulation - Effect of Pb(II) Distribution between the PAA Polymer Film and α-Al_2O_3 Surface

(Yoon *et al.*, *Langmuir 21*, 4503, 2005)

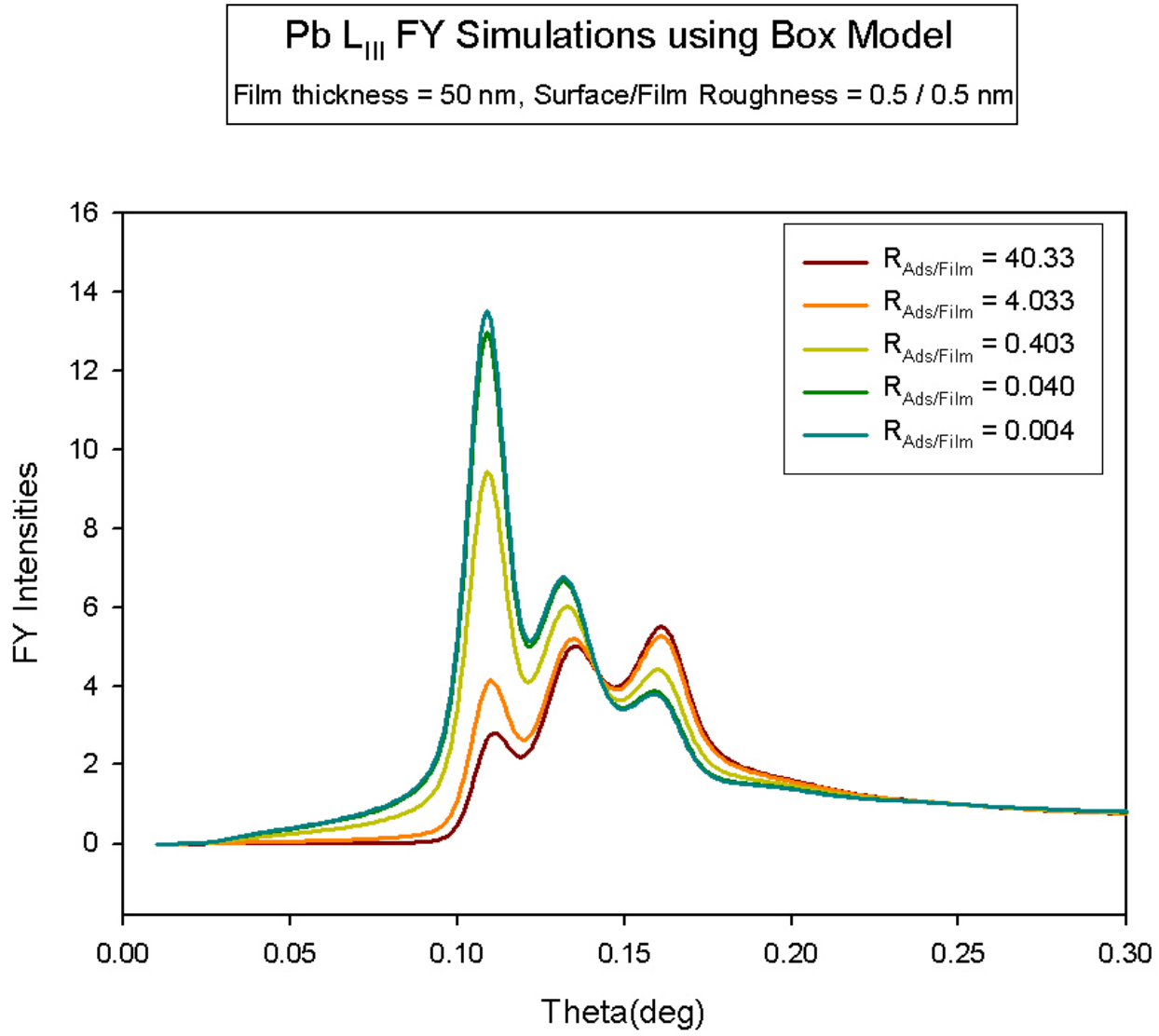

XSW-FY Determination of Pb(II) Distribution between PAA Film and Al- and Fe(III)-Oxide Surfaces: Effect of Different Substrates

(Yoon *et al.*, *Langmuir 21*, 4503, 2005)

(All samples: pH = 4.5, [Pb] = 20 μM)

α-Al_2O_3(0001)

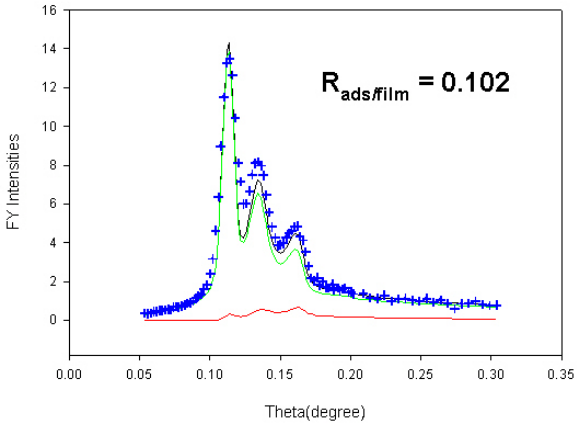

α-Al_2O_3(1-102)

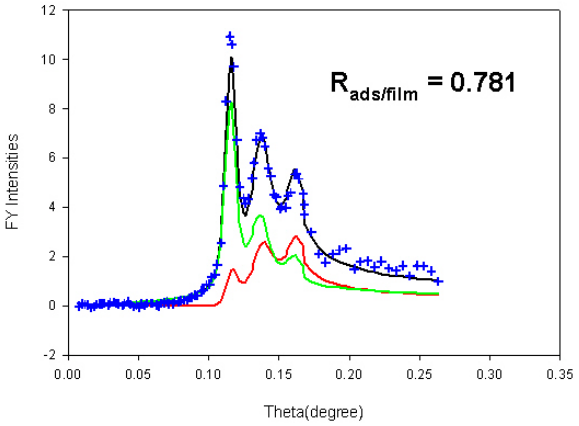

α-Fe_2O_3(0001)

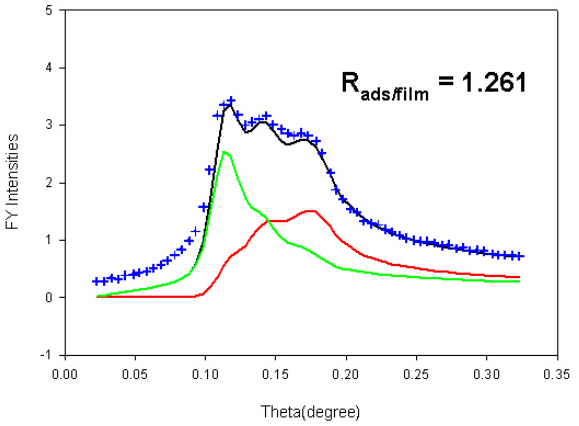

Order of reactivity of PAA-coated surfaces wrt Pb(II):

α-Fe_2O_3(0001) > α-Al_2O_3(1-102) >> α-Al_2O_3(0001)

Approaching Natural Complexity in Model Systems: Pb Sorption on Biofilm-Coated Metal Oxides

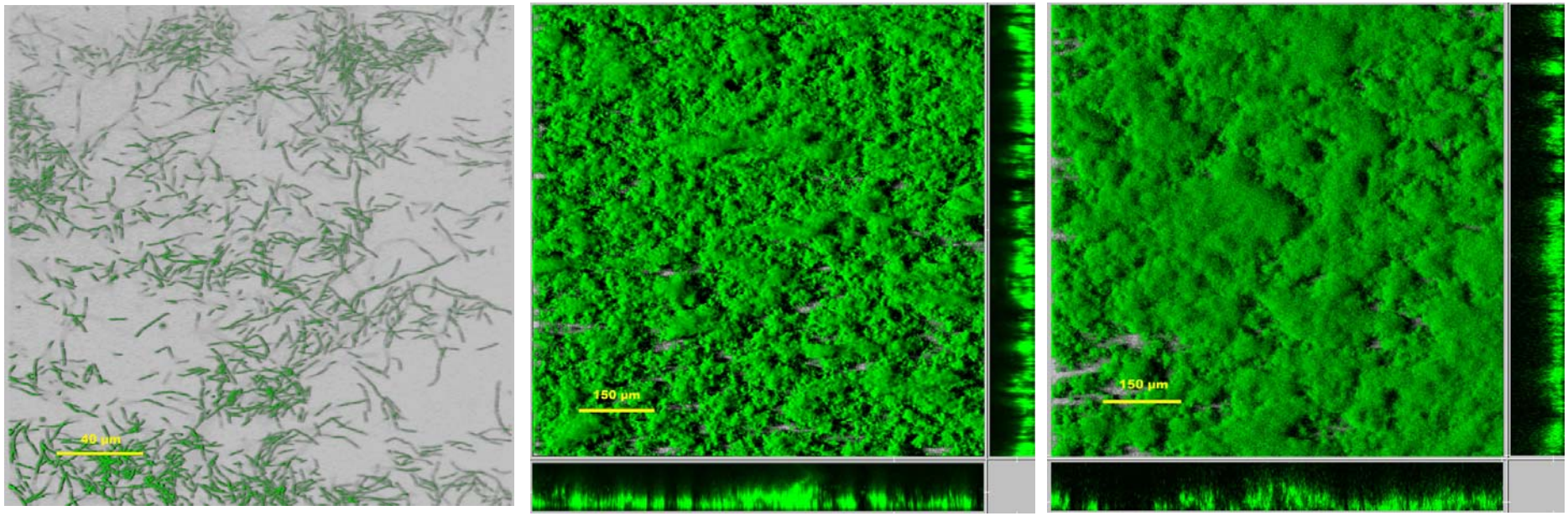

7 hrs 24 hrs 48 hrs

Confocal Laser Scanning Microscopy of *Shewanella oneidensis* Biofilm Formation on a Glass Slide as a Function of Time

(Thormann *et al.*, unpublished)

Comparison of Surface Binding Site Densities for Various Microorganisms, Natural Organic Matter, and Polyacrylic Acid

Type of organic matter	Functional group	Total site concentrations (mol/g , dry weight)
Bacterial cells[16-18,36,37]	carboxylic	3.2×10^{-5} ~1.2×10^{-3}
	phosphoryl	8.9×10^{-6} ~ 8.3×10^{-4}
SRFA[41]	carboxylic	6.1×10^{-3}
	total acidity	10.5×10^{-3}
SRHA[41]	carboxylic	4.9×10^{-3}
	total acidity	9.0×10^{-3}
PAA	carboxylic	1.4×10^{-2}

(Yoon *et al.*, *Langmuir 21*, 4503, 2005)

Comparison of Pb(II) Binding Affinities for Various Microorganisms, Natural Organic Matter, and PAA

Type of organic matter		Stability constant
Cyanobacteria[16]	log K (cell wall)	4.67
	log K (sheath)	5.07
Enterobacteriaceae[17]	$\log K_{carboxyl}$	3.9
	$\log K_{phosphoryl}$	5.0
B. Subtilis[18]	$\log K_{carboxyl}$	4.2
	$\log K_{phosphoryl}$	5.6
B. licheniformis[37]	$\log K_{carboxyl}$	4.7
	$\log K_{phosphoryl}$	5.7
Humic Acid[19]	$\log K_{Pb\text{-}S1}$	3.40
	$\log K_{Pb\text{-}S2}$	8.75
PAA[22]	$\log \beta_{102}$	6.75
PAA[21]	$\log \beta_{102}$	7.00

(Yoon *et al.*, *Langmuir 21*, 4503, 2005)

Heavy Metal Partitioning and Speciation at Biofilm/Mineral Interfaces

(Templeton *et al., Proc. Nat. Acad. Sci. USA 98*, 11897, 2001)

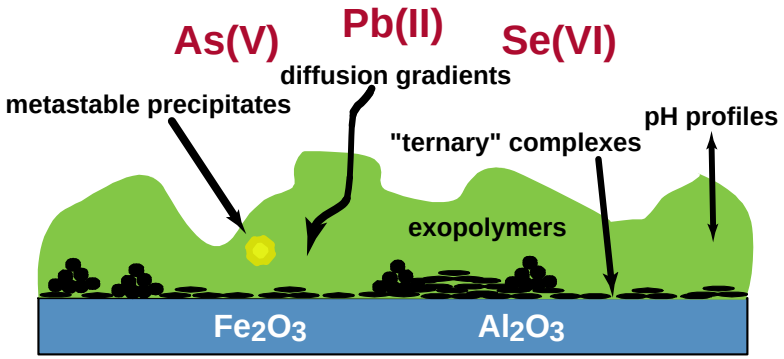

X-ray standing waves are well suited for determining the position of atoms at complex interfaces such as these

Vertical (z) Position of Metal Ion

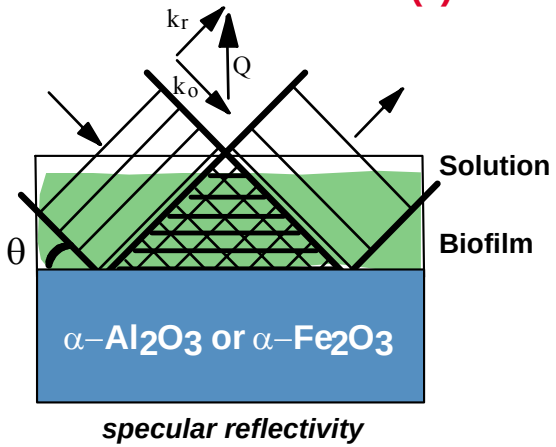

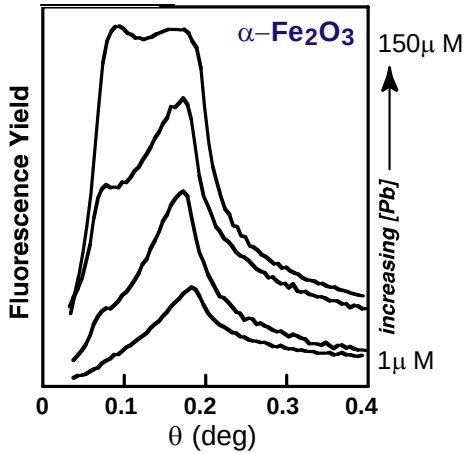

Grazing-incidence XAFS provides complementary information on the types of species present at both the interface and in the biofilm

Speciation in Biofilm *vs.* on Mineral Surface

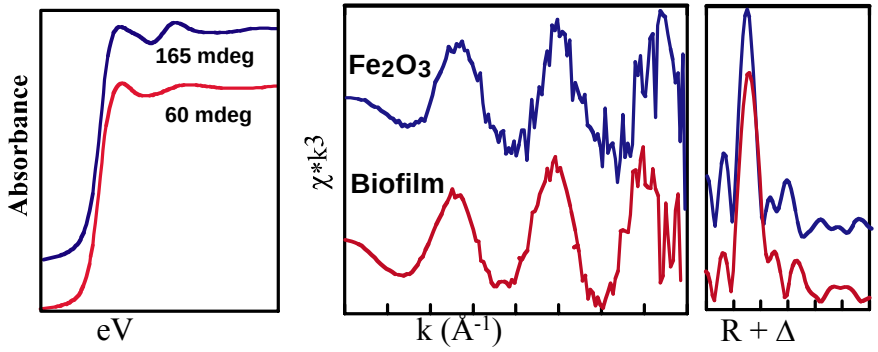

(SSRL)

Grazing-Incidence Apparatus and Array Detector on SSRL BL 11-2
Used for XSW and XAFS Measurements on Biofilm-Coated Metal Oxides

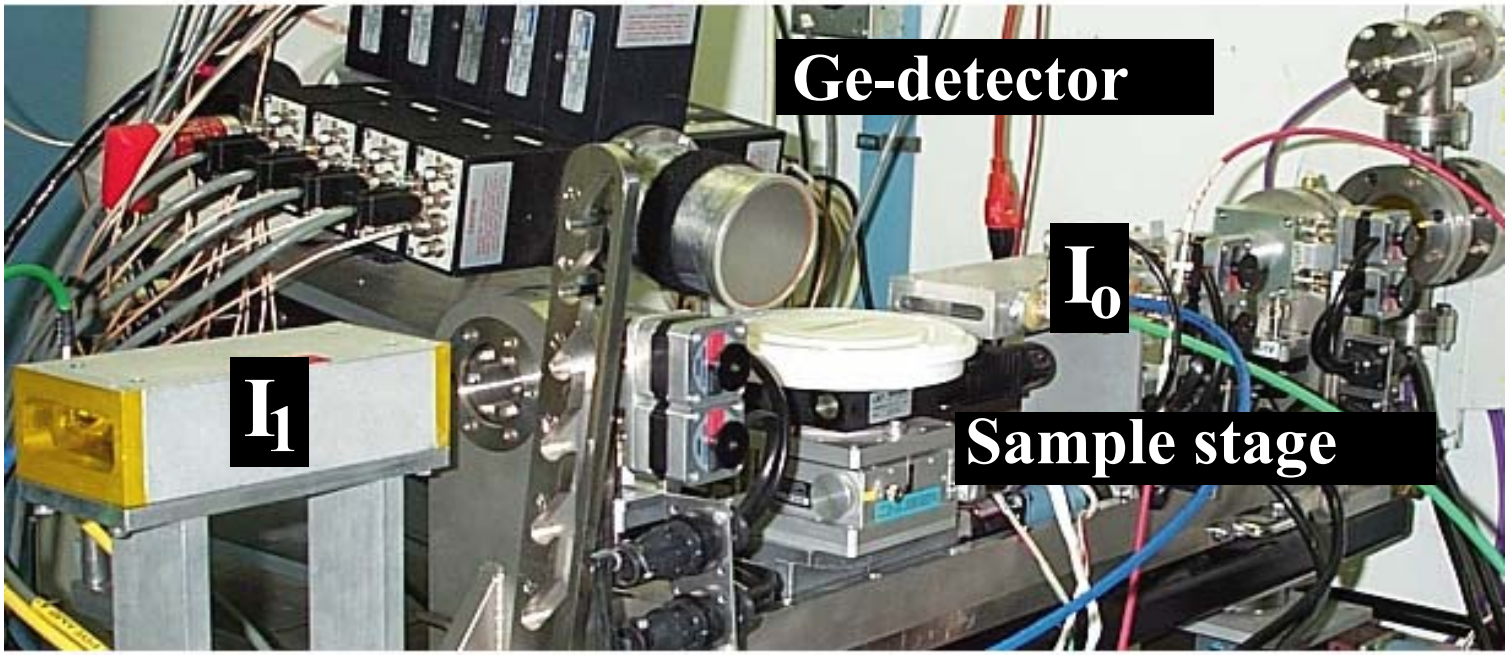

XSW Spectra of Pb(II) at Metal Oxide/Biofilm Interfaces

(Templeton *et al., Proc. Nat. Acad. Sci. USA 98*, 11897, 2001)

B. cepacia biofilms

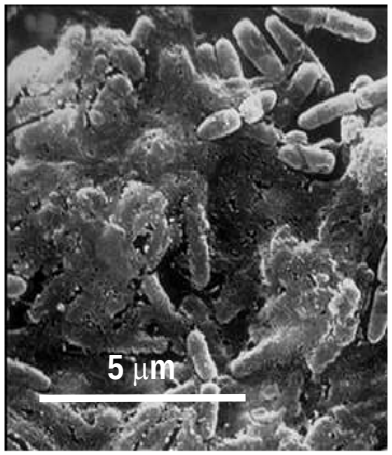

X-ray standing waves

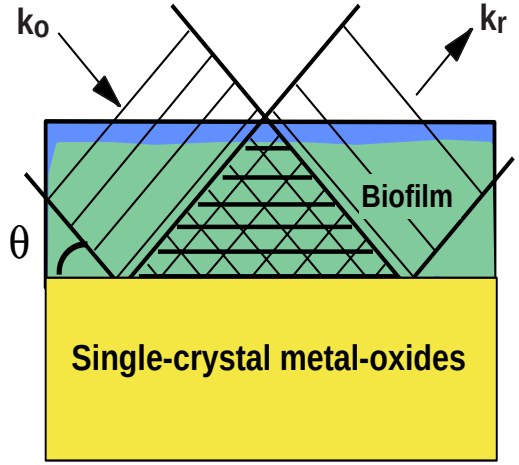

Vertical Metal(oid) distributions

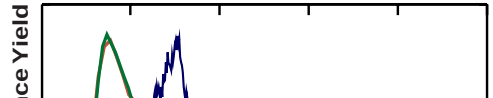

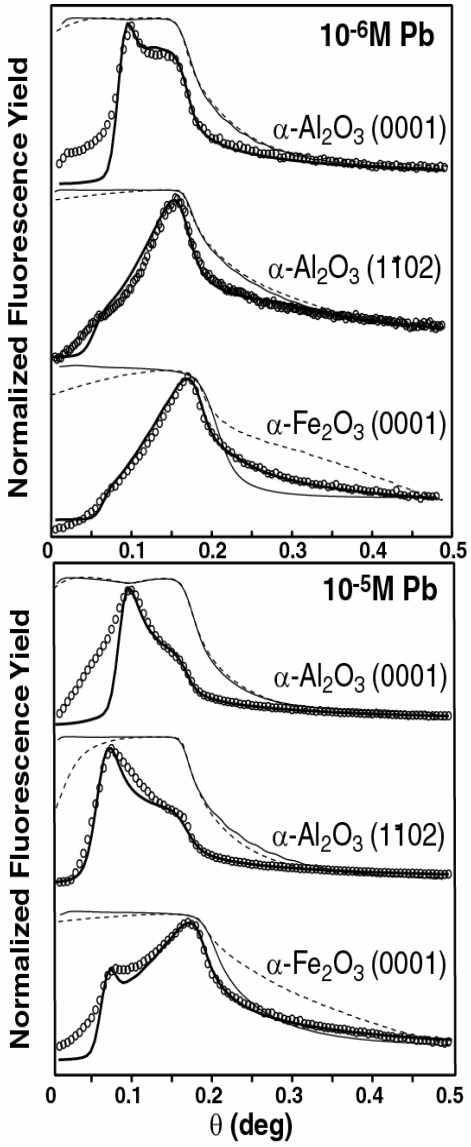

These XSW data show that Pb at 10^{-6} M occurs at the mineral/biofilm interface for the α-Fe_2O_3(0001) and α-Al_2O_3 (1-102) surfaces. Pb occurs mainly in biofilm for the α-Al_2O_3 (0001) surface.

For Pb ≤ 10^{-5} M, Pb occurs mainly in the biofilm for the alumina samples and ispartitioned between the surface and biofilm for the Fe_2O_3 (0001) sample.

These results indicate that the intrinsic differences in reacti-vity of these surfaces are notaffected by the biofilm coating.

(SSRL)

Comparison of XSW FY-Results for Pb^{2+}/B. cepacia/M_2O_3

(Templeton *et al.*, *Proc. Nat. Acad. Sci. USA 98*, 11897, 2001)

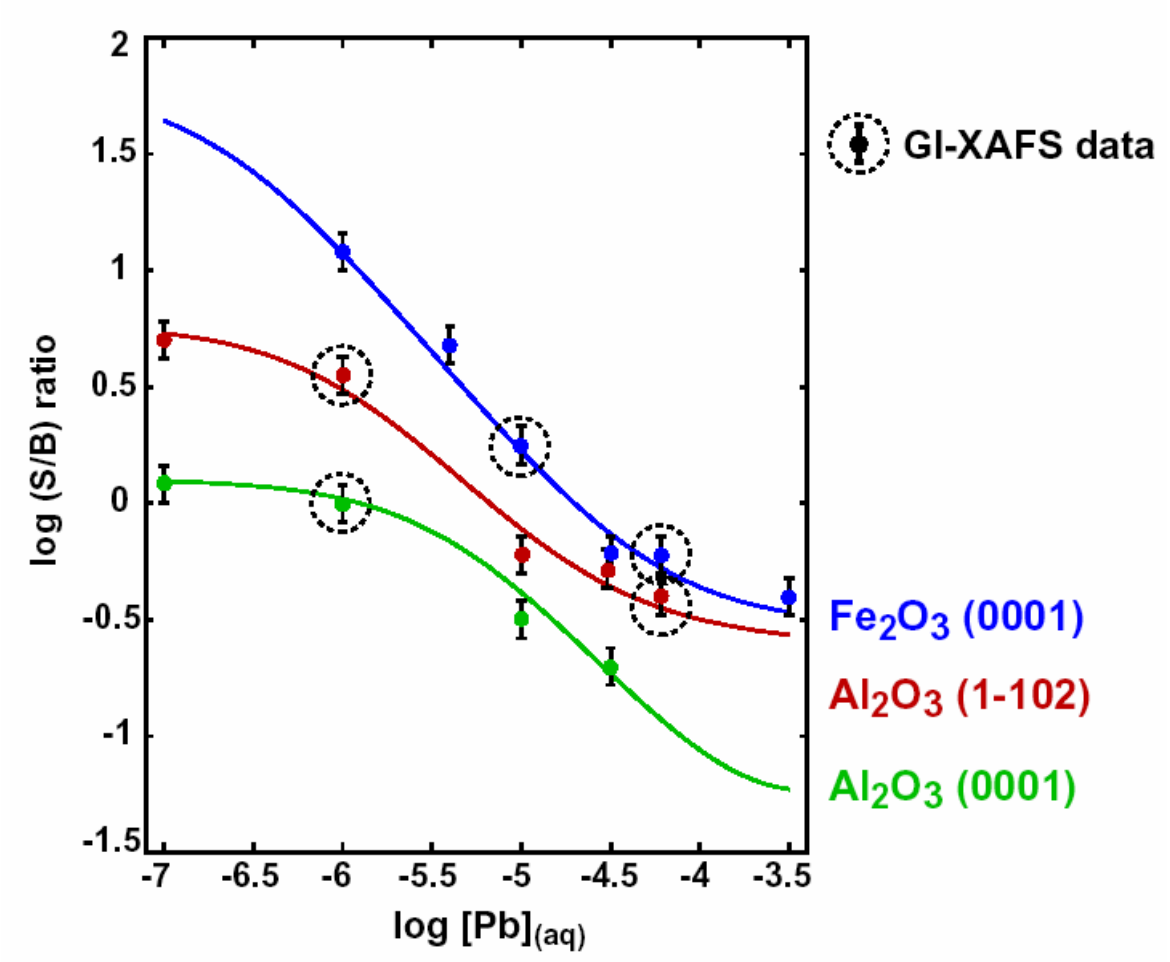

Order of Reactivity for Pb(II) Adsorption on Al- and Fe-oxide Surfaces Coated by Microbial Biofilm in Contact with Aqueous Solution

α-Fe_2O_3(0001) > α-Al_2O_3(1-102) >> α-Al_2O_3(0001)

SEM, Optical, and X-ray Microprobe Maps and GI-EXAFS Spectra of B. cepacia/α-Al_2O_3 after Reaction with $10^{-4.2}$M Pb(II)*

(Templeton *et al.*, *Environ. Sci. Technol. 37*, 300, 2003)

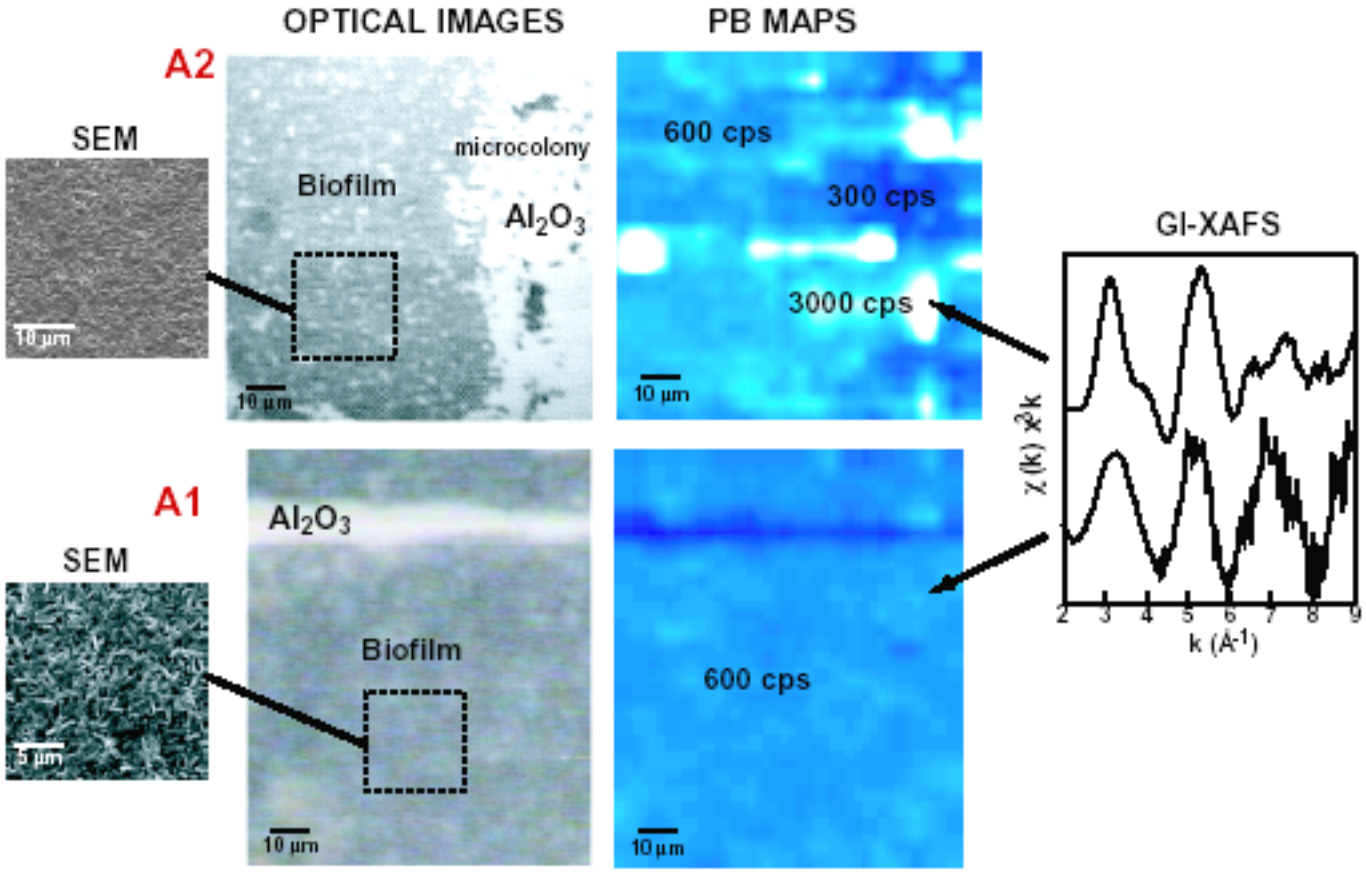

***X-ray spot size was 5x5 µm. Data taken at APS on ID-13.**

(APS)

Crystal Truncation Rod Diffraction Studies of Surface Structure Under Hydrous Conditions: Understanding Reactivity Differences at Different Metal Oxide/Aqueous Solution Interfaces

Possible Adsorption Sites on the α-Al_2O_3 (0001) and (1-102) Surfaces

(Towle *et al.*, *J. Colloid Interface Sci. 217*, 312, 1999)

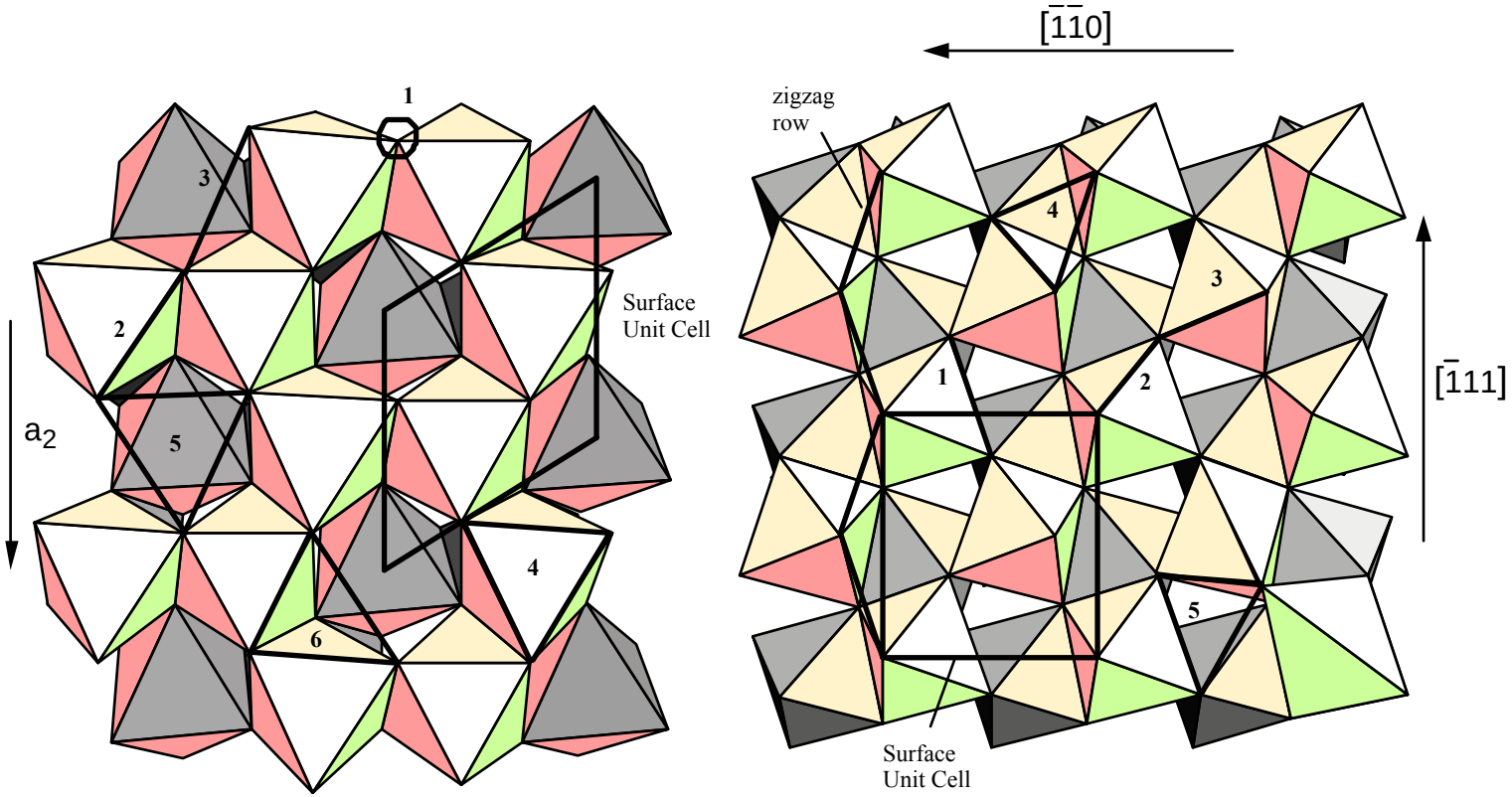

A. α-Al_2O_3 (0001)

B. α-Al_2O_3 ($1\bar{1}02$)

Surface Diffraction Studies of Hydrated Metal Oxides

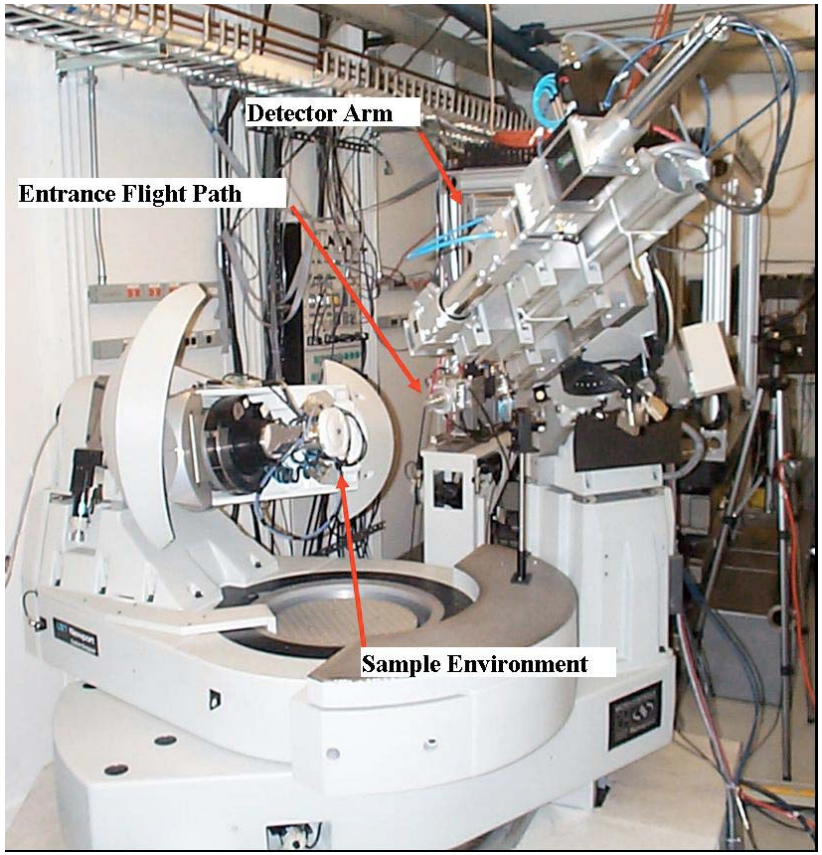

GSECARS Kappa diffractometer on BL 13-ID-C at the APS used for crystal truncation rod diffraction studies of hydrated metal oxide surfaces

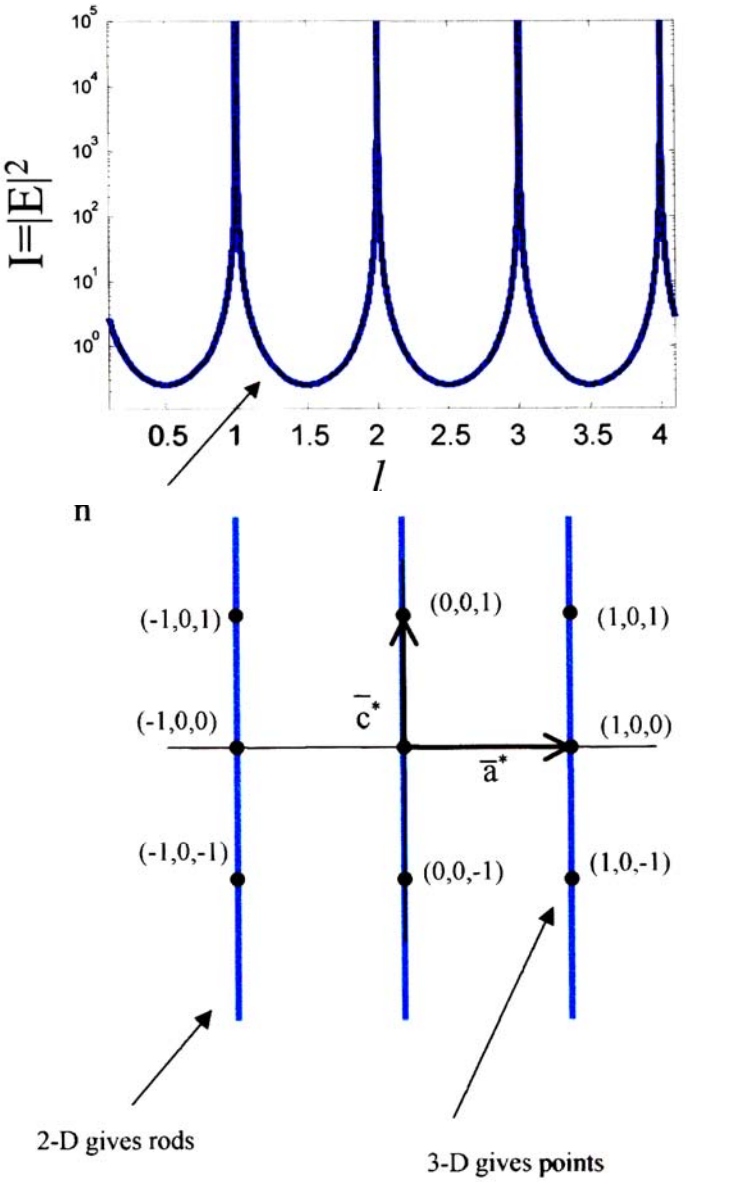

(I.K. Robinson, *Phys. Rev. B 33*, 3830, 1986)
(G. Renaud, *Surf. Sci. Rep. 32*, 1, 1998)

Crystal Truncation Rod Diffraction Study of the Hydrated Al_2O_3 (0001) Surface

(Eng *et al.*, *Science 288,* 1029, 2000)

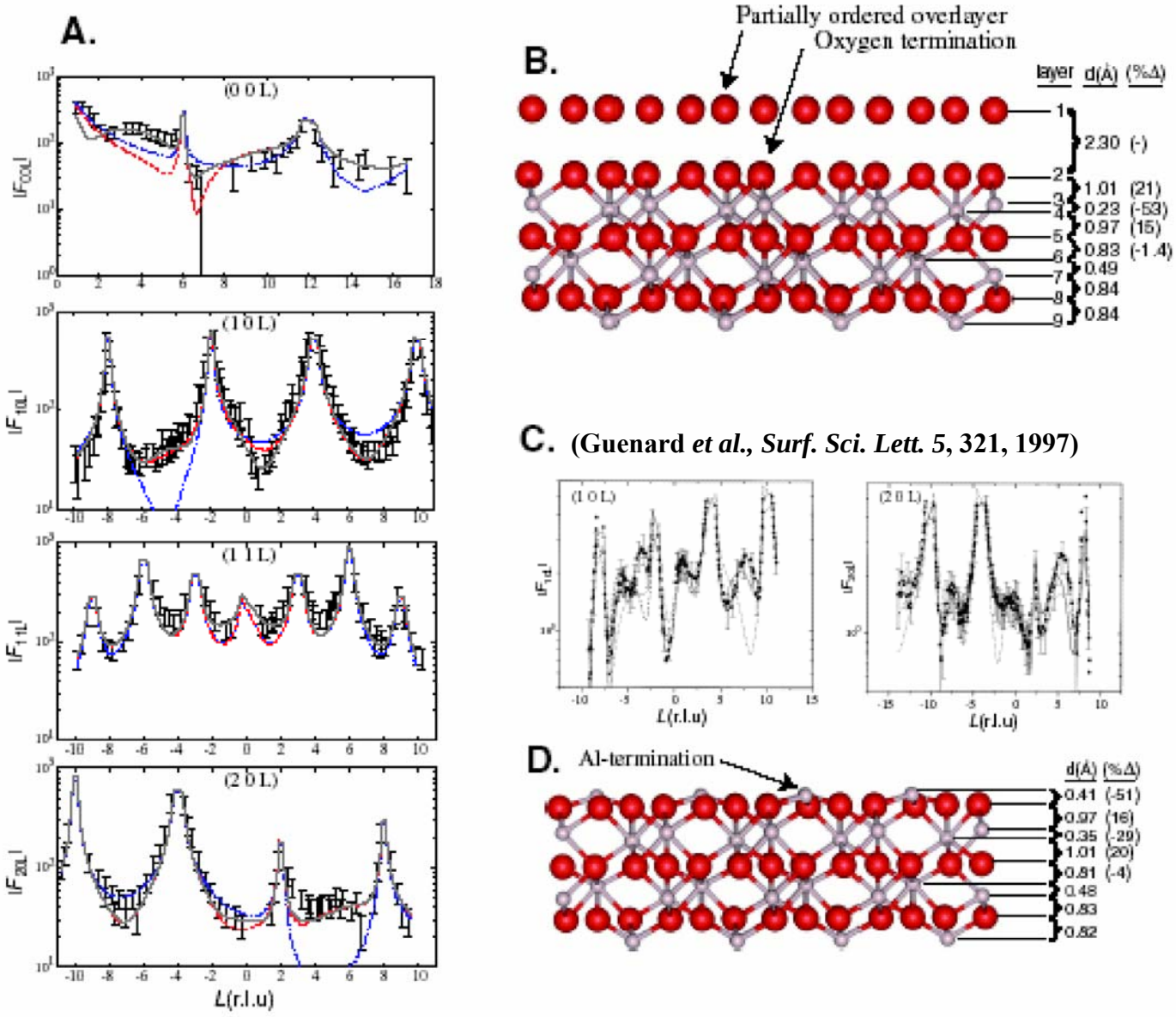

Crystal Truncation Rod Diffraction Study of the Hydrated α-Fe_2O_3(0001) Surface

(Trainor *et al.*, *Surf. Sci. 573*, 204, 2004)

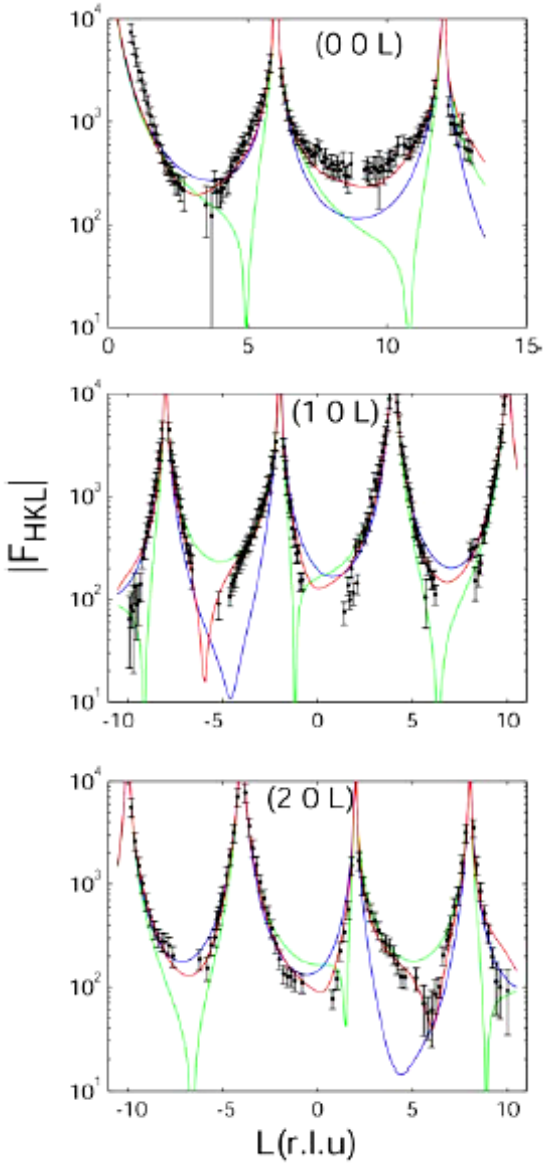

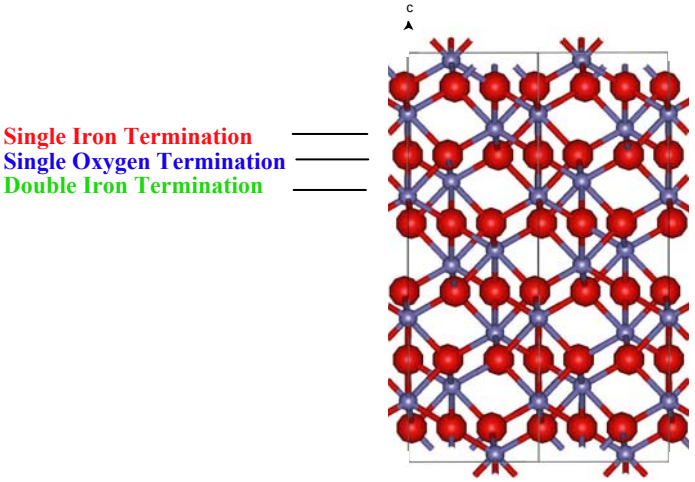

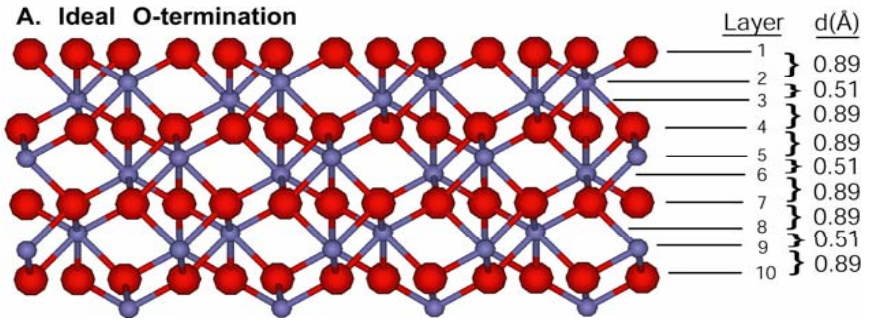

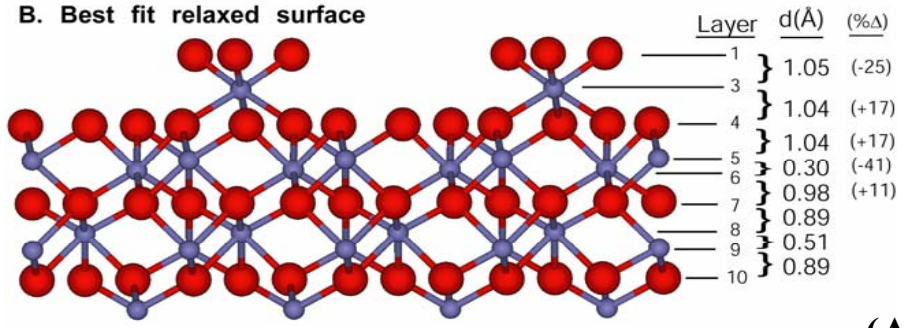

(APS)

Analysis of Multi-Domain Hematite Surfaces

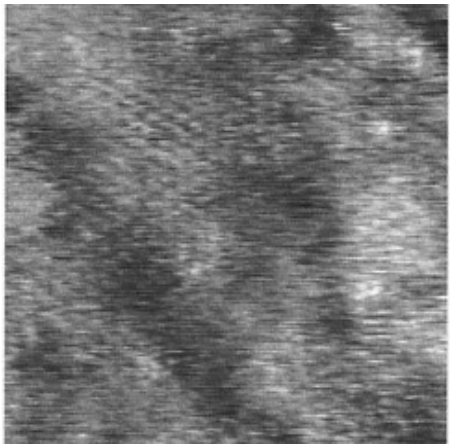

20 nm x 20 nm STM image of α-Fe_2O_3 (0001) in water.

(Eggleston *et al. Geochim. Cosmochim. Acta* 67, 985, 2003)

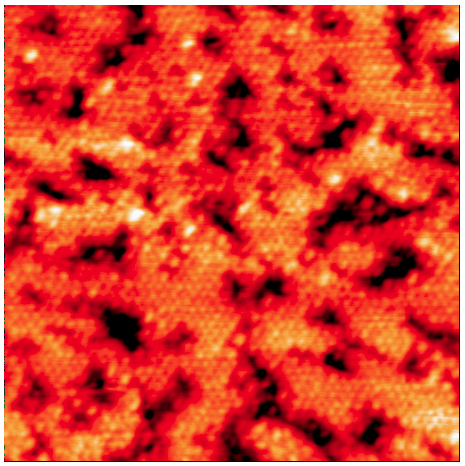

30 nm x 30 nm STM image of α-Fe_2O_3 (0001) prepared at 10^{-2} mbar O_2.

(Lemire *et al.*, *Phys. Rev. Lett.* 94, 166101, 2005)

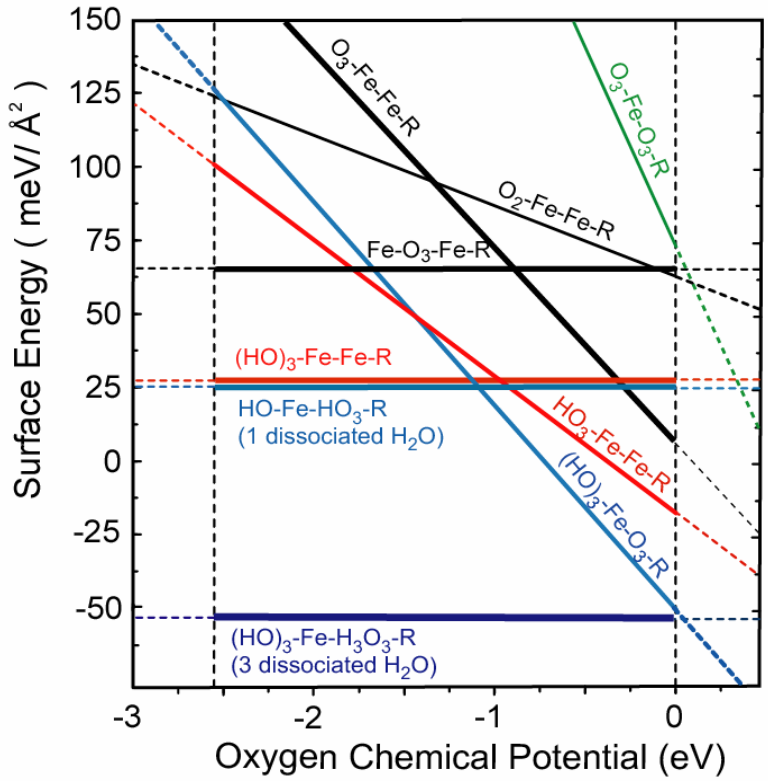

- **Calculated surface energies in equilibrium with water vapor.**
- **Predict lowest energy stoichiometry and structure (relaxations) for direct comparison with experiment.**
- **Best fit to CTR data based on linear combination of theory models:**

~1/3 $(HO)_3$-Fe-H_3O_3-R

~2/3 $(HO)_3$-Fe-Fe-R

(Trainor *et al., Surf. Sci. 573*, 204, 2004)

Structural Models of Hydrated Al- and Fe-Oxide Surfaces

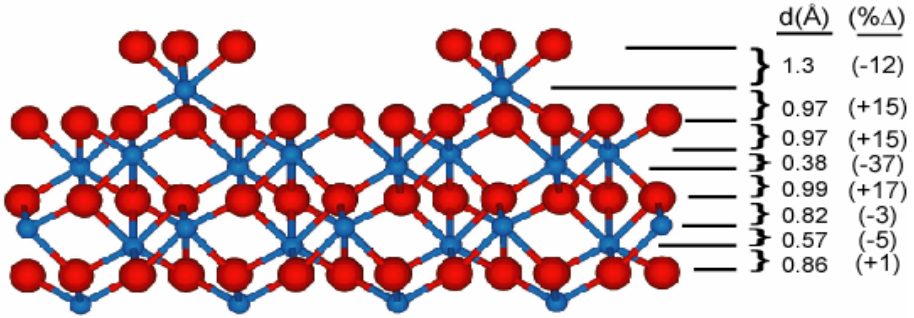

α-Fe_2O_3 (0001)

(Trainor *et al.*, *Surf. Sci. 573*, 204, 2004)

Gibbsite, γ-$Al(OH)_3$

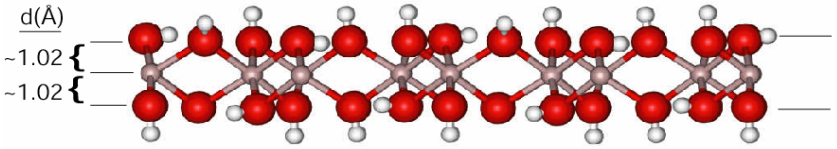

α-Al_2O_3 (0001)

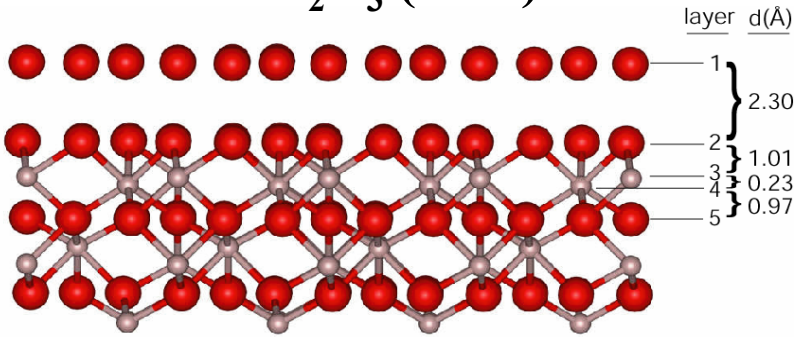

(Eng *et al.*, *Science 288,* 1029, 2000)

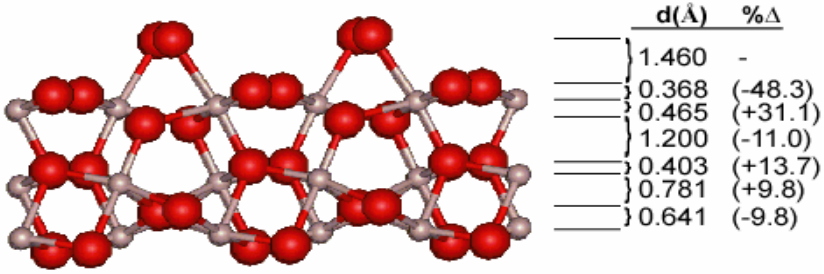

(Trainor *et al.*, *Surf. Sci. 496,* 238, 2002)

α-Al_2O_3 (1-102)

and

α-Fe_2O_3 (1-102)

(Trainor *et al.*, 2005, in preparation)

Applications of Microbeam and Spectromicroscopy Synchrotron Radiation Methods to Environmental Problems

X-ray Microprobes in the U.S.

Beam Line	Source	Energy Range (KeV)	Microbeam Apparatus	Beam Size	Flux (ph/s 0.01% BW)
NSLS (X26A)	Bend Magnet (2.8 GeV)	5 - 15	KB mirrors	10 μm	2×10^{8}
APS (13-ID)	Undulator (7 GeV)	6 - 45	KB mirrors	1 μm	4×10^{11}
APS (20-ID)	Undulator (7 GeV)	6 - 45	KB mirrors	1 μm	4×10^{11}
APS(2-ID)	Undulator (7 GeV)	4 - 20	Zone plate	0.l μm	1×10^{8}
ALS (10.3.2)	Bend Magnet (1.9 GeV)	5 - 12	KB mirrors	5 μm	3×10^{9}

Scanning Transmission X-ray Microscopes in the U.S.

NSLS (X1A1)	Bend Magnet (2.8 GeV)	0.25 - 0.50	Zone plate	30 nm	1×10^{8}
NSLS (X1A2)	Bend Magnet (2.8 GeV)	0.25 - 1.00	Zone plate	30 nm	1×10^{8}
ALS (5.3.2)	Bend Magnet (1.9 GeV)	0.25 - 0.70	Zone plate	40 nm	1×10^{7}
ALS (11.0.2)	Ellip. Undulator (1.9 GeV)	0.13 - 2.20	Zone plate	30 nm	2×10^{9}

X-ray Fluorescence Microprobe
BL X26A, NSLS

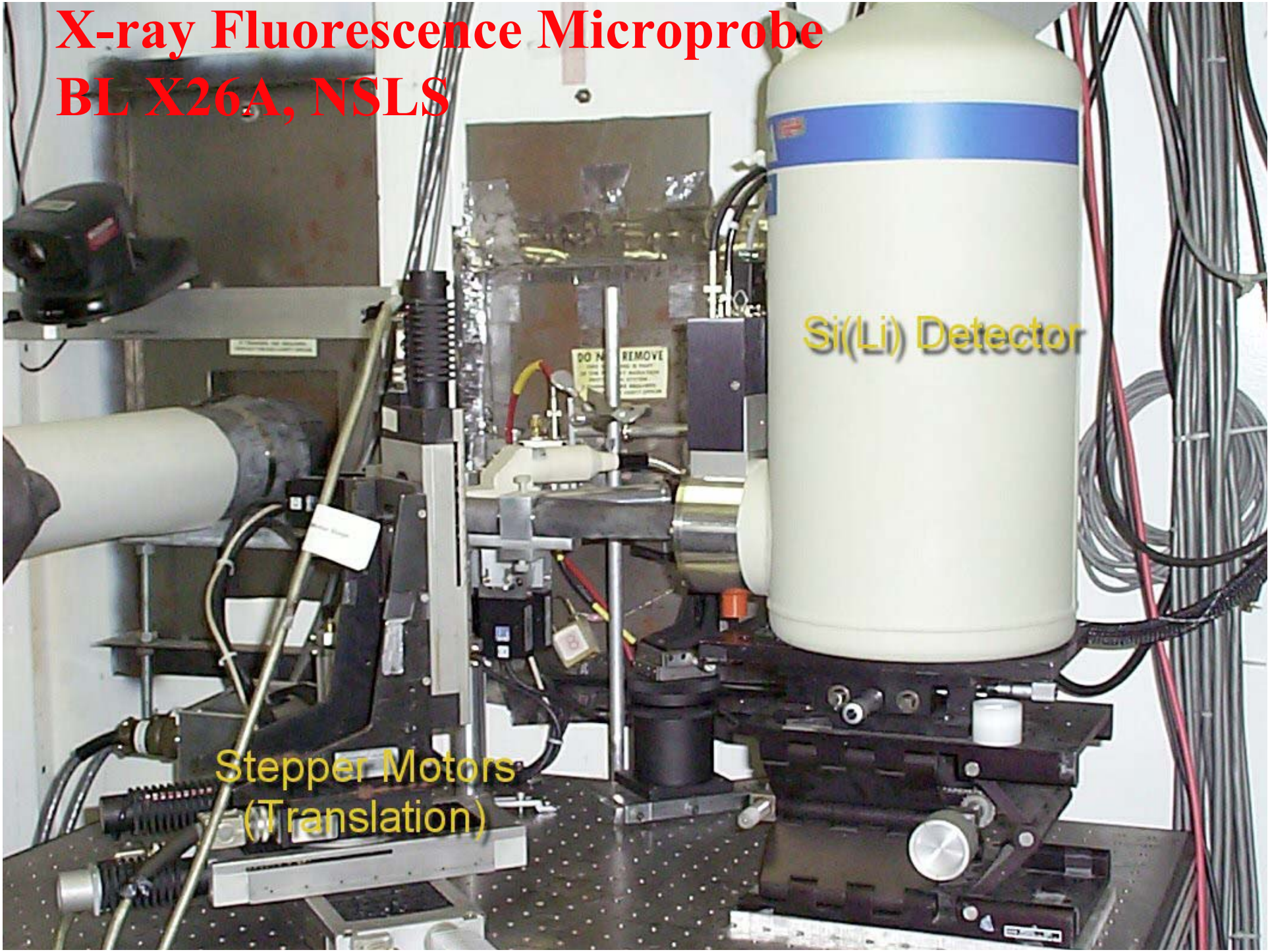

Pu Sorbed on Smectite Grains in Yucca Mountain Tuff

(Duff *et al.*, *Environ. Sci. Technol. 33*, 2163-2169, 1999)

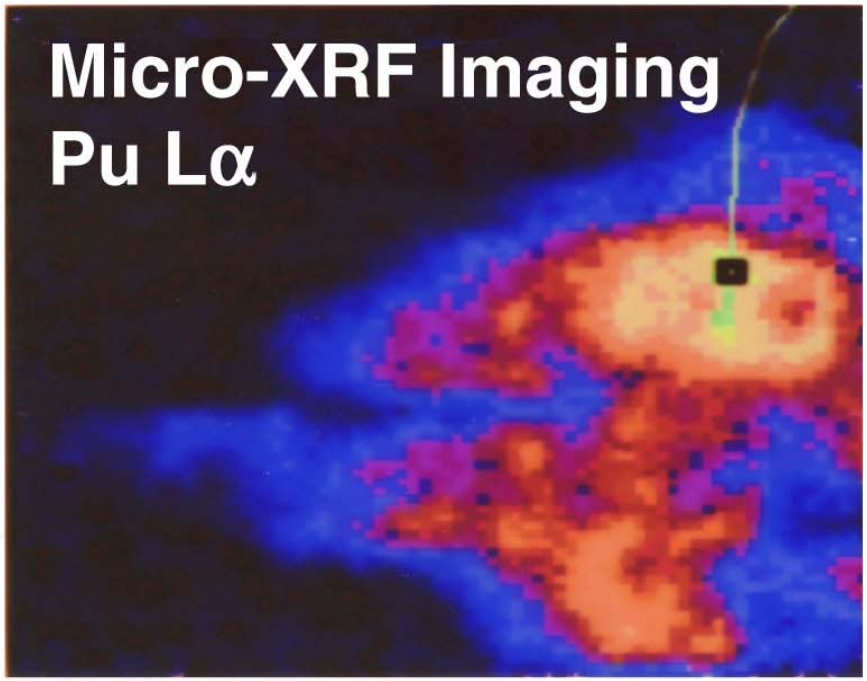

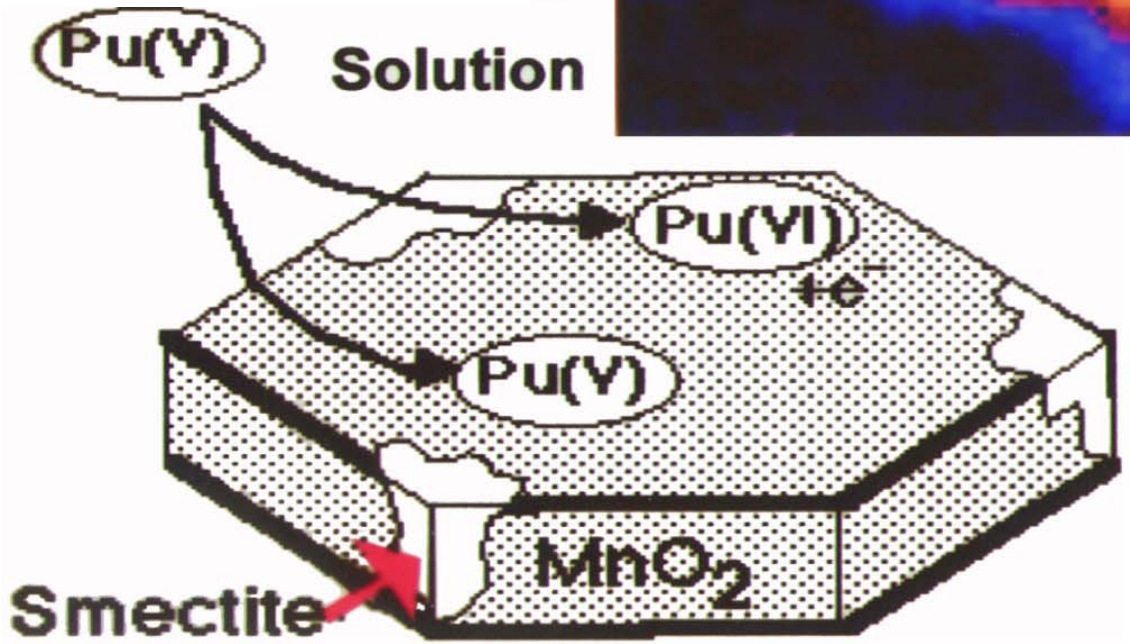

Formation of ZnS Nanoparticles in Natural Biofilms of the Sulfate-Reducing Bacterium Desulfobacteriaceae in a Flooded Pb-Zn Mine

(Labrenz *et al.*, *Science 290*, 1744, 2000)

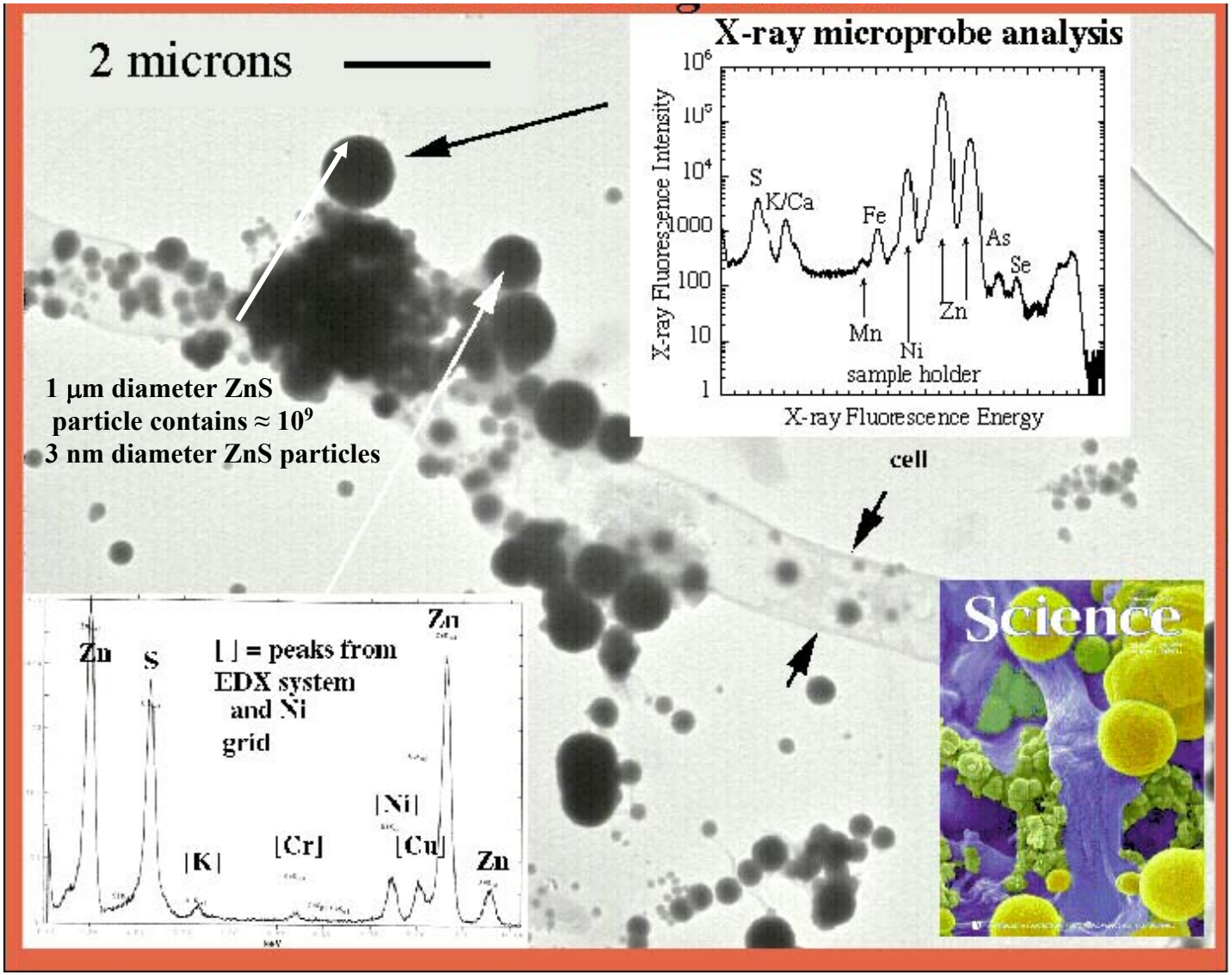

Speciation and Transformation of Se(VI) and Cr(VI) in Aquatic Fern Roots (Salvinia rotundifolia)

(Hunter *et al.*, *J. Phys. IV 7*, 767, 1997)

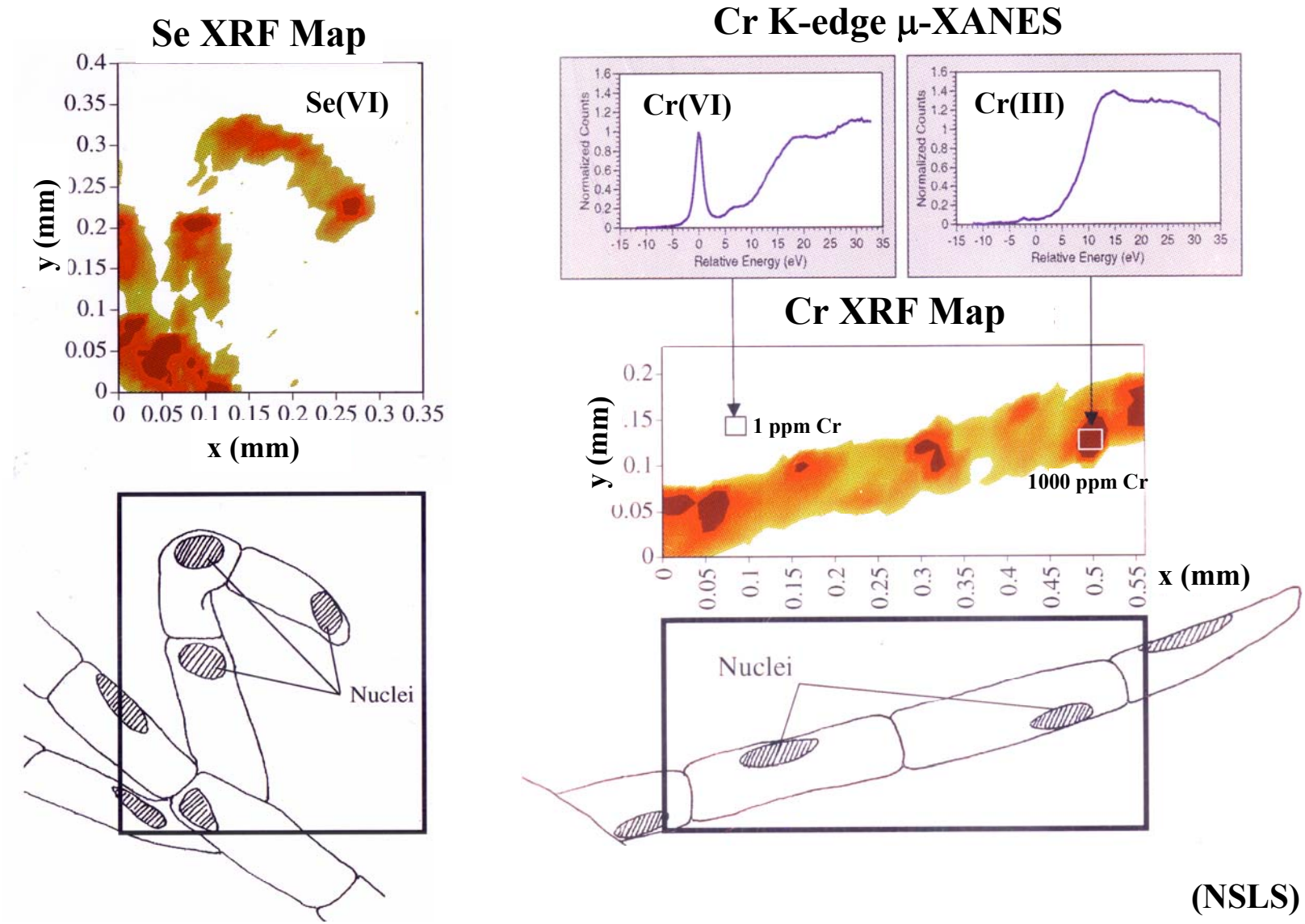

(NSLS)

Schematic Illustration of Fluorescence Computed Microtomography

(Sutton *et al.*, *Rev. Mineral. 49*, xxx, 2002)

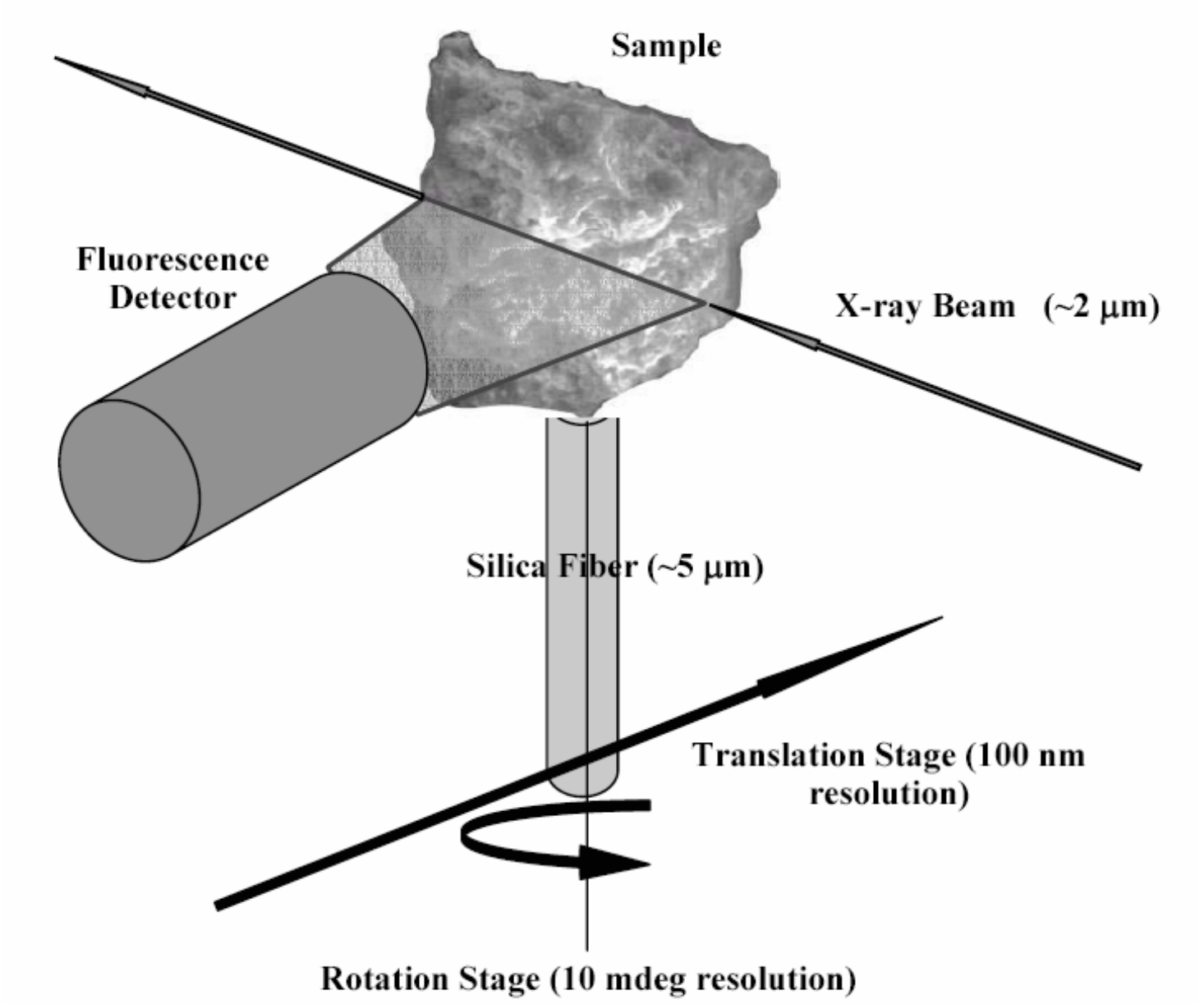

X-ray fluorescence μ-tomographic images of the distribution of metals on and within a grass root (Phalaris arundinacea)

(Hansel *et al.*, *Environ. Sci. Technol. 35*, 3863, 2001)

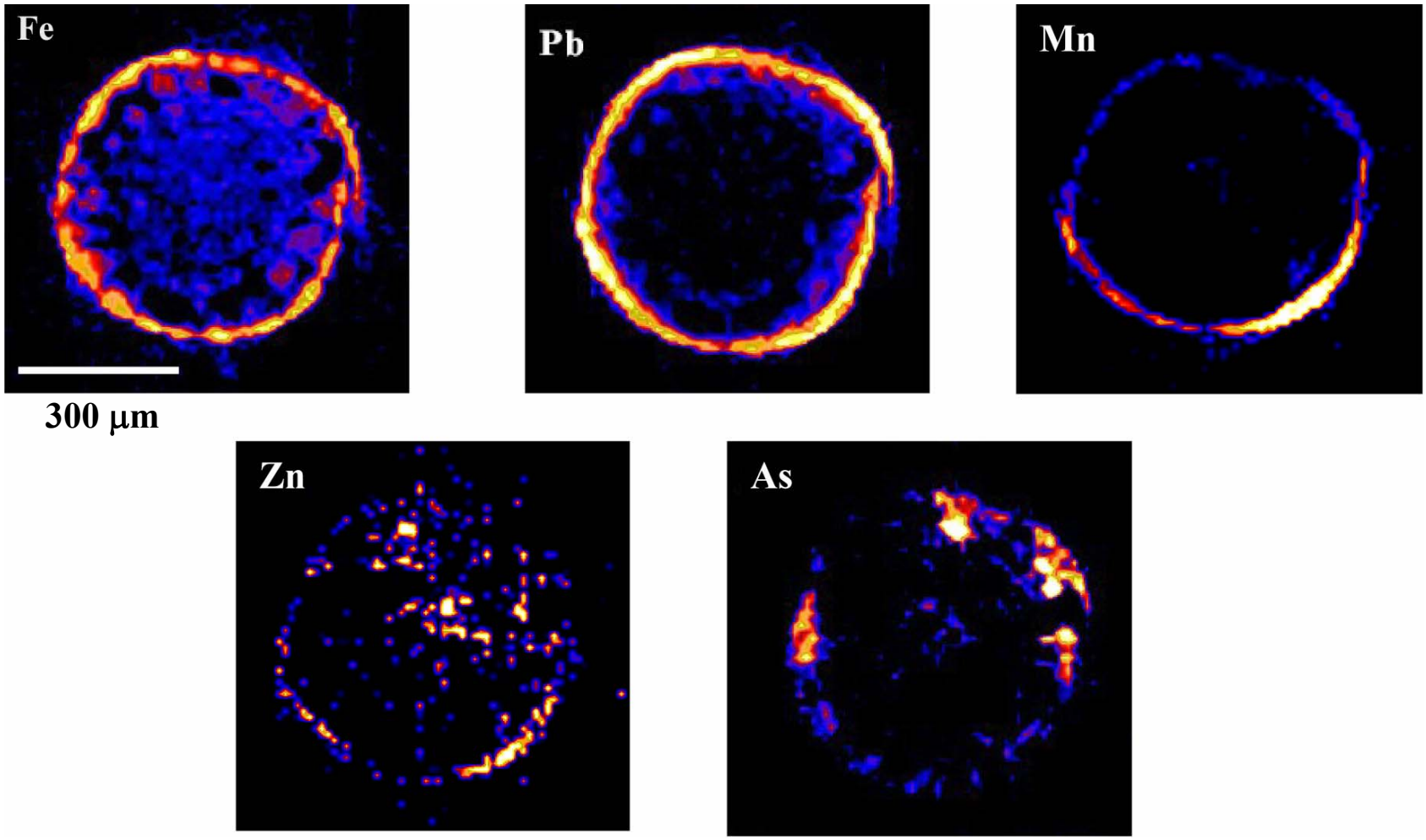

(APS & SSRL)

Soil Nodule Elemental (μXRF) Maps

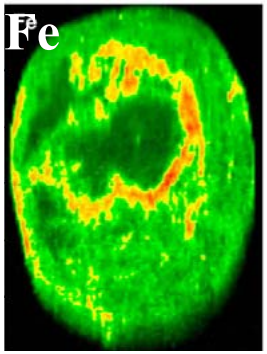

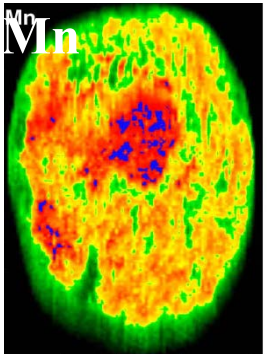

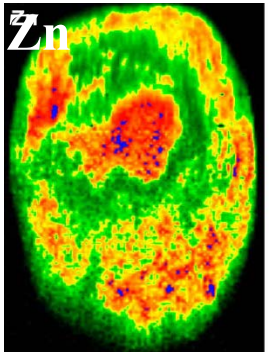

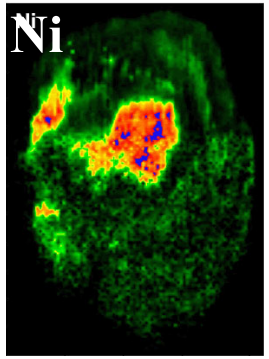

Soil Nodule Mineral Species (μXRD) Maps

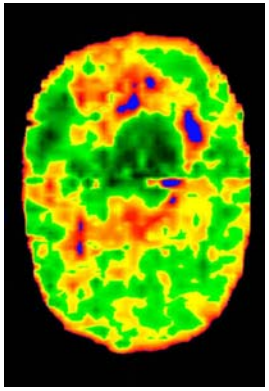

4.19 Å

Goethite (α-FeOOH)

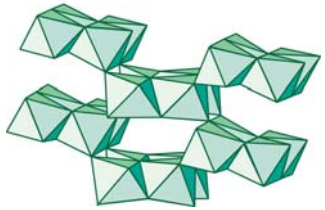

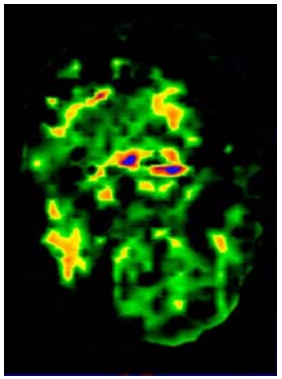

7.1 Å

Hexagonal birnessite

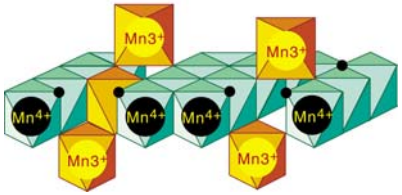

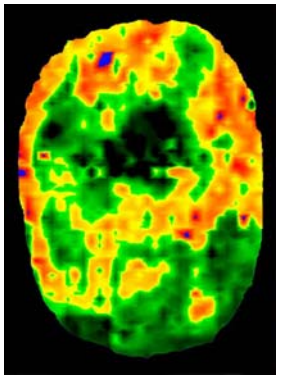

2.57 Å

2:1 phyllosilicate

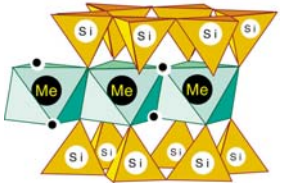

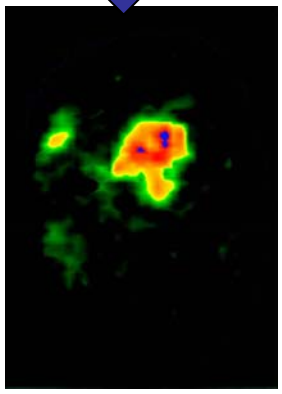

9.4 Å

Lithiophorite

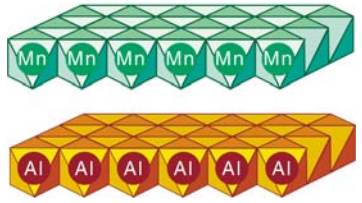

(Manceau *et al.*, *Am. Mineral. 87*, 1494, 2002)

(ALS)

Applications of STXM to MES: Organic Acids, Microbes, Colloids, Bioweathering, and Biomineralization

Transmission X-ray Microscope

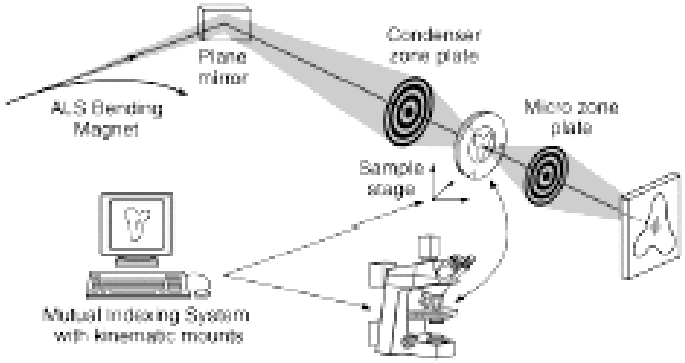

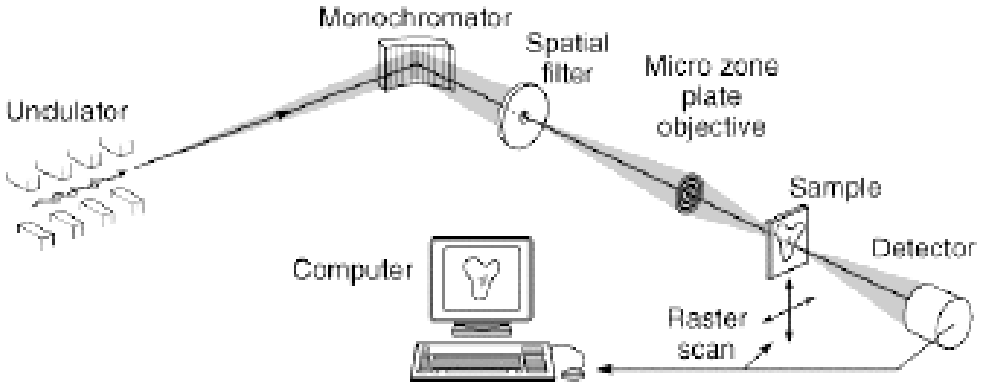

Scanning Transmission X-ray Microscope

(20-40 nm spot size)

ALS Molecular Environmental Science Beam Line 11.0.2

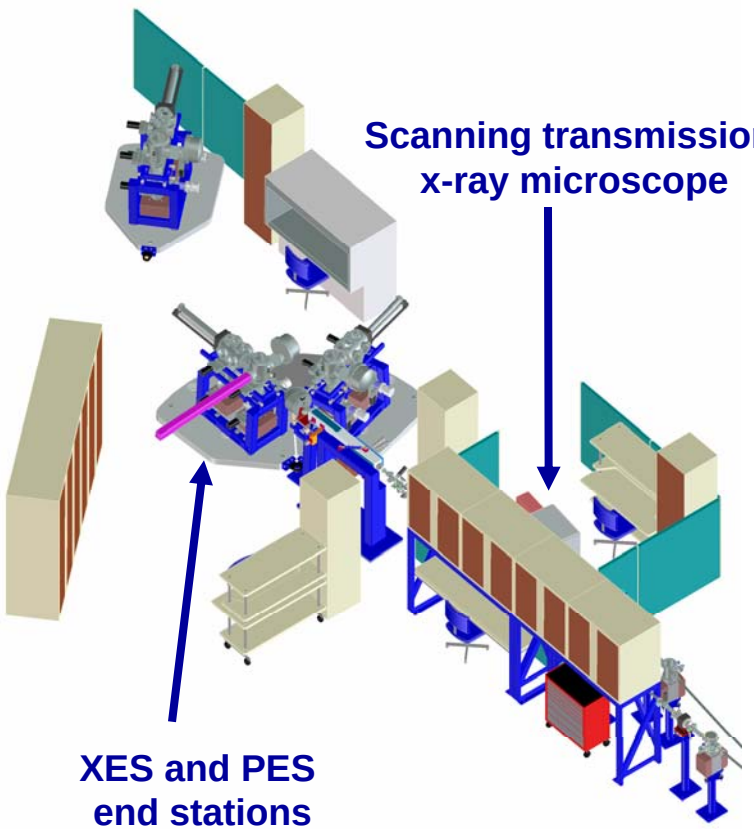

STXM= Scanning Transmission X-ray Microscopy

Advanced Light Source, LBNL, beam station 11.0.2.2

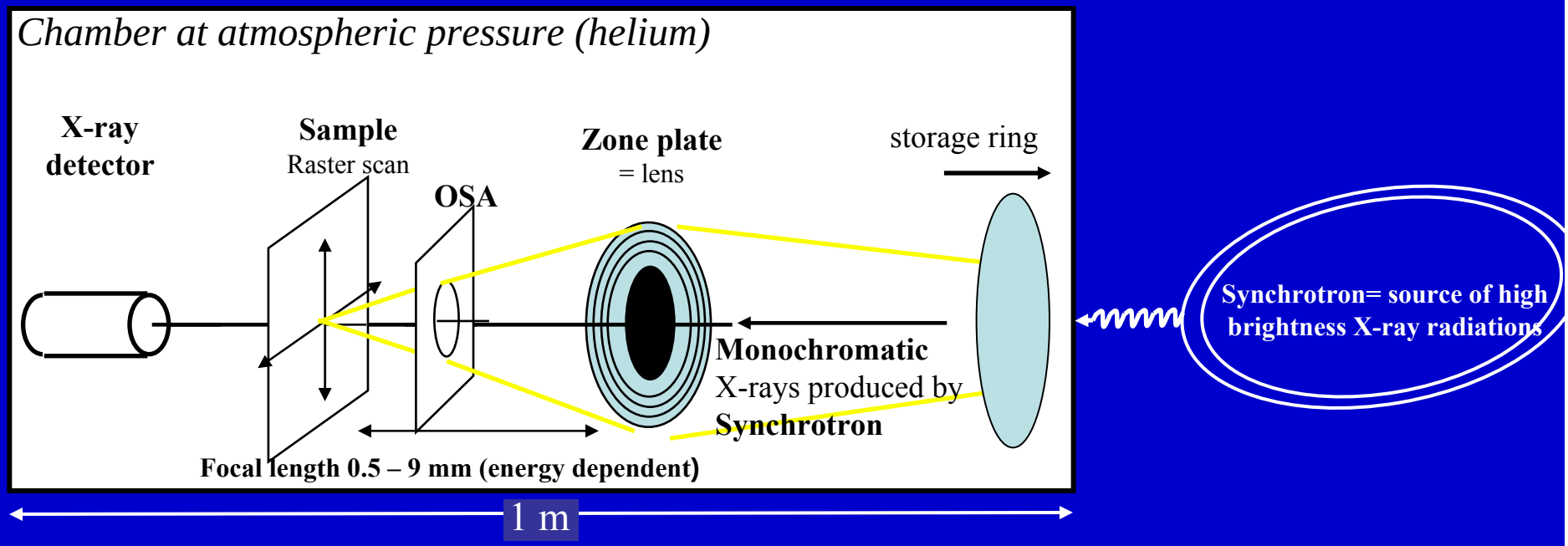

- Transmission microscopy
- Spatial Resol: ~25 nm
- Spectral Resol: <0.1 eV
- Photon flux: 10^9 ph/s (full spatial resolution & energy resolving power > 3000)

⟹

- Energy Range 130 - 2200 eV
- Energy-filtered Imaging
- Chemical Mapping
- X-ray spectroscopy (NEXAFS)

Penetration of Soft X-rays through Water and Soft Matter

(from Jacobsen and Kirz - http://xray1.physics.sunysb.edu/research/intro.php)

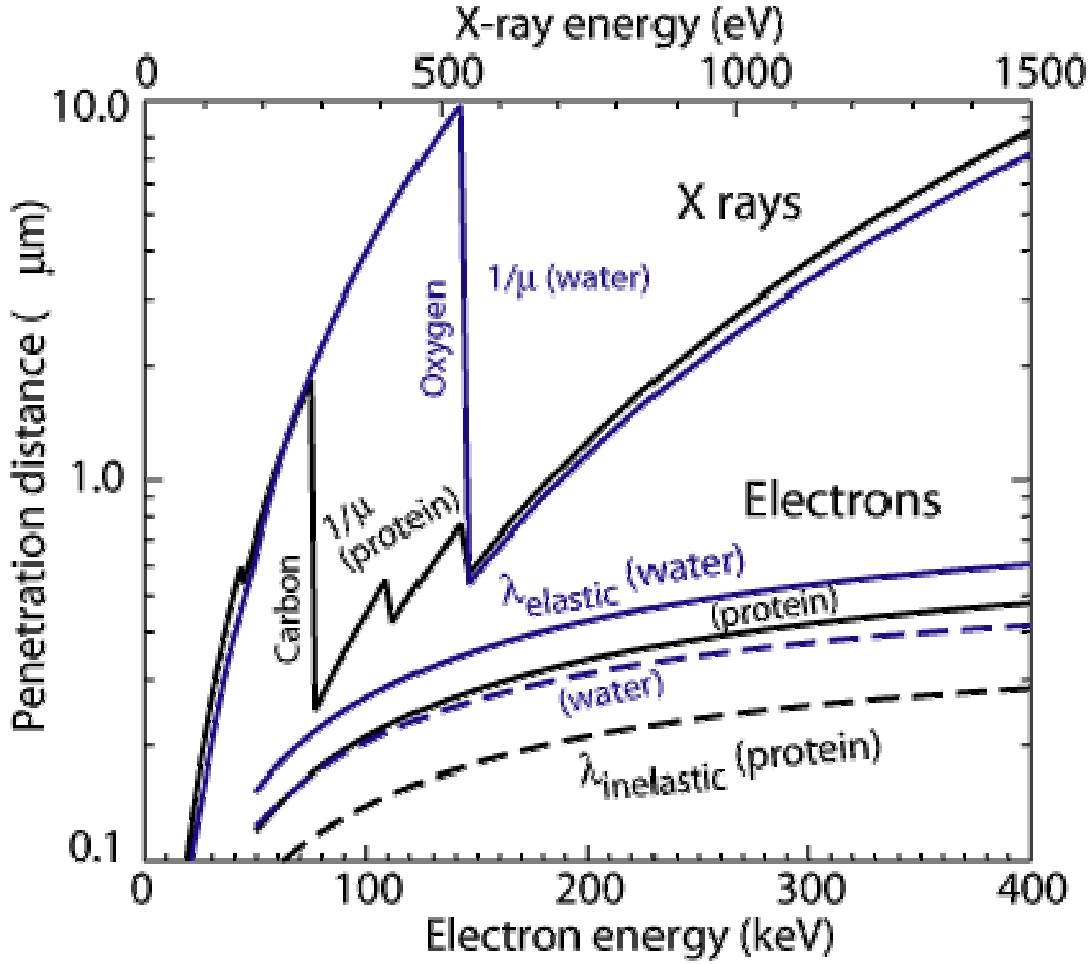

The "water window" between the carbon and oxygen K-edges permits good contrast to be achieved in imaging organic matter in water.

X-ray transmission microscope images at the C K-edge of Suwannee River fulvic acid in aqueous solution at a function of pH and ionic strength

(Myneni *et al.*, *Science 286*, 1335, 1999)

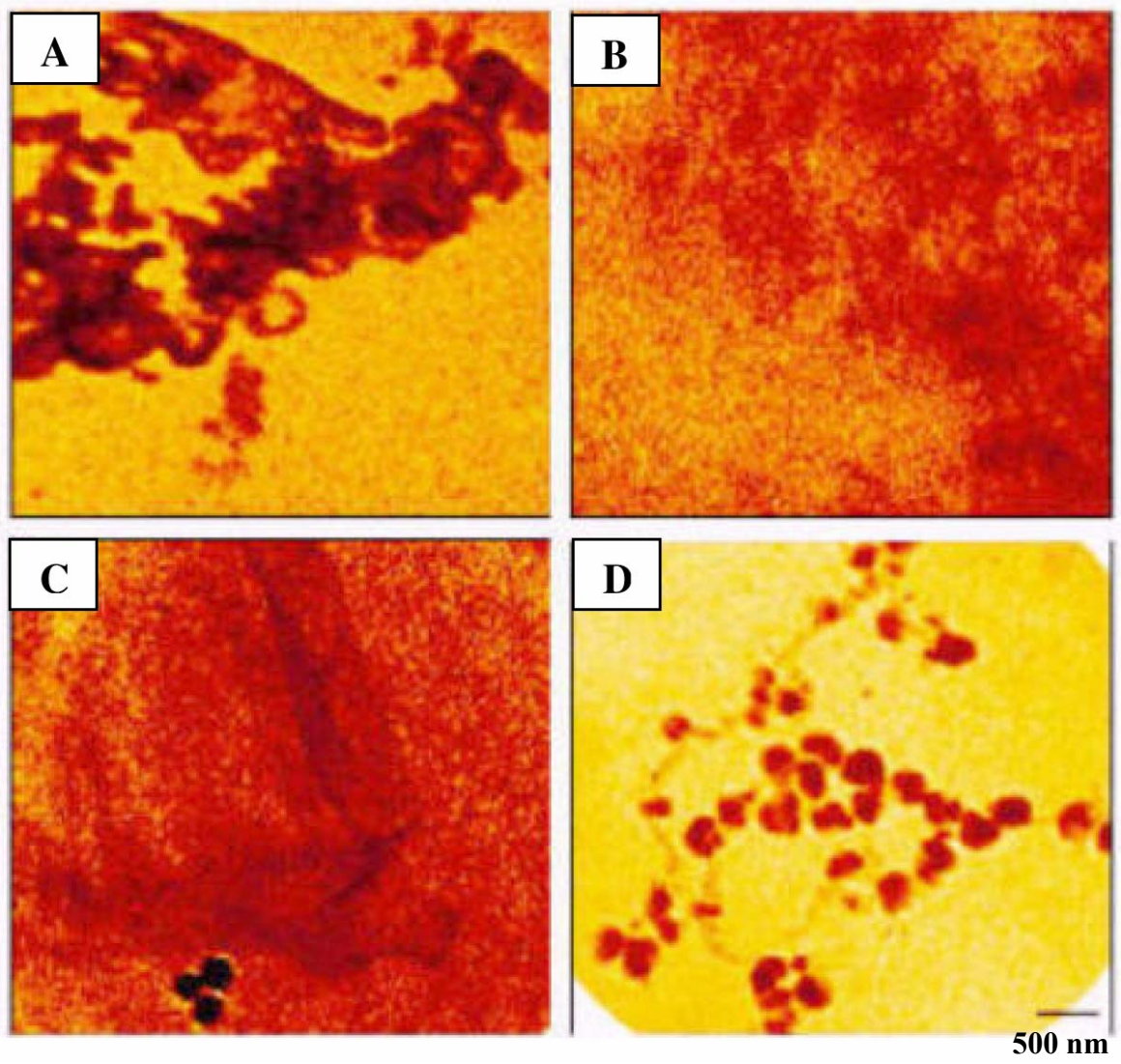

pH 3.0

pH 9.0

pH 4.0

$[Ca^{2+}]$ = 0.018 M

pH 4.0

$[Fe^{3+}]$ = 0.001 M

Cr(VI) Interactions with Microorganisms - A Soft X-ray Spectromicroscopy Approach Using STXM

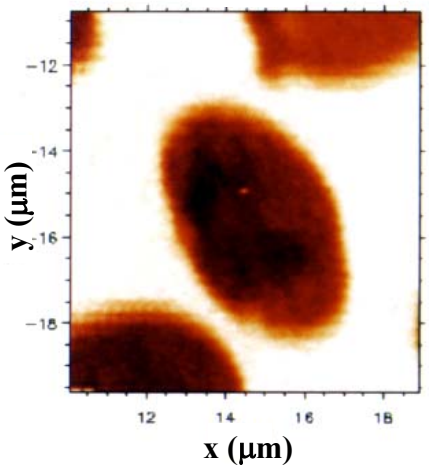

Before Reaction

C K-edge XANES

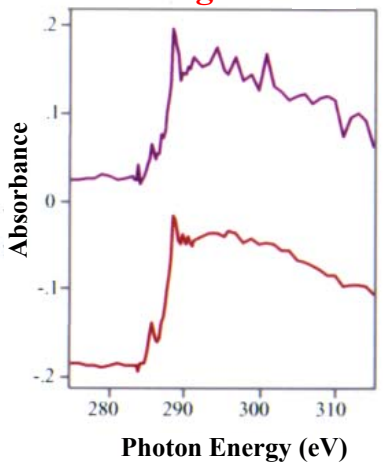

O K-edge XANES

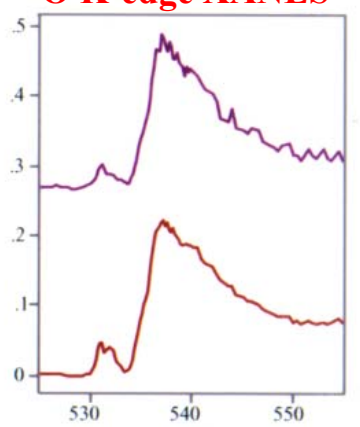

After Reaction

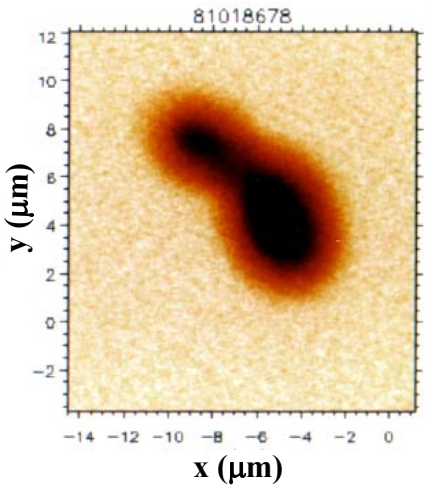

Cr L-edge XANES

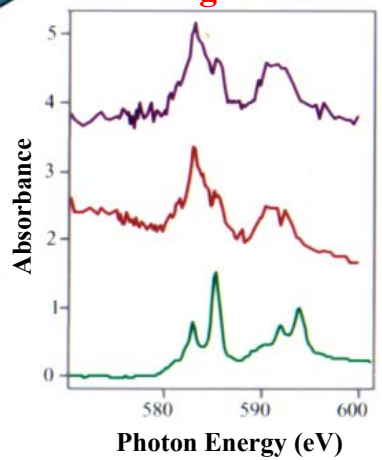

C K-edge XANES

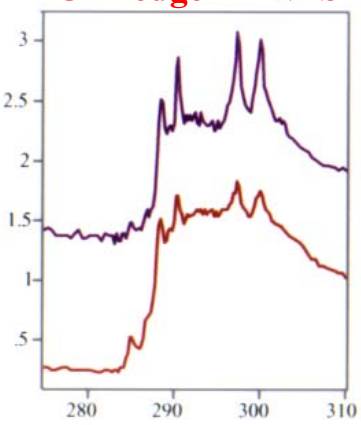

O K-edge XANES

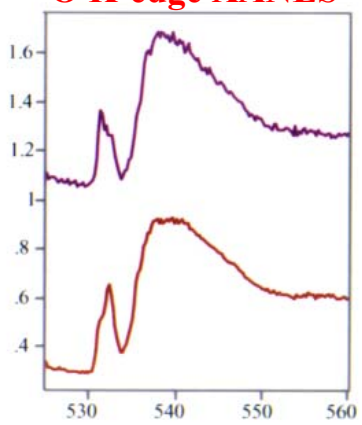

(Myneni, 2002, unpublished) (ALS)

Comparisons of C- and Al K-edge Images from Mineral-Bacteria Suspensions (Biocolloid Aggregates)

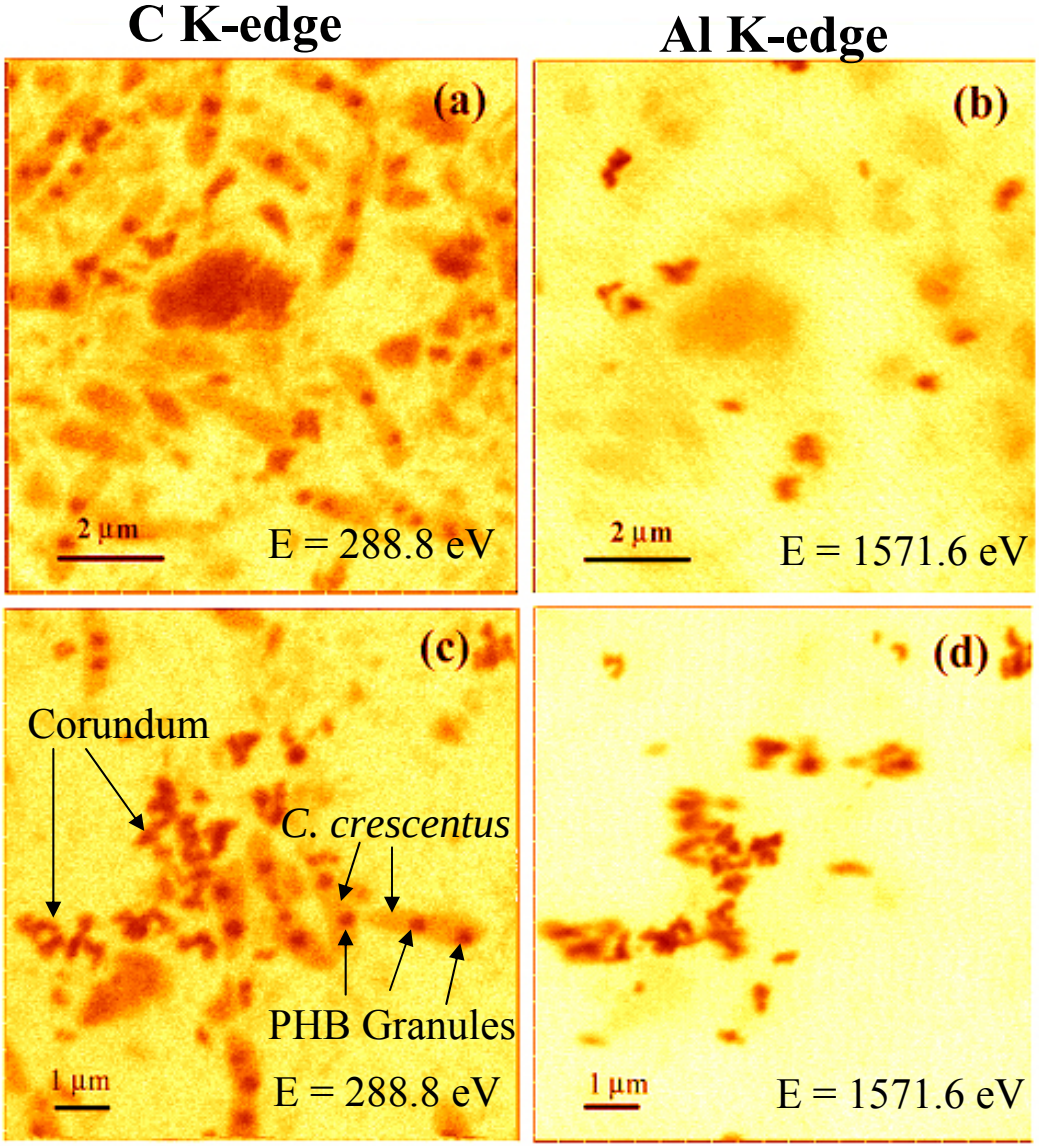

STXM image of *Caulobacter crescentus*-corundum-montmorillonite suspensions under hydrous conditions.

Key Observation - Bacteria (tan objects) are not in direct contact with corundum particles (orange irregular objects),

- exopolysaccharides form bridges between bacteria and corundum surfaces

- such aggregation changes the properties of the mineral nanoparticles

(Yoon *et al.*, *Langmuir Lett. 20,* 10361, 2004)

(ALS)

STXM Imaging and Al K-edge Spectromicroscopy of Al-Containing Nanoparticles

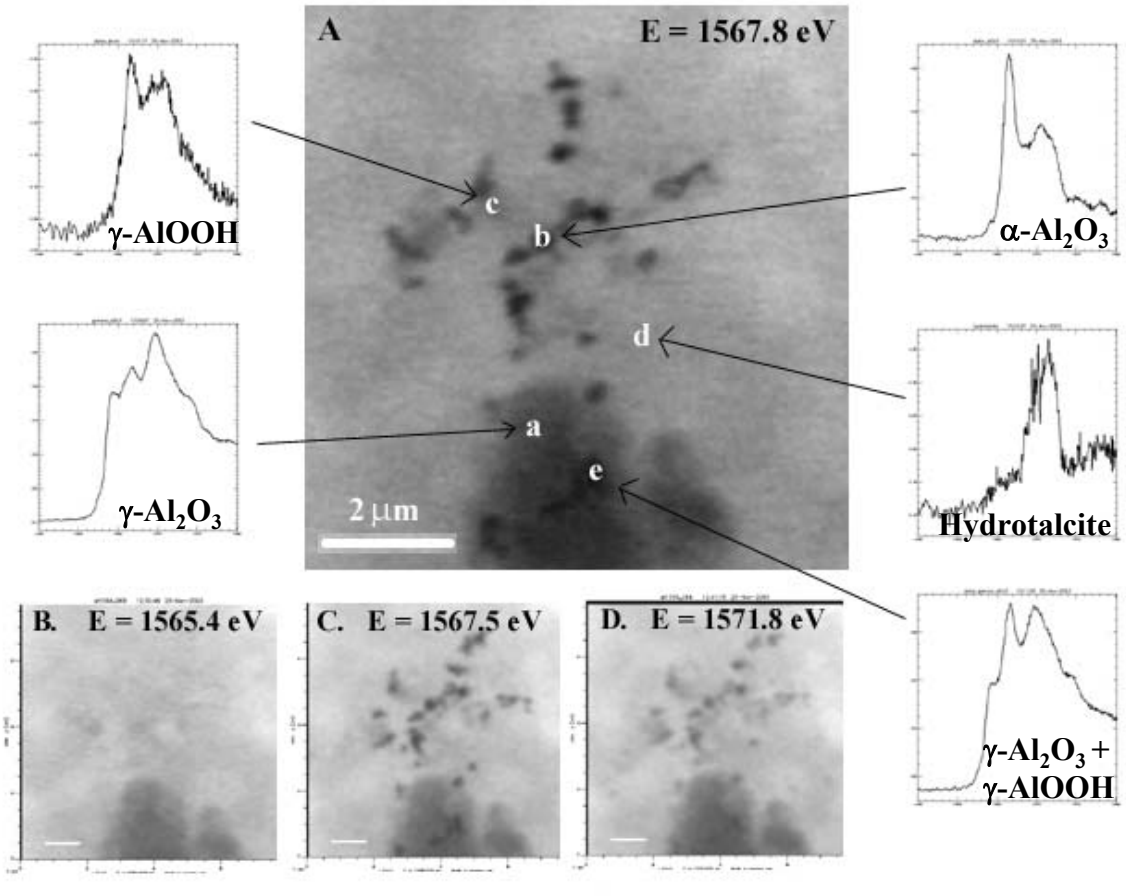

(Yoon *et al.*, *Langmuir Lett. 20,* 10361, 2004)

C K-edge Image and XANES Spectrum of Shewanella oneidensis

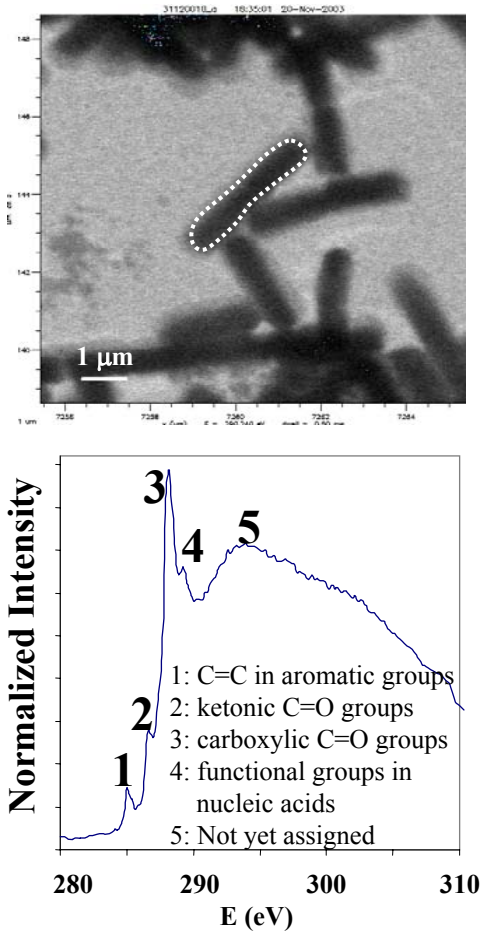

(Benzerara *et al.*, 2004, unpublished)

Tatahouine Meteorite - Unique Example of Biotic Weathering of an Fe-Silicate

(Benzerara *et al.*, *Proc. Nat. Acad. Sci. U.S.A. 204*, 979-982, 2005)

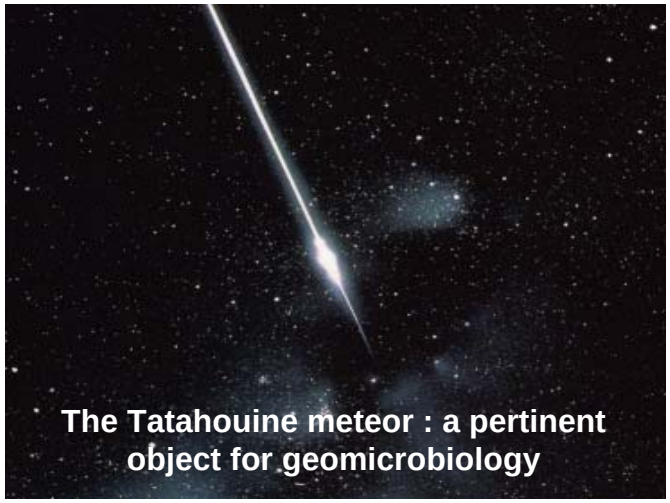

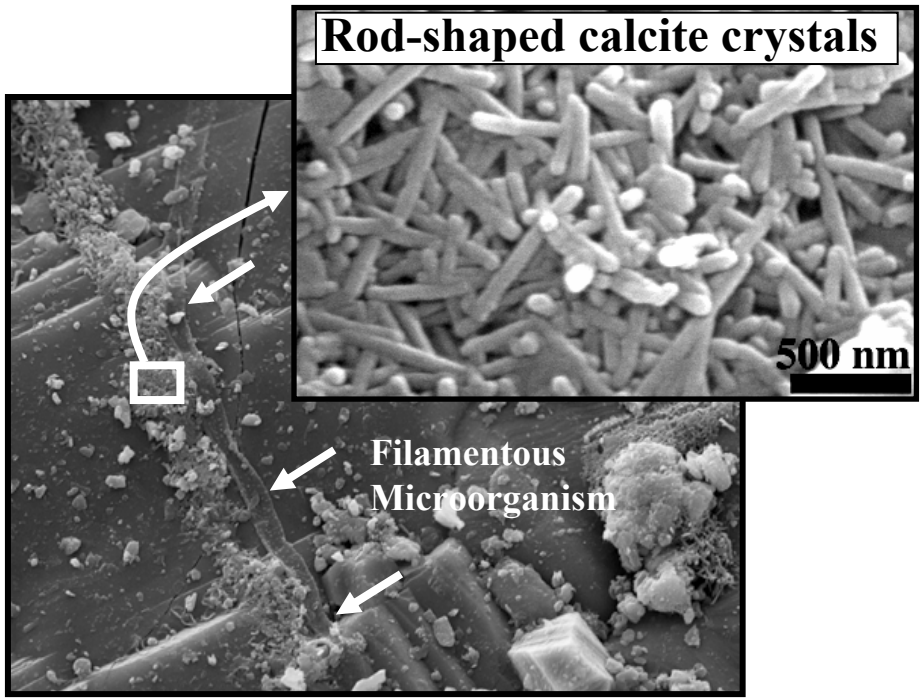

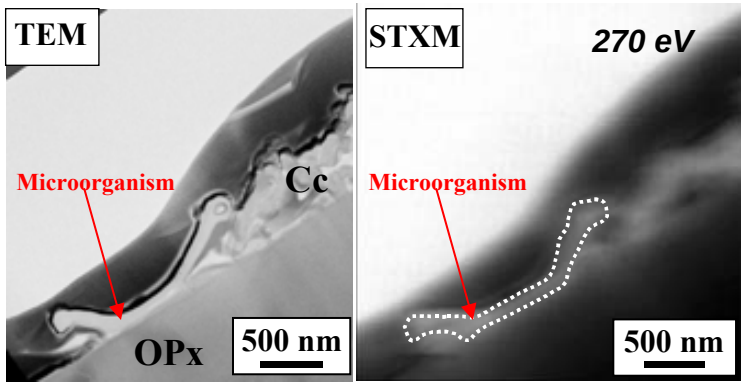

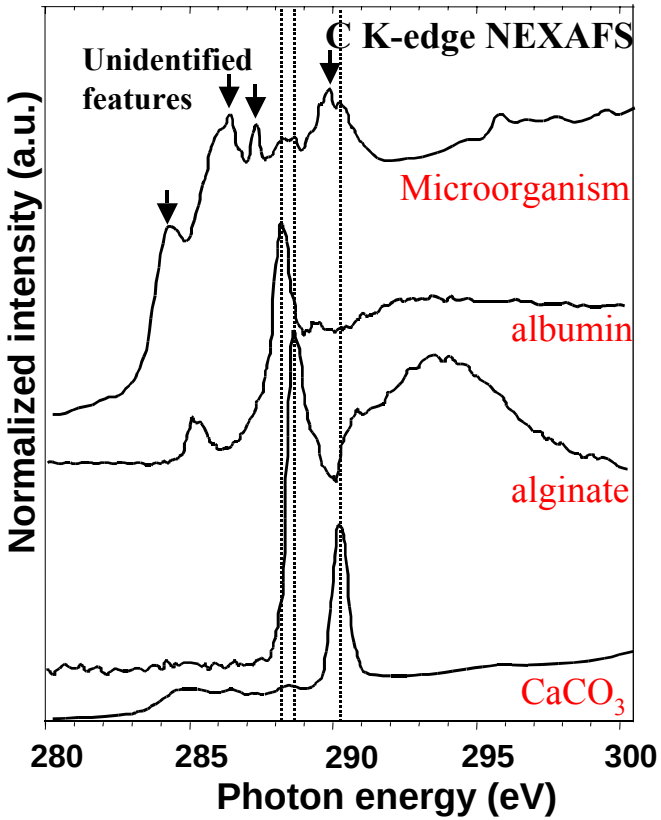

Calcite Nanocrystals - Biosignatures of Life

(Benzerara *et al.*, *Proc. Nat. Acad. Sci. U.S.A. 204*, 979-982, 2005)

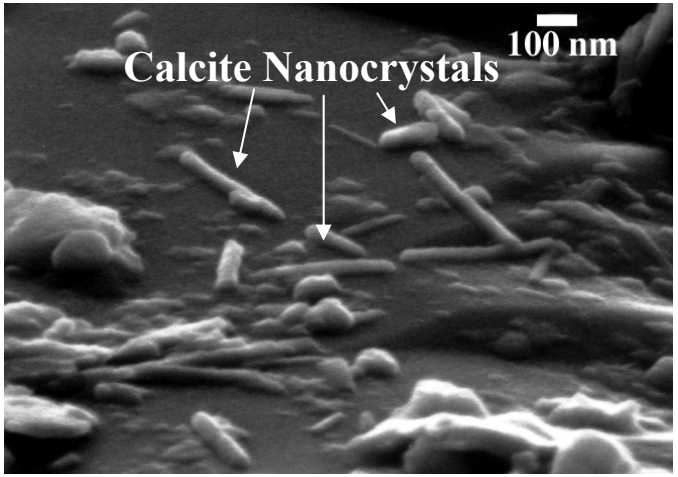

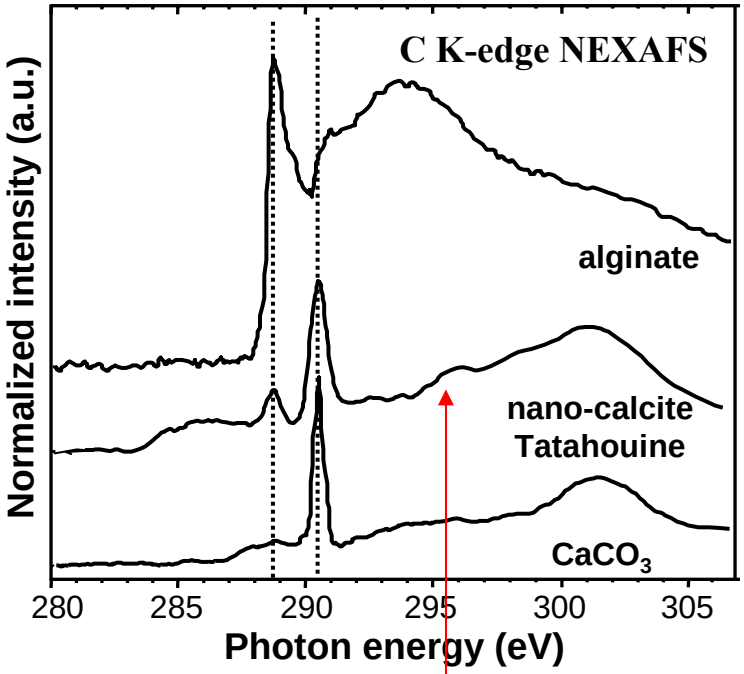

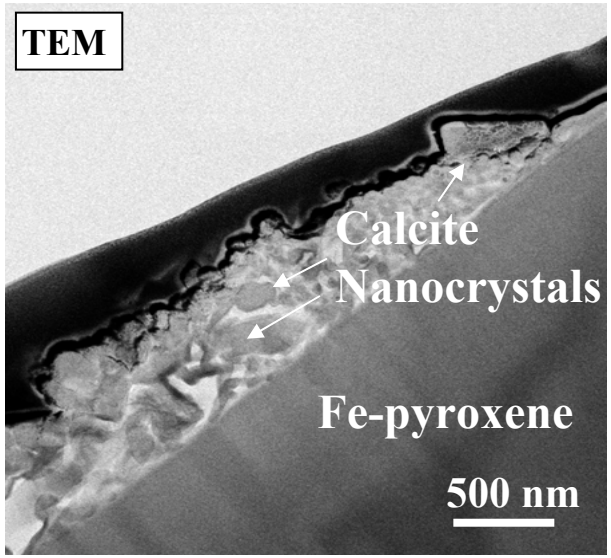

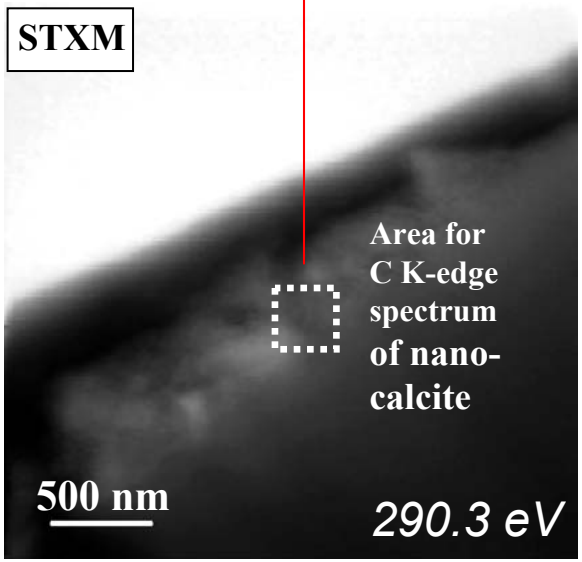

STXM/TEM Study of the Tatahouine Pyroxene/Microbe Interface

(Benzerara *et al.*, *Proc. Nat. Acad. Sci. U.S.A. 204*, 979-982, 2005)

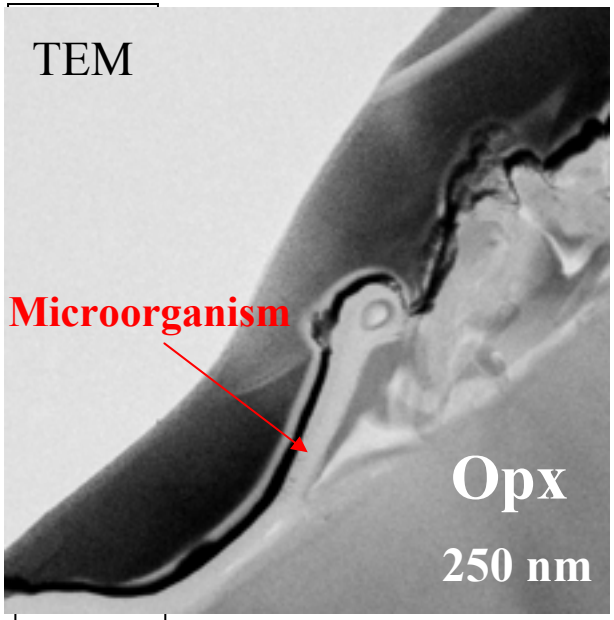

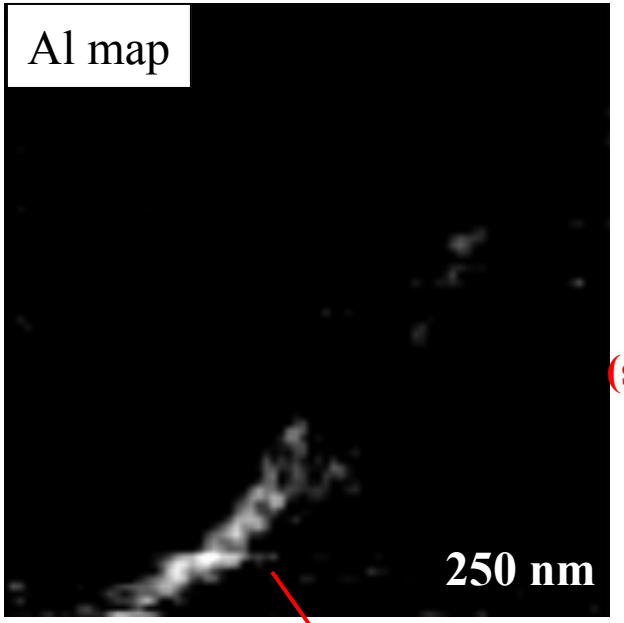

Al -rich layer beneath the microorganism (serves as anchor substrate)

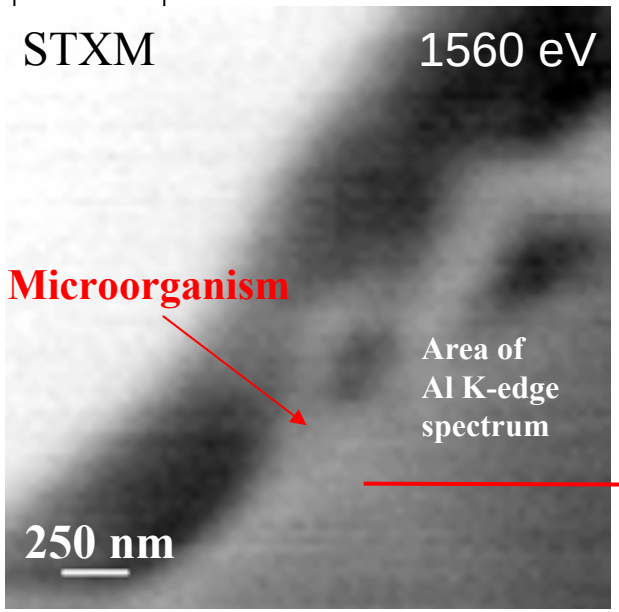

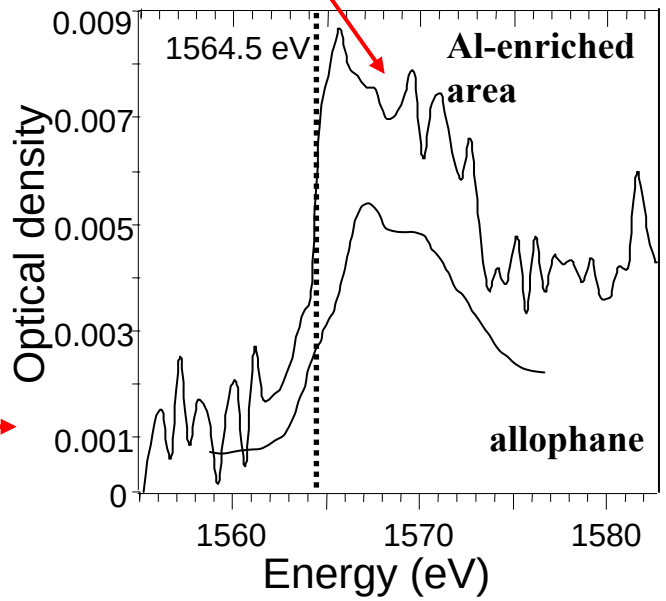

Al K-edge NEXAFS

= Al^{IV} + Al^{VI}
in poorly crystalline aluminosilicate

STXM/TEM Study of the Tatahouine Pyroxene/Microbe Interface

(Benzerara *et al.*, *Proc. Nat. Acad. Sci. U.S.A. 204*, 979-982, 2005)

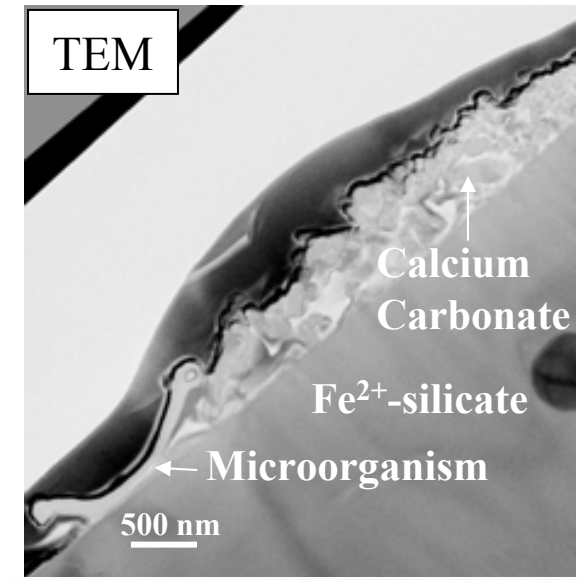

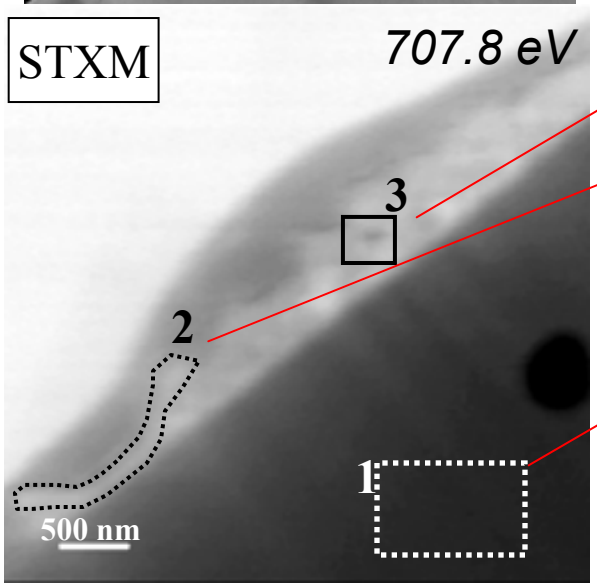

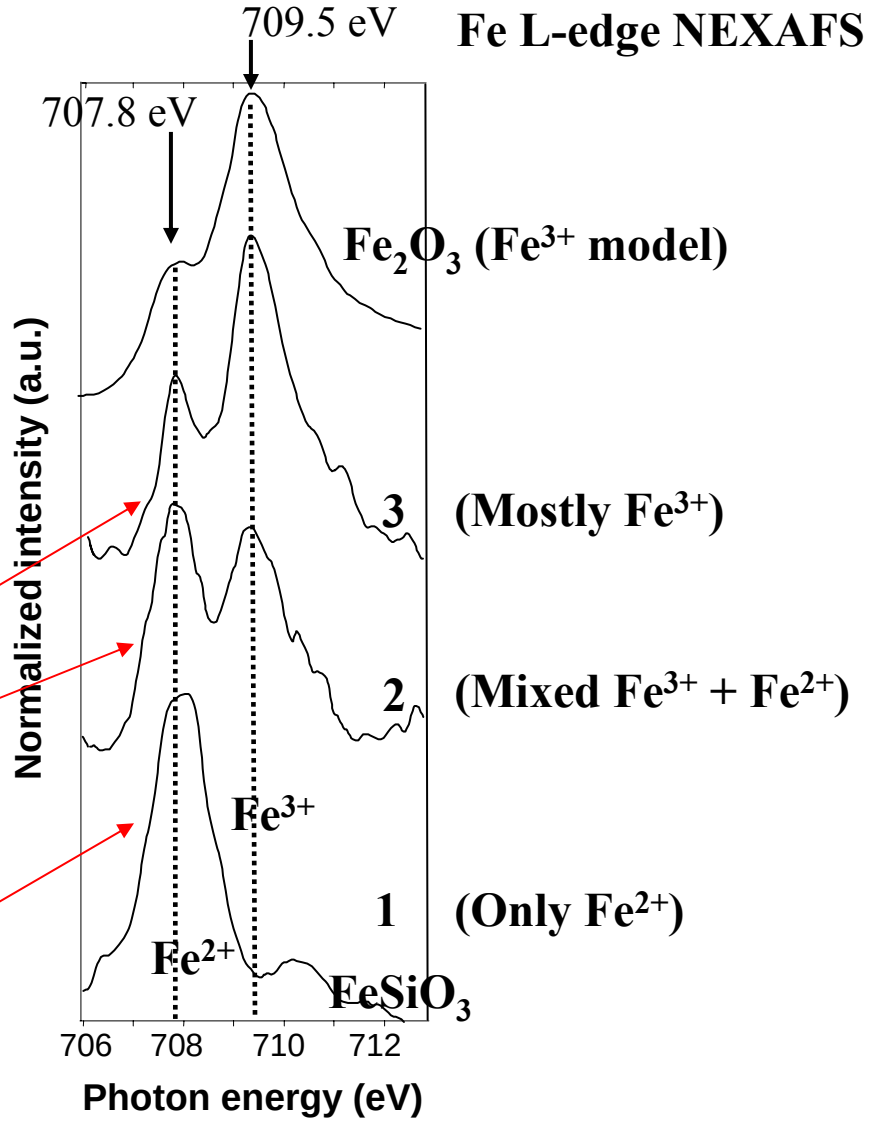

→ *Evidence for distinct nanoenvironments with different pO_2 values*

X-ray Microscopy (STXM) and TEM Study of Microbial Calcification

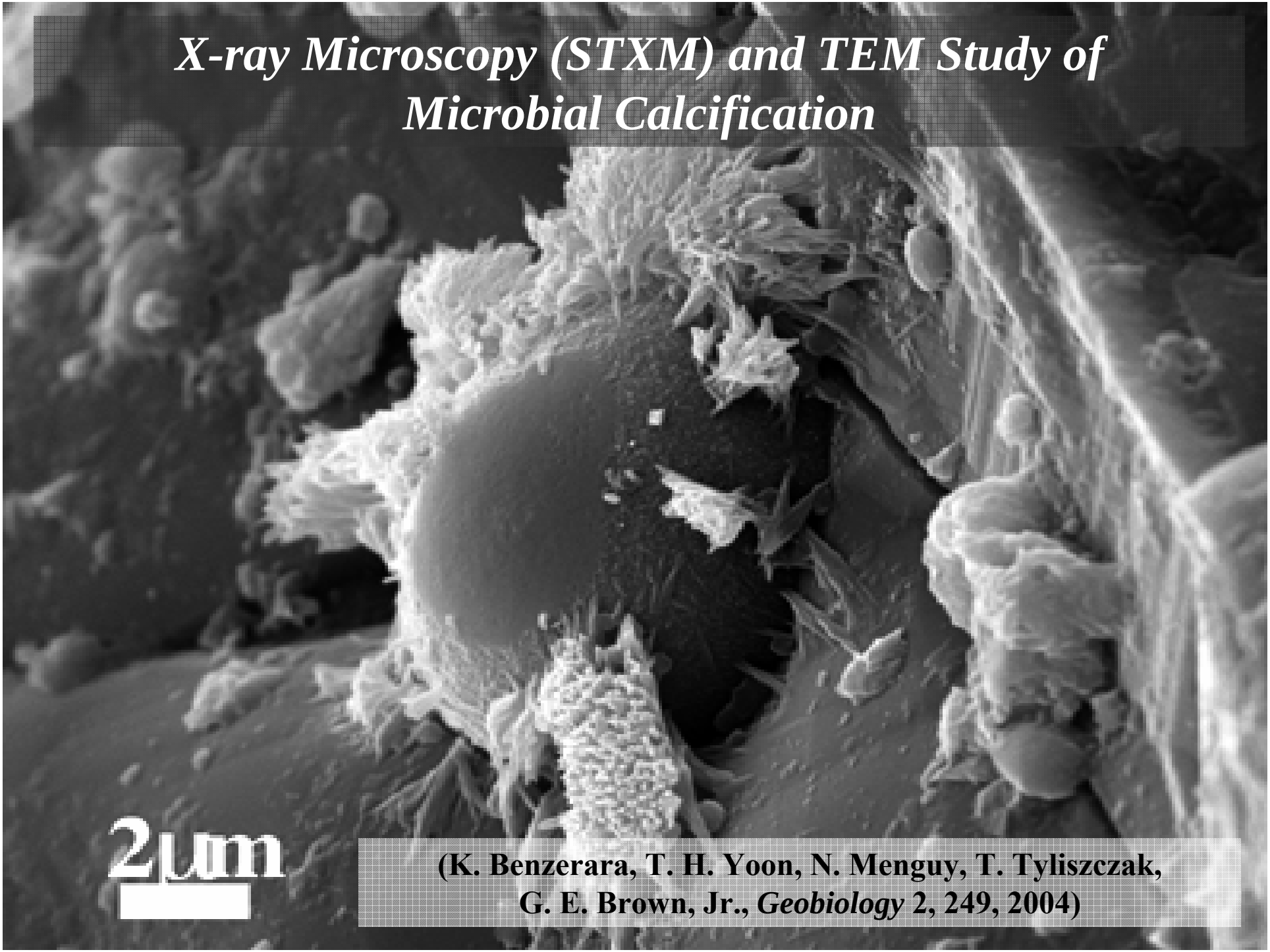

(K. Benzerara, T. H. Yoon, N. Menguy, T. Tyliszczak, G. E. Brown, Jr., *Geobiology* 2, 249, 2004)

Basics of Soft X-ray Spectromicroscopy

X-ray absorption intensity depends on the speciation of an element

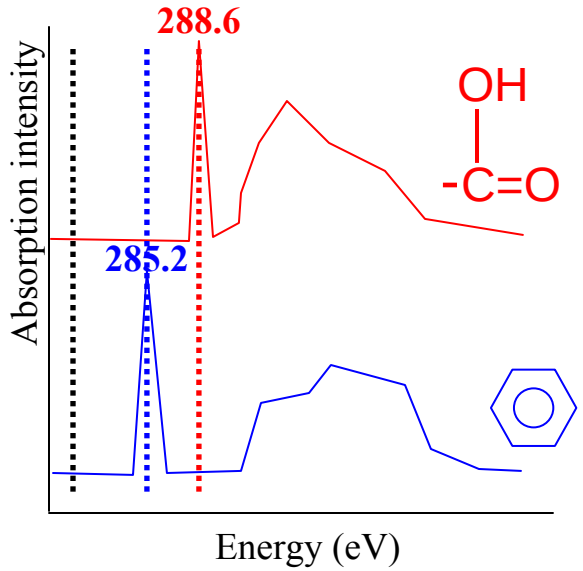

2 objects: one rich in aromatics, the other in carboxylic groups

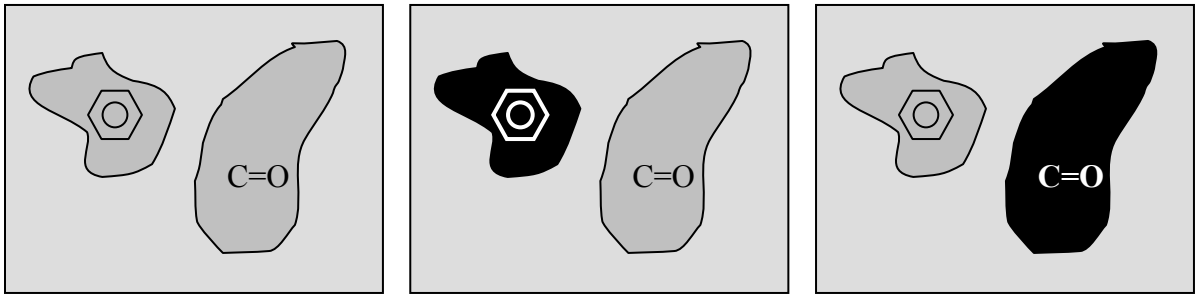

280 eV

285.2 eV
Aromatics absorb

288.6 eV
Carboxylics absorb

Near Edge X-Ray Absorption Fine Structure (NEXAFS)

Image contrast = Differential absorption of X-rays depending on speciation

Calcified Microorganisms at the Calcium $L_{2,3}$ Edge

Energy-filtered Imaging

Below Ca edge (340 eV)

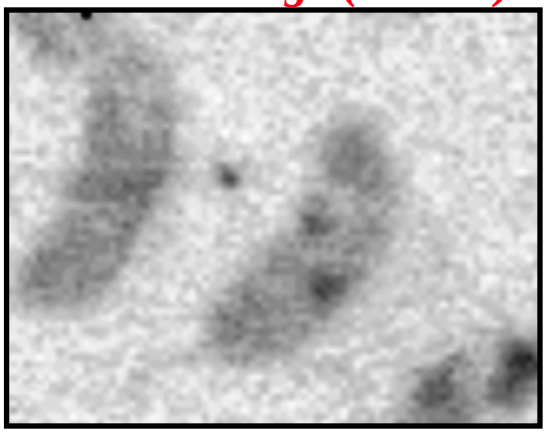

Above Ca edge (349.3 eV)

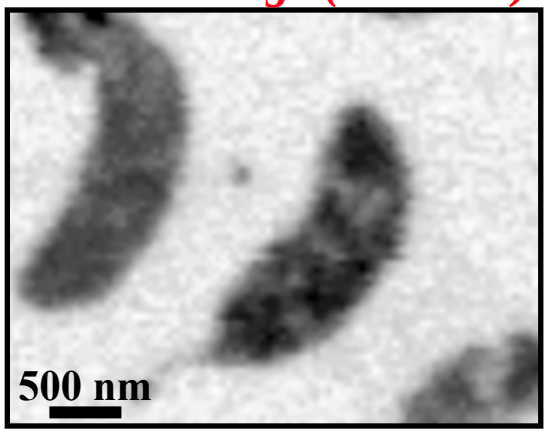

Ca map

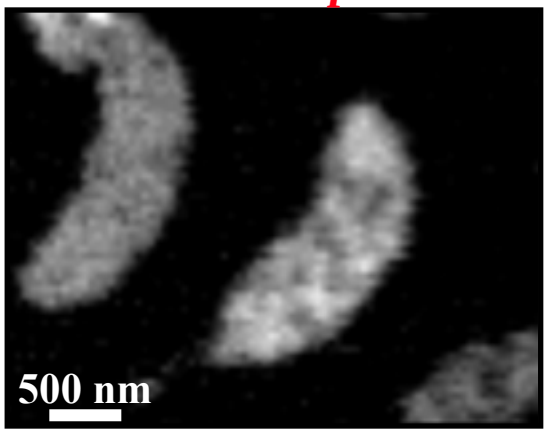

1 Pixel = 25 nm x 25 nm

Acquisition time for one image ≈ 30 s

Spectroscopy:

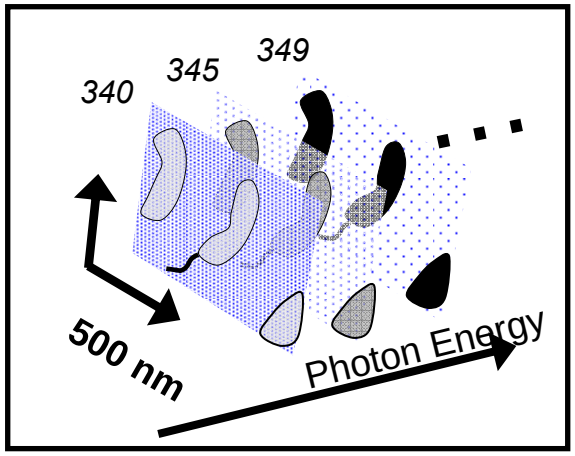

Acquisition of image stacks:

1 image every 0.1 eV

3-D volume of data (x,y, E)

(Benzerara *et al.*, *Geobiology 2*, 249, 2004)

NEXAFS Spectrum of Calcified Bacteria at the Ca $L_{2,3}$ Edge

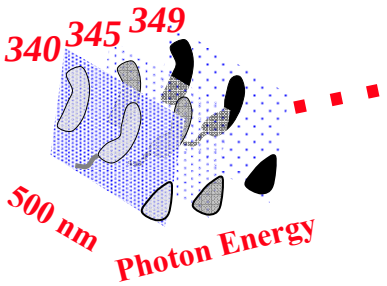

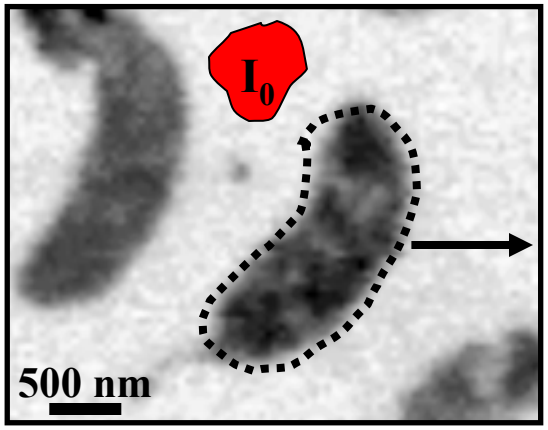

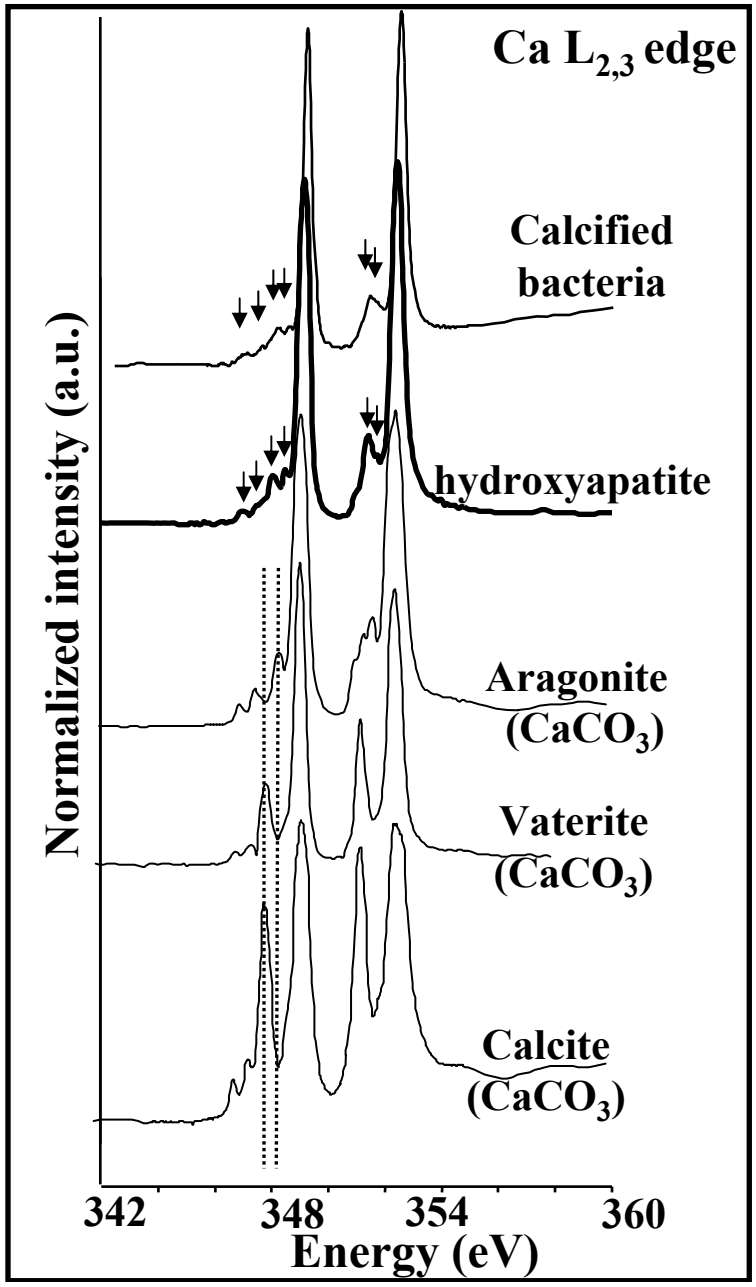

(Benzerara *et al.*, *Geobiology 2*, 249, 2004)

STXM Images of C. crescentus above and below the P $L_{2,3}$-edge

(Benzerara *et al*., *Geobiology 2*, 249-259, 2004)

130 eV

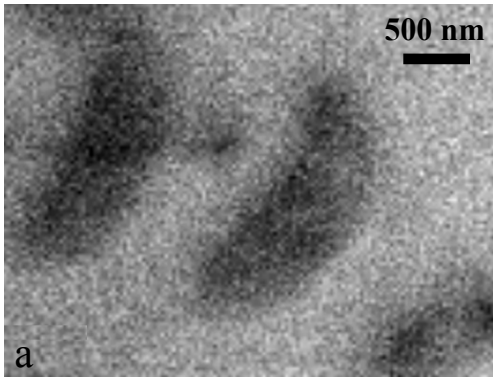

145 eV

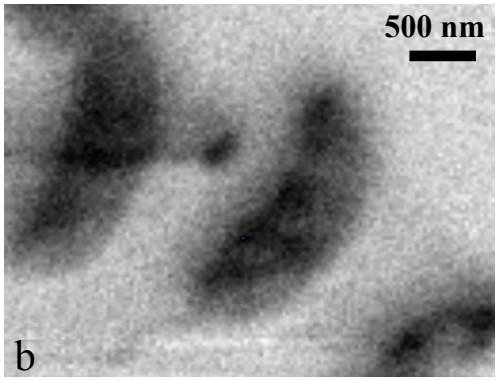

Δ Map

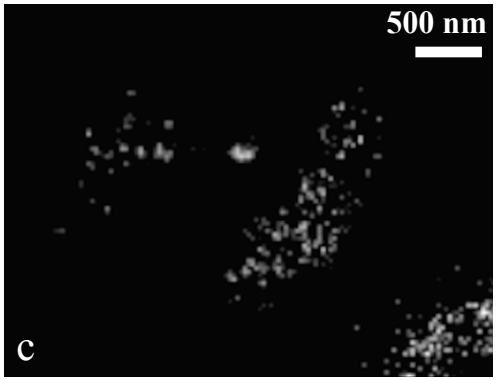

P in cells

STXM Images of C. crescentus at and below the C K-edge Resonance of Carboxyl Groups in Proteins and C K-edge Spectra

(Benzerara *et al.*, *Geobiology 2*, 249-259, 2004)

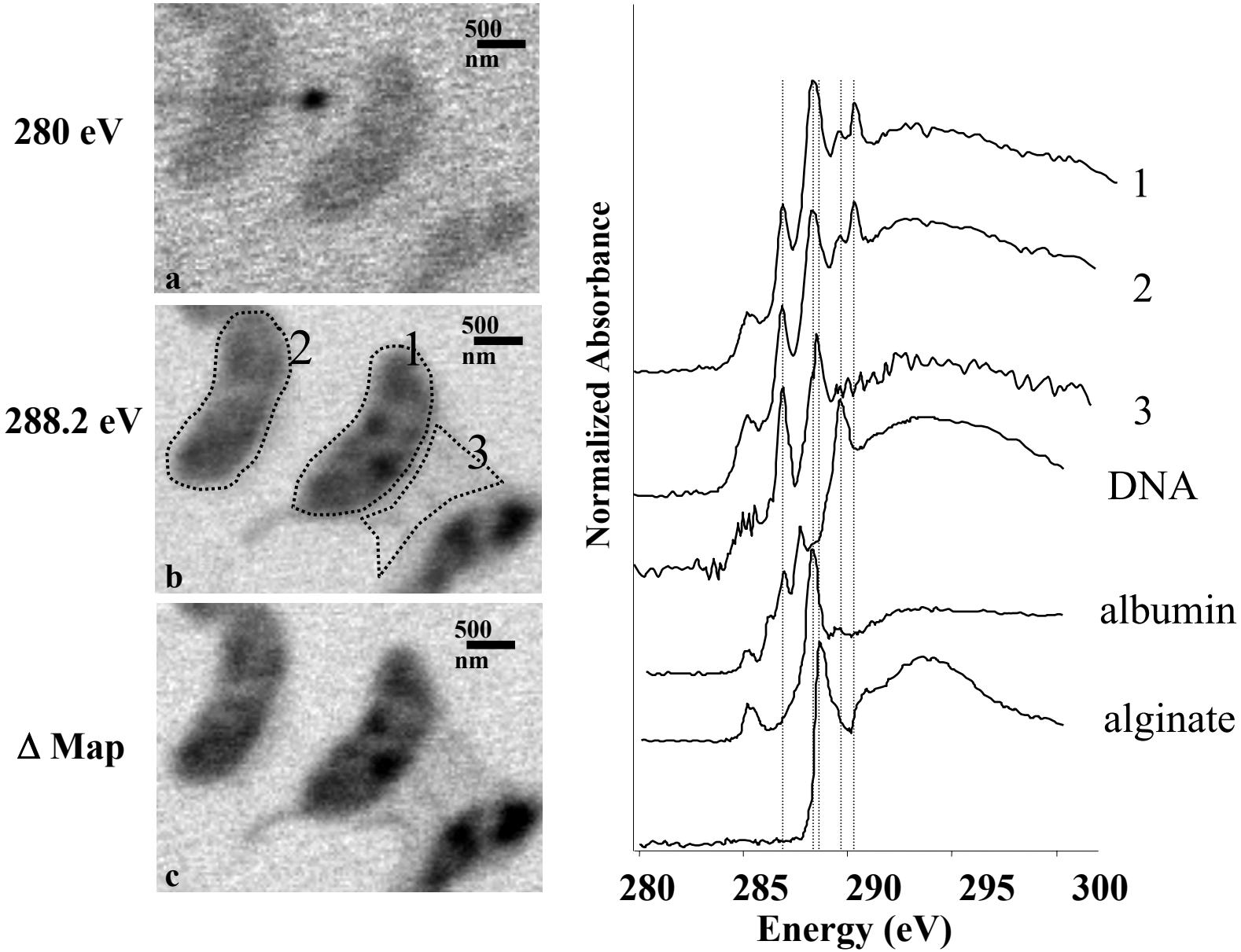

Applications of Photoemission and Soft X-ray XAFS Spectroscopy to Acid Mine Drainage

Acid Mine Drainage - A Significant Environmental Problem

Acid Mine Drainage Pond below Main Waste Dump at New Idria Mercury Mine California

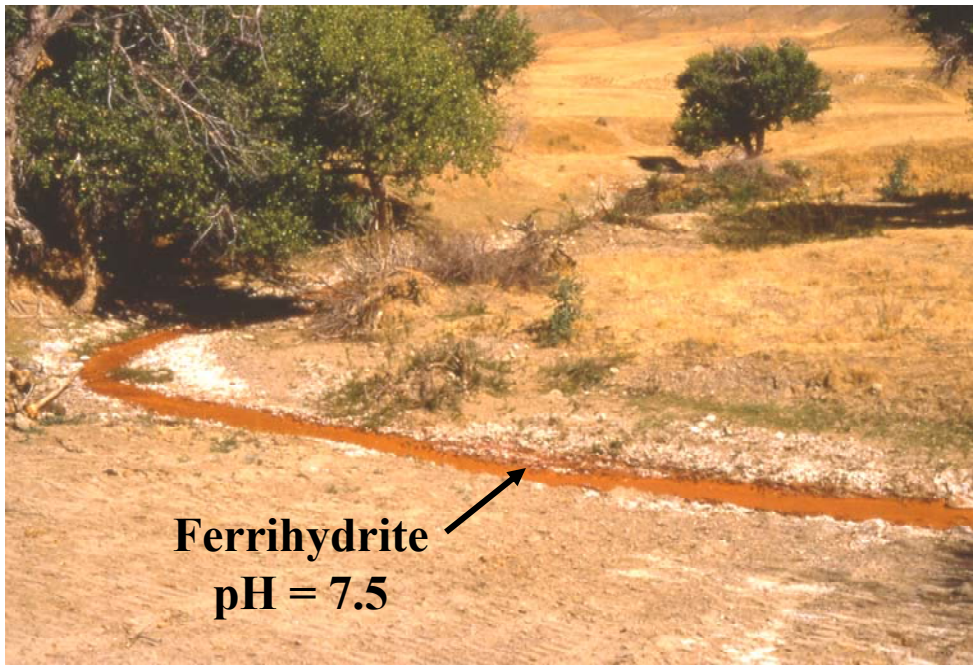

Typical Acid Mine Drainage Stream showing Ferrihydrite Precipitate

Uptake of Aqueous Metal Cations and Oxoanions on HFO Surfaces as a Function of pH

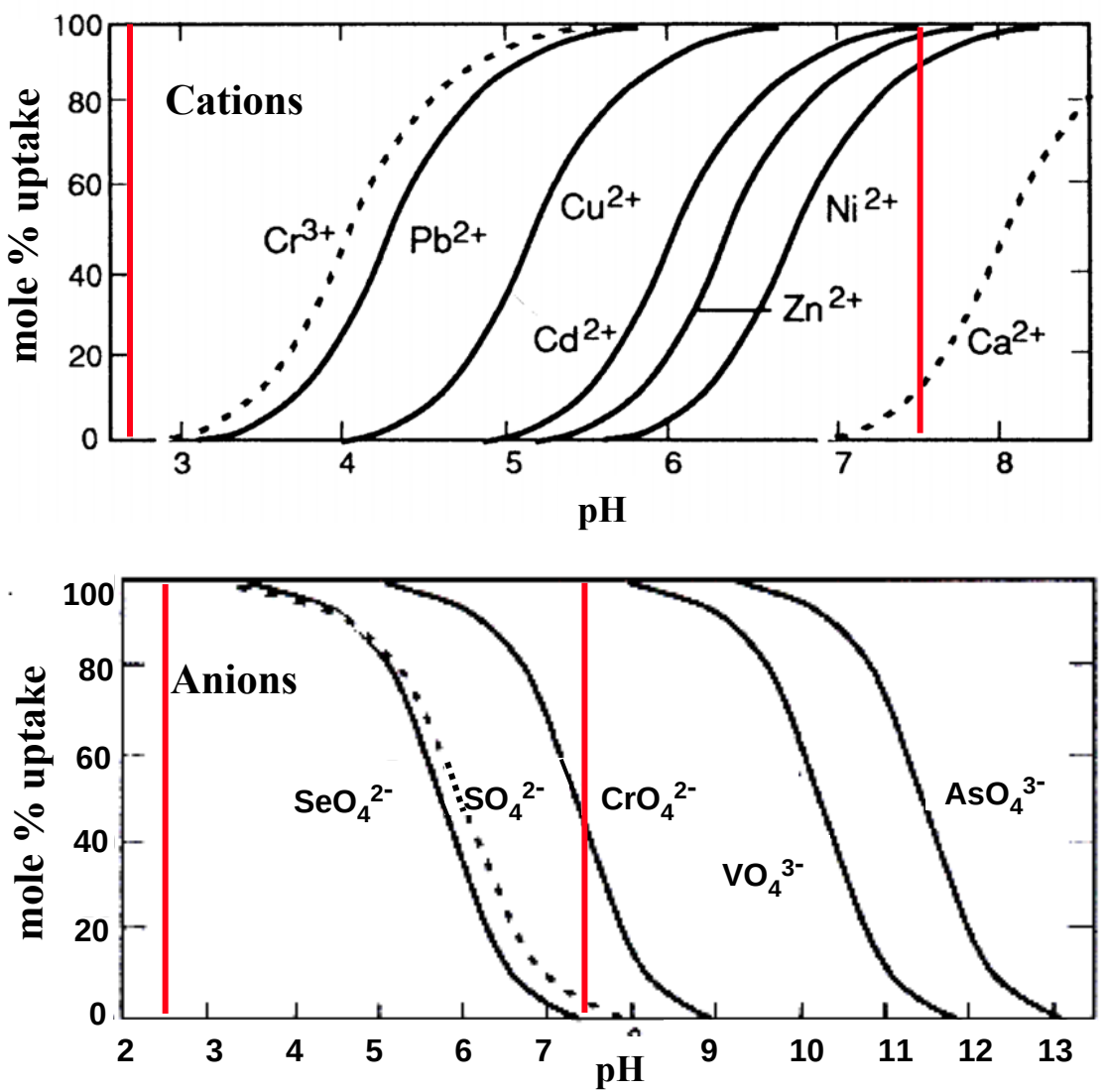

(after Stumm, *Chemistry of the Solid-Water Interface,* Wiley, 1992)

Microbially Mediated Oxidation of Pyrite

Pyrite: FeS_2

$$FeS_2 + H_2O + 7/2\ O_2 = Fe^{2+}(aq) + 2\ SO_4^{2-} + 2\ H^+$$

$$Fe^{2+}(aq) + 5/2\ H_2O + 1/4\ O_2 = Fe(OH)_3(solid) + 2\ H^+$$

Ferrihydrite: $Fe(OH)_3$

without bacteria (abiotic)

$$FeS_2 + 14\ Fe^{3+} + 8\ H_2O \rightarrow 14\ Fe^{2+} + Fe^{2+} + 16\ H^+ + 2\ SO_4^{2-}$$

$\uparrow$ $\downarrow$

A. ferrooxidans

$$7\ H_2O + 14\ Fe^{3+} \leftarrow 14\ Fe^{2+} + 3.5\ O_2 + 14\ H^+$$

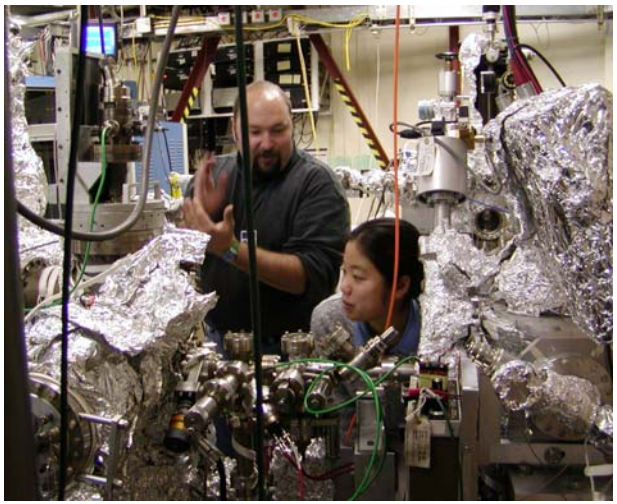

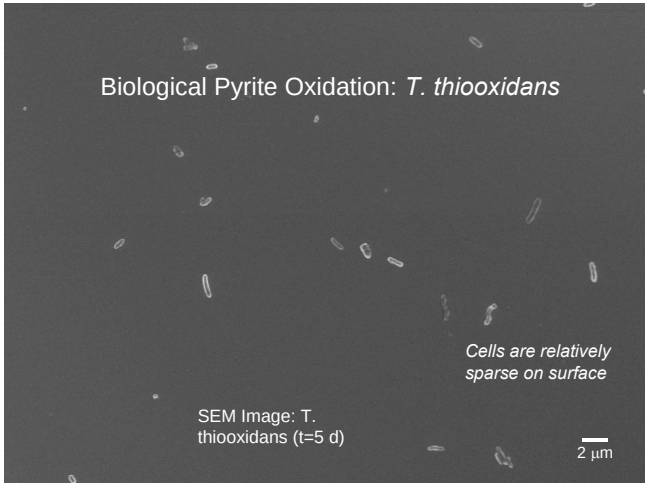

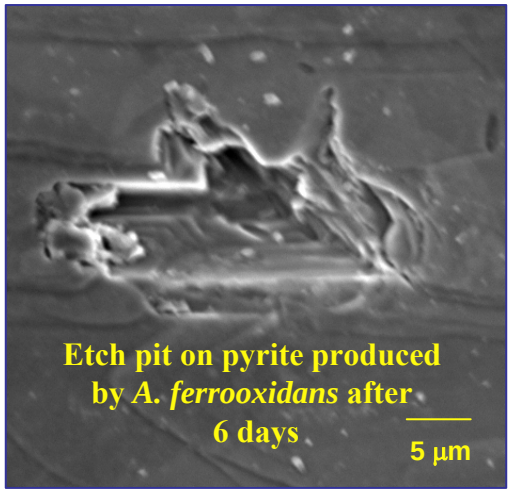

(Bostick *et al.*, in preparation)

Biological Pyrite Oxidation: Acidothiobacillus ferrooxidans

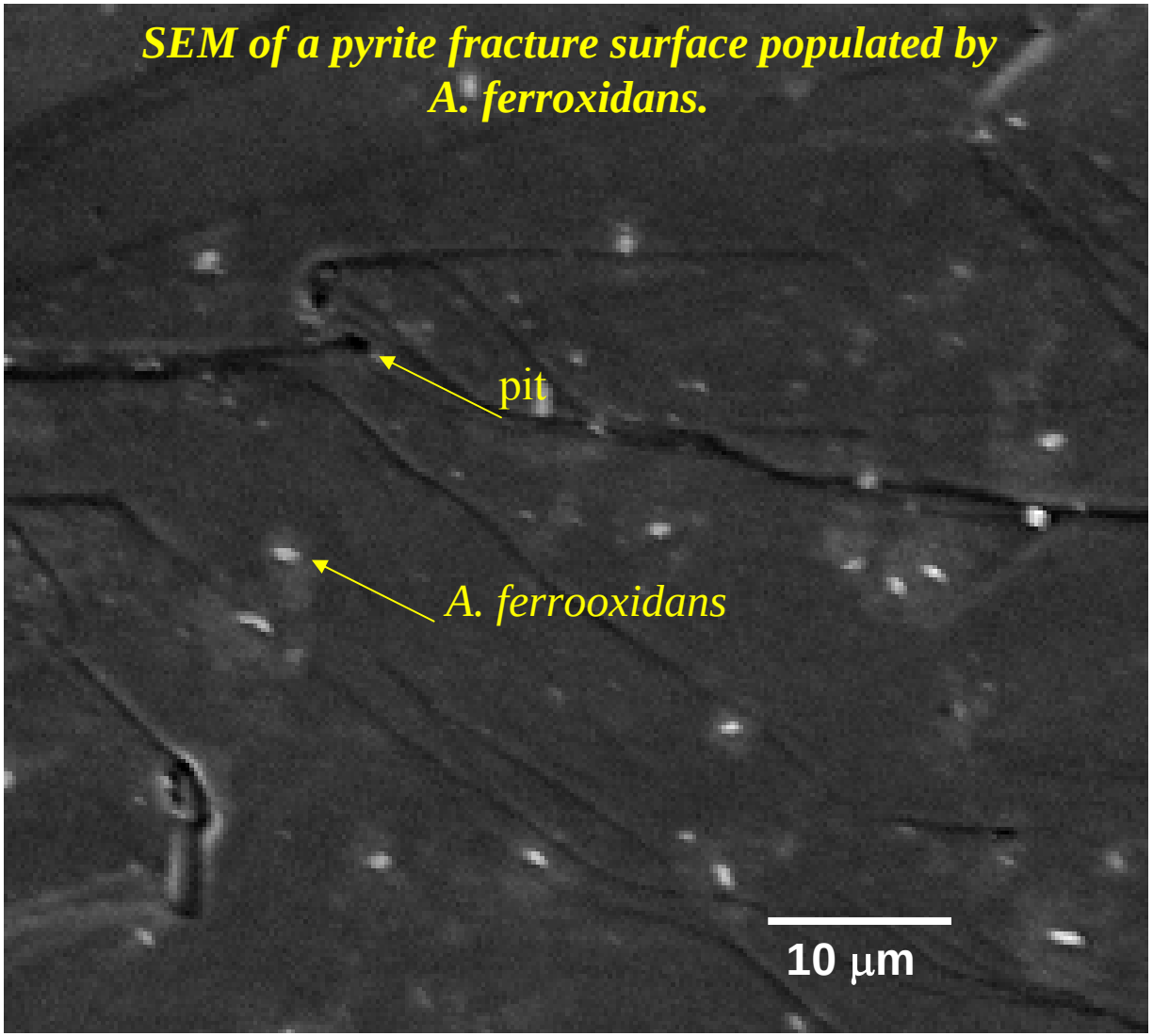

- **Bacteria populate the surface, resulting in the presence of localized regions of oxidation around the bacteria**
- **Bacterial populations and localized oxidized regions are not correlated with surface defects**

(Bostick *et al.*, in preparation)

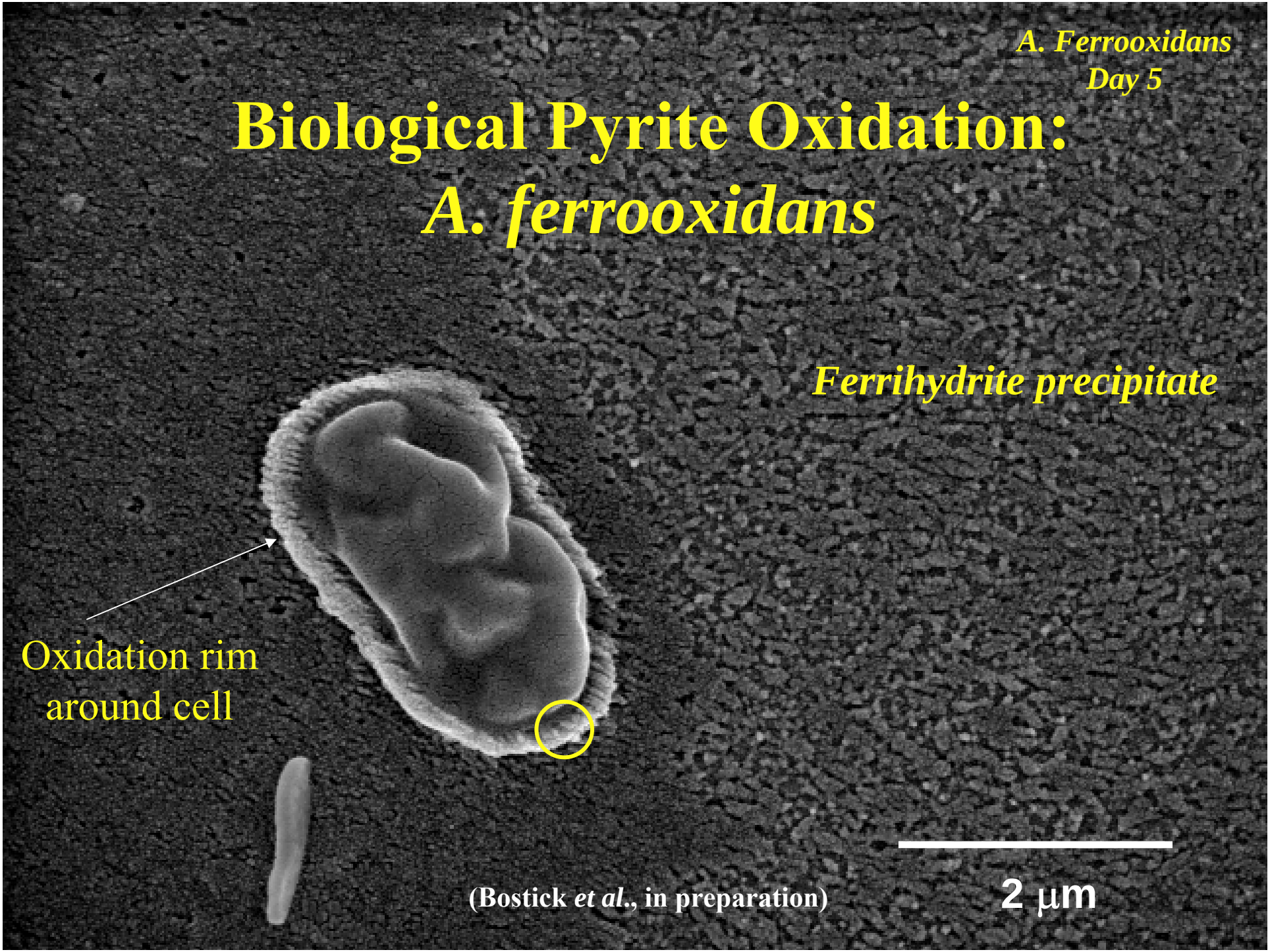
A. Ferrooxidans
Day 5
Biological Pyrite Oxidation:
A. ferrooxidans
Ferrihydrite precipitate
Oxidation rim
around cell
(Bostick et al., in preparation)
2 μm

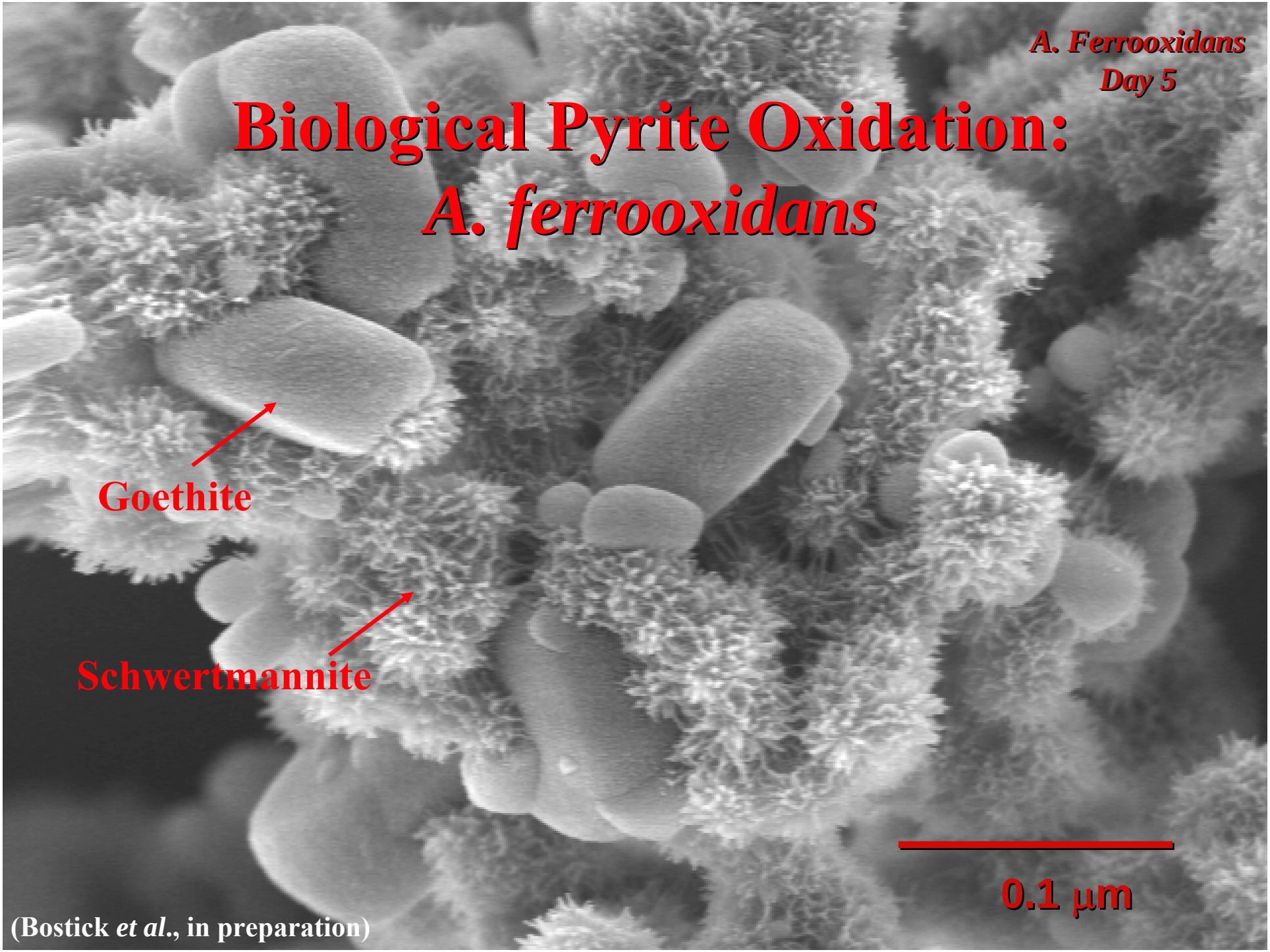
A. Ferrooxidans
Day 5
Biological Pyrite Oxidation:
A. ferrooxidans
Goethite
Schwertmannite
0.1 μm
(Bostick et al., in preparation)

Fitting S 2p XPS Data

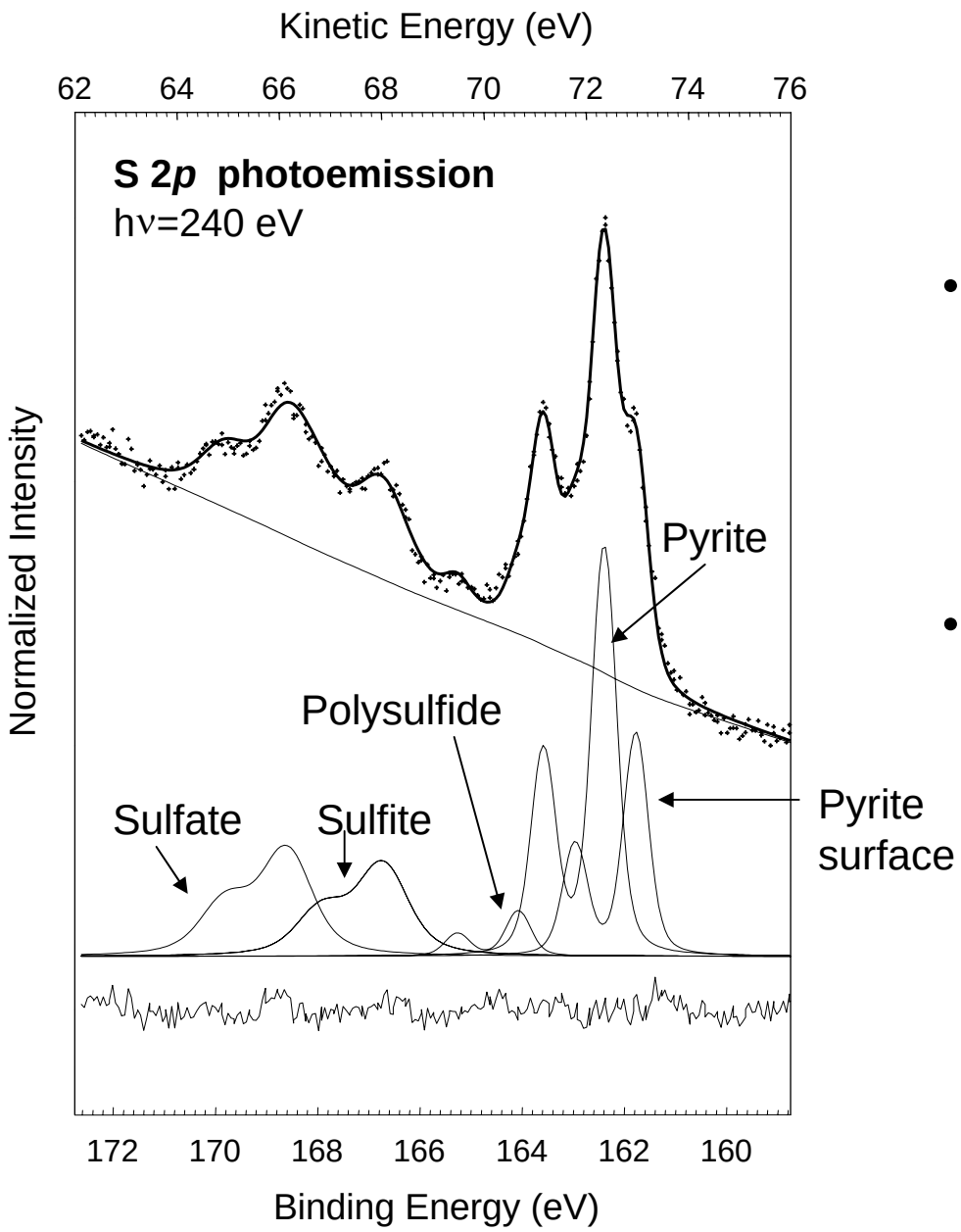

- Each species is a doublet with an ratio of areas of 2:1 and separated by known energy (S: 1.19 eV)
- More oxidized species have higher binding energies (binding energy related to effective nuclear charge)

(Bostick *et al.*, in preparation)

Abiotic (Chemical) Pyrite Oxidation

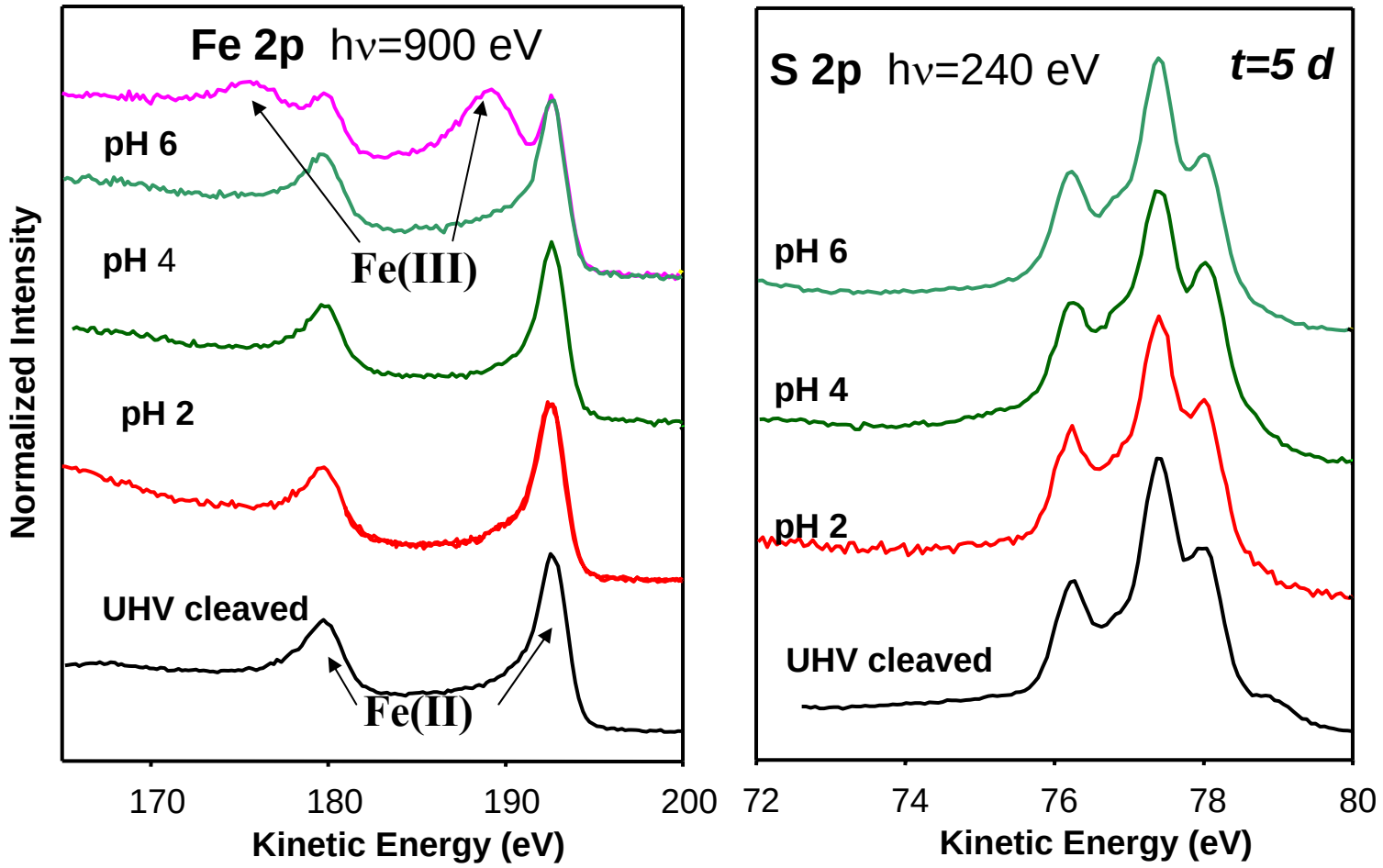

- **Significant surface oxidation not observed for chemical system—diffusion from surface rapid enough that oxidation product concentrations do not build up on surface**
- **Sulfur oxidation products do not build up on surface**

(Bostick *et al.*, in preparation)

Biological Pyrite Oxidation: A. ferrooxidans

(Bostick *et al.*, in preparation)

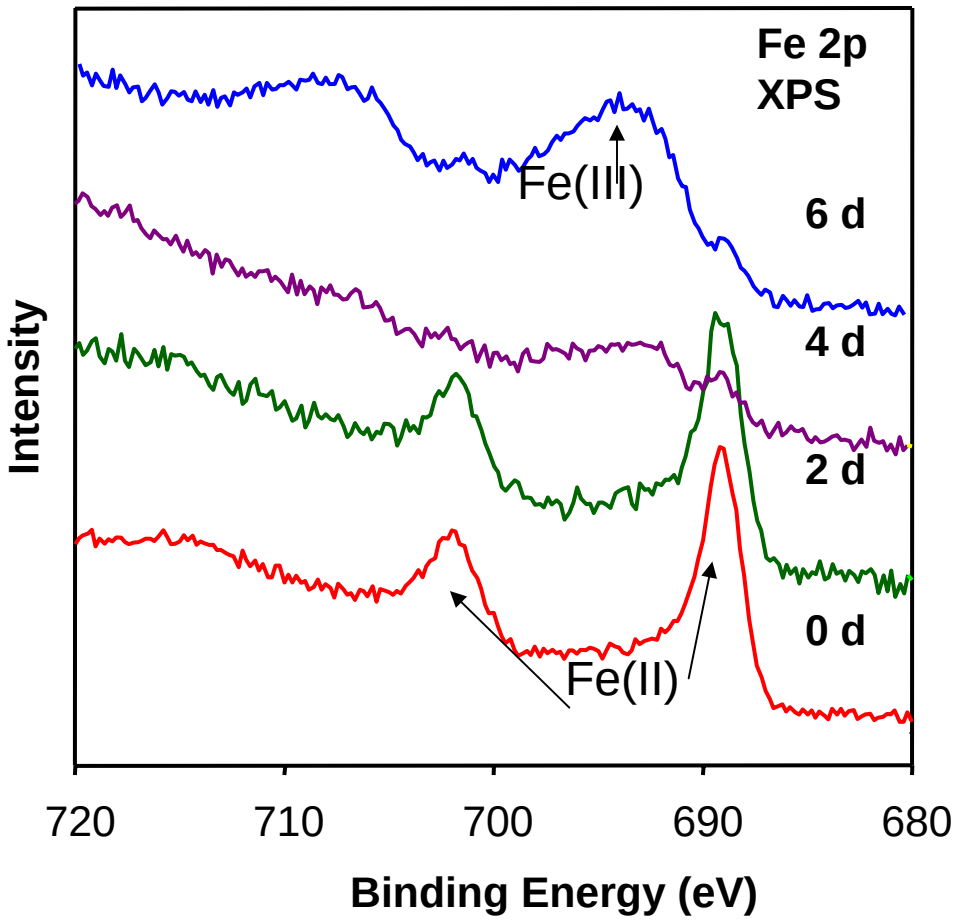

Fe oxidation products build up rapidly on the FeS_2 surface over time, first occurring in a spotty fashion (not reproducible on a scale of μm) and then gradually thickening to 10-20 monolayers after 6 days of microbial oxidation.

Biological Pyrite Oxidation: A. ferrooxidans

(Bostick *et al.*, in preparation)

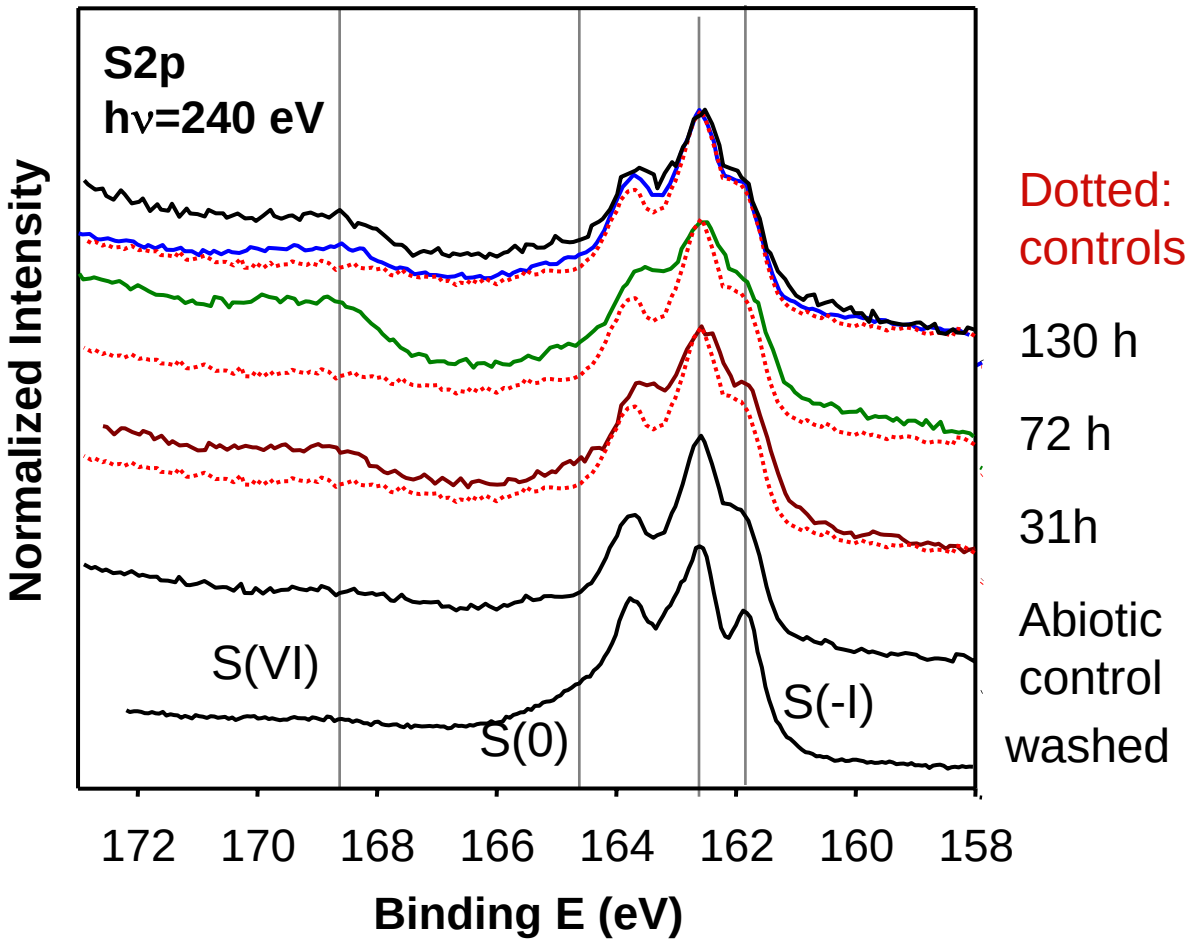

- **Some oxidized sulfur species are formed on the surface**
- **Extent of oxidation is variable, depending on spot location**

Biological Pyrite Oxidation: A. ferrooxidans

(Bostick *et al.*, in preparation)

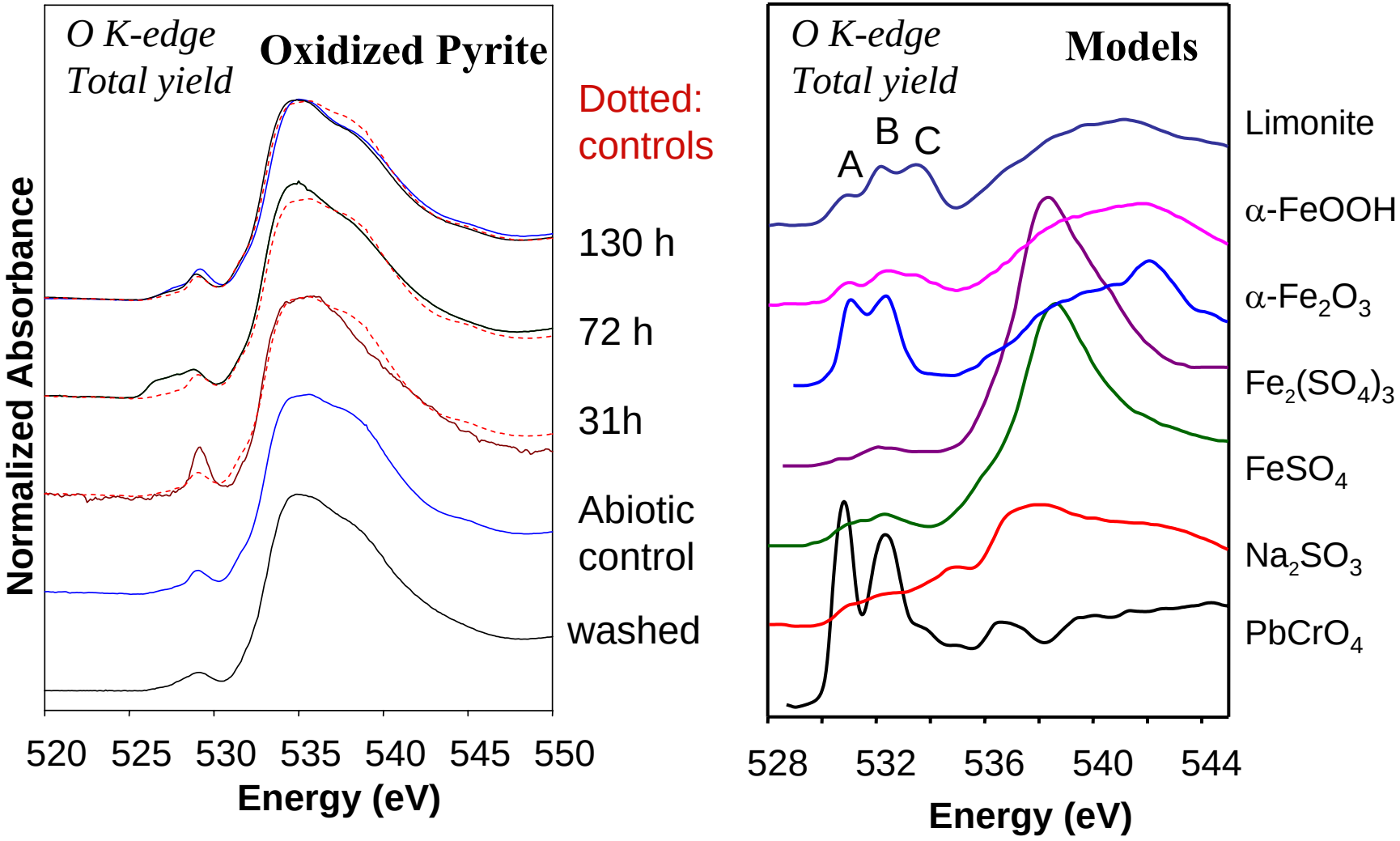

- **O K-edge also shows considerable surface hydroxylation (peak C) and oxidation, with some evidence for the formation of goethite**

Biological Pyrite Oxidation: *A. ferrooxidans and A. thiooxidans* in mixed cultures

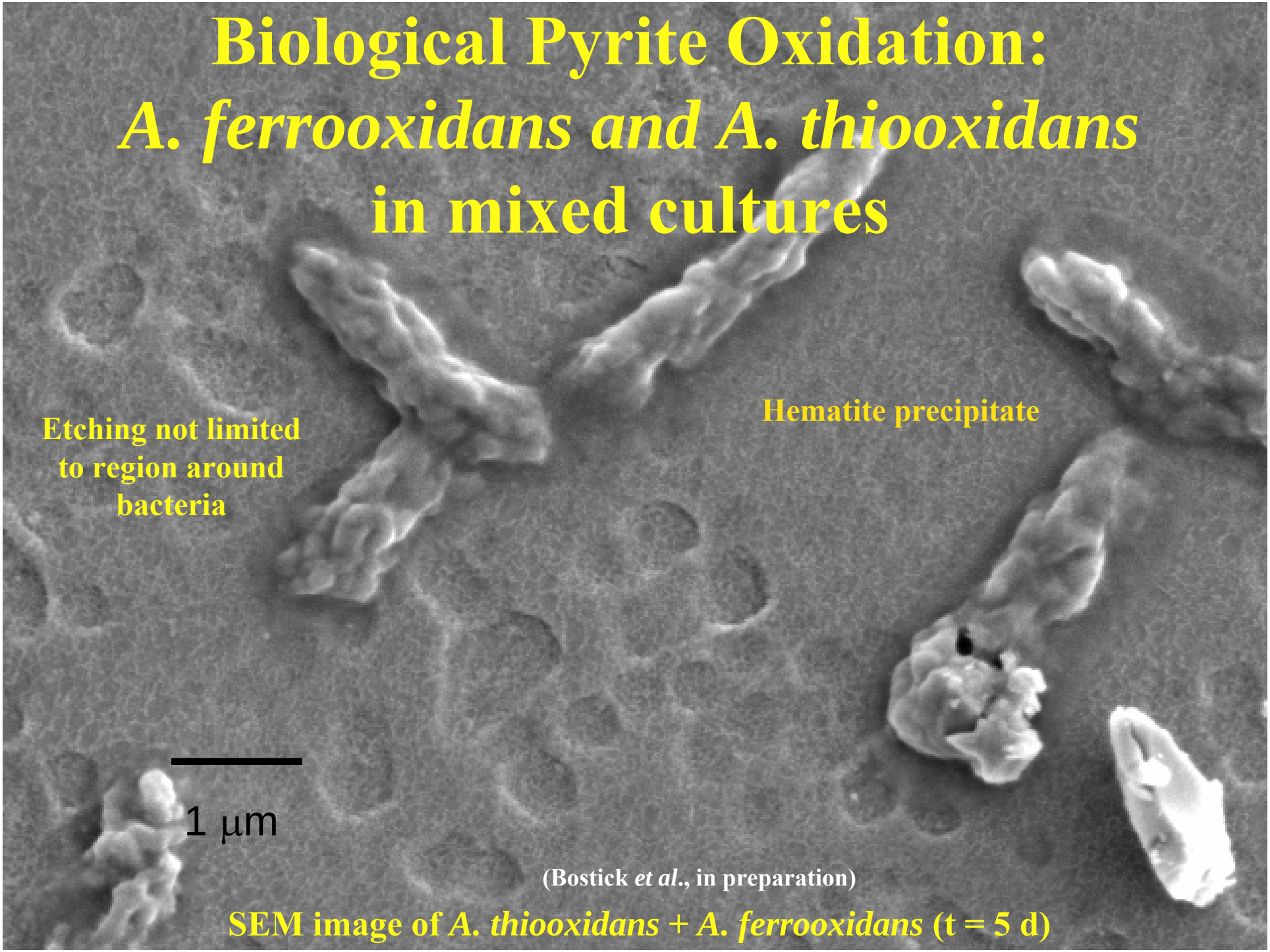

(Bostick *et al.*, in preparation)

SEM image of *A. thiooxidans* + *A. ferrooxidans* (t = 5 d)

Biological Pyrite Oxidation: A. ferrooxidans and A. thiooxidans

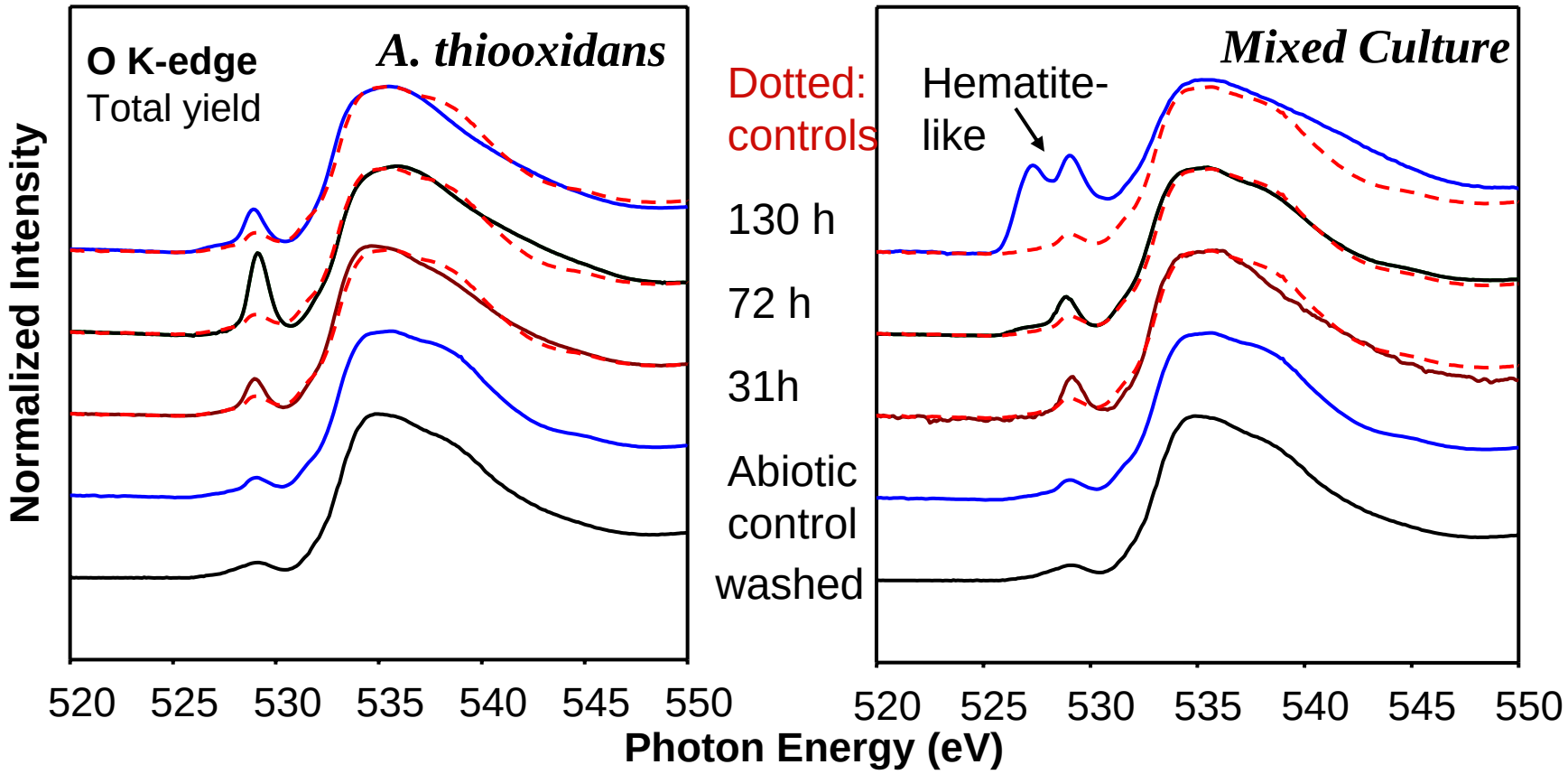

- **Sulfide mineral surface is hydroxylated in the presence of *A. thiooxidans*; hematite forms when the consortium is present.**

(Bostick *et al.*, in preparation)

Biological Pyrite Oxidation: A. ferrooxidans and A. thiooxidans

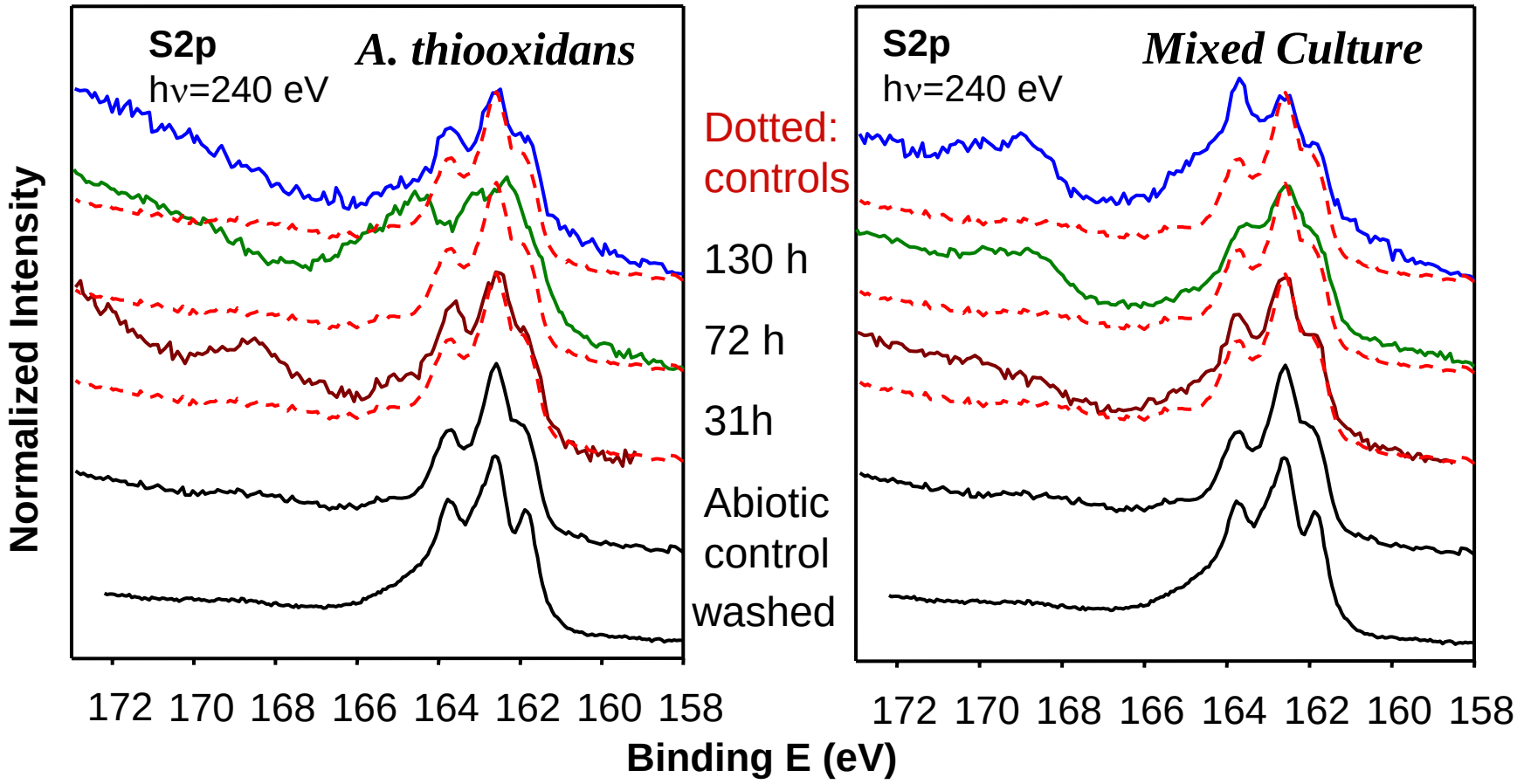

- **Little oxidized sulfur species other than S^0 is retained on the sulfide mineral surface when *A. thiooxidans* is present.**

(Bostick *et al.*, in preparation)

Applications of XAFS Spectroscopy to Environmental Pollution Problems

- **Zn Speciation in Contaminated Soils from N. France**
- **Arsenic in Bangladesh**
- **Selenium in the Central Valley of California**
- **Chromium and Radionuclides at U.S. DOE Sites**

Zn Speciation in Polluted Soils from Northern France

(Juillot *et al.*, *Am. Mineral.* *88*, 509, 2003)

Different Possibilities for the Sequestration of Zinc in Contaminated Soils from XAFS Experimental Studies of Model Systems

Adsorption

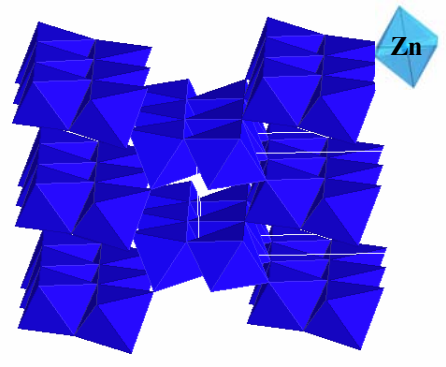

Schlegel et al. (1997)
Trainor et al. (2002)
Waychunas et al. (2002)

Layered Double Hydroxides (LDHs)

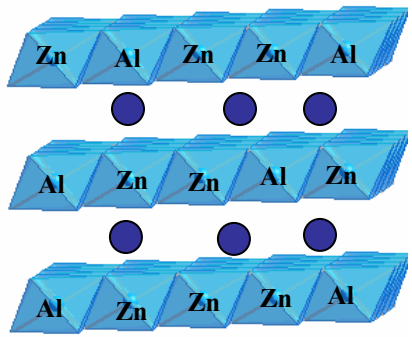

Paulhiac and Clause (1993)
D'espinose de la Caillerie et al., (1995)
Trainor et al. (2000)
Ford and Sparks (2000)

Phyllosilicates

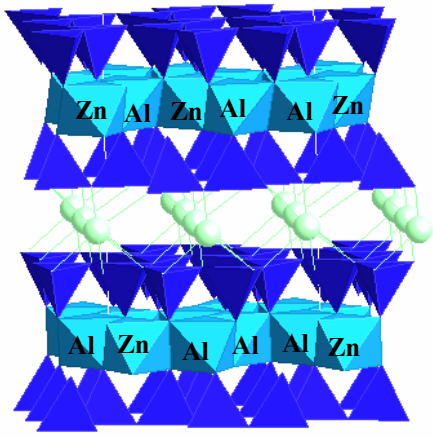

Manceau et al. (2000)
Shlegel et al. (2001)

Suggestions from Studies of Zn-Contaminated Soils

Neoformation of phyllosilicates — Manceau et al. (2000)

Zn sulfide and oxides and adsorption — Roberts et al. (2002)

Approach

EXAFS Spectroscopy and Selective Chemical Extractions

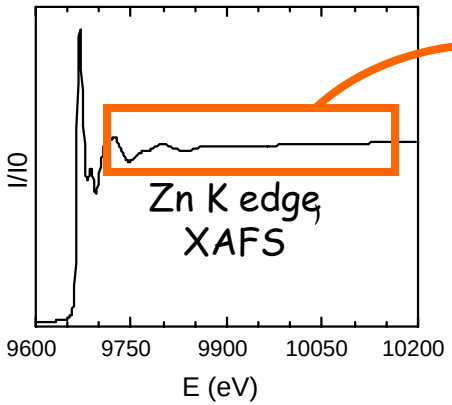

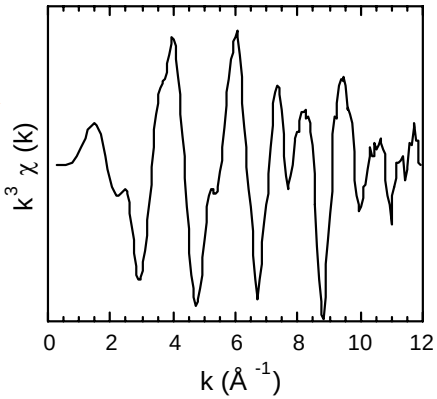

Model Comparisons

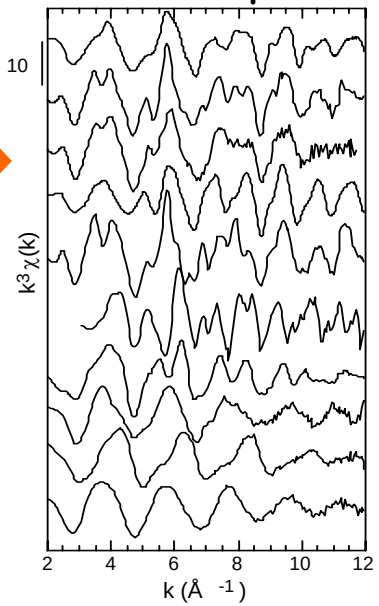

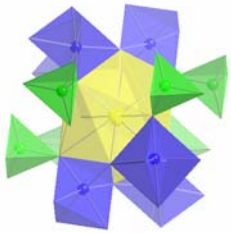

MOLECULAR SPECIATION

$CaCl_2$ 10^{-2} M : Zn exchangeable

HNO_3 4 10^{-1} M : Zn acid-soluble

(Juillot *et al.*, 2003) (SSRL)

French Soils from Evin-Malmaison

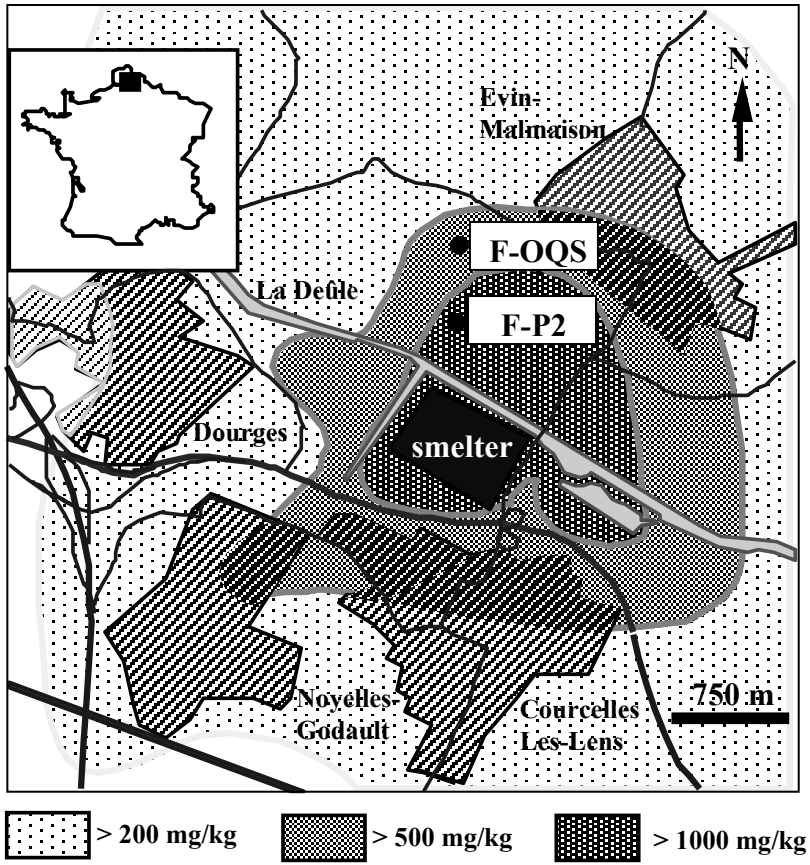

Soils contaminated by Pb/Zn from pyrometallurgical wastes

Soil 2: forested
1900 ppm Zn at surface

Soil 1: cultivated
600 ppm Zn at surface

(Juillot *et al.*, 2003)

French Soil 1: EXAFS before/after chemical extractions

(Juillot *et al.*, 2003)

Soil Profile

Fractions

% Zn extracted

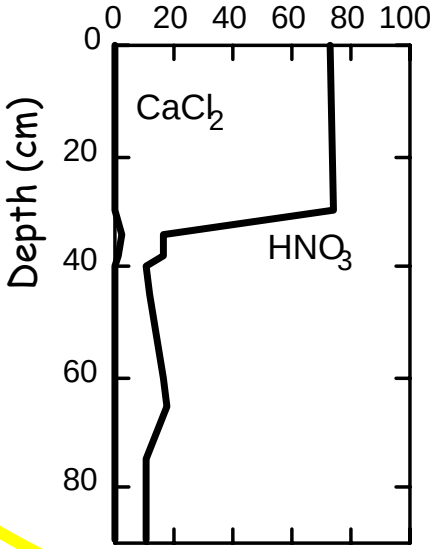

EXAFS

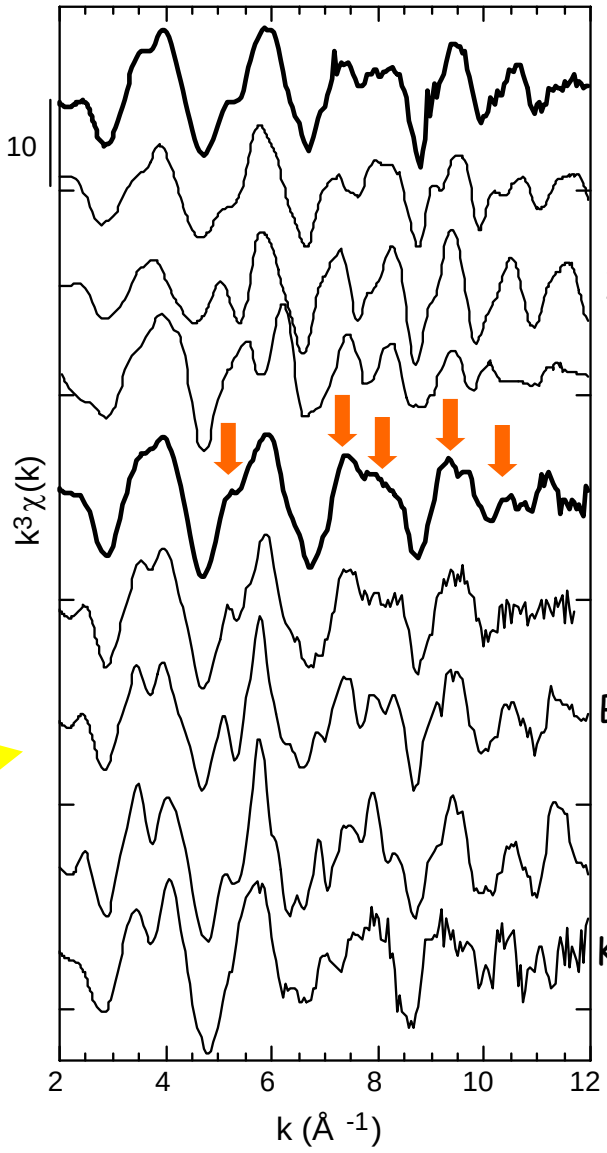

French Soil 1 not treated

Zn/Al LDH

$Zn_3Si_4O_{10}(OH)_2$ Talc

Zn/birnessite

French Soil 1 treated w/HNO_3

Illite (140ppm Zn)

Biotite (800ppm Zn)

Talc (4000ppm Zn)

Kaolinite (40ppm Zn)

Incorporation of zinc in LDHs and/or phyllosilicates

Evidence for incorporation of zinc in illite-type phyllosilicates after HNO_3

(SSRL)

French Soils: EXAFS before/after chemical extractions

(Juillot *et al.*, 2003)

Soil 1

70% Zn extracted by 0.4 M HNO_3

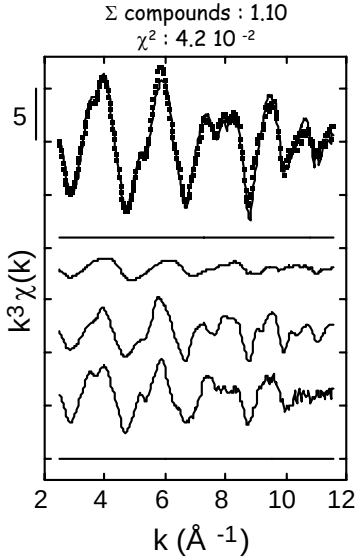

0%	Zn Humate	34%
22%	Zn/HFO	0%
51%	Zn/Al LDH	0%
38%	Zn Illite	62%
0%	Franklinite	5%

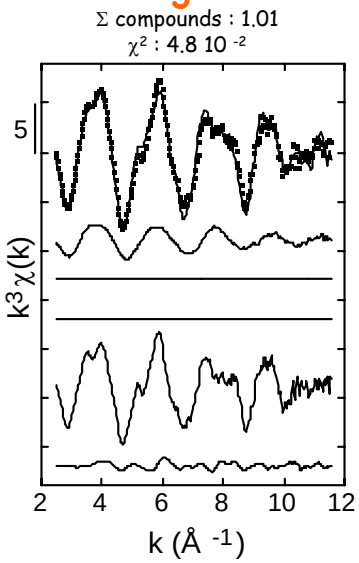

Soil 2

65% Zn extracted by 0.4 M HNO_3

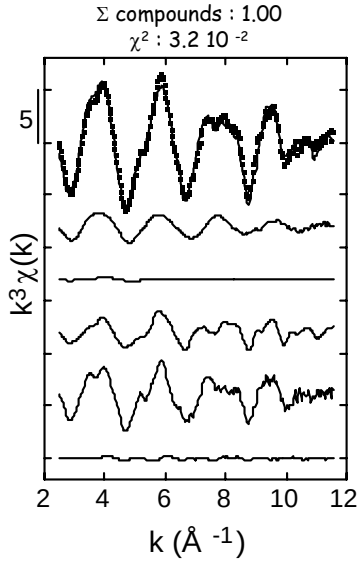

27%	Zn Humate	31%
3%	Zn/HFO	0%
31%	Zn/Al LDH	0%
32%	Zn Illite	43%
2%	Franklinite	24%

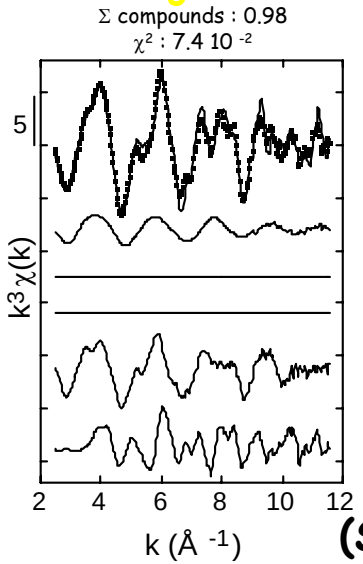

(SSRL)

XAFS Spectroscopic Study of Arsenic Speciation: Preliminary Results from Bangladesh Soils and Aquifer Sediments

Andrea Foster (USGS)

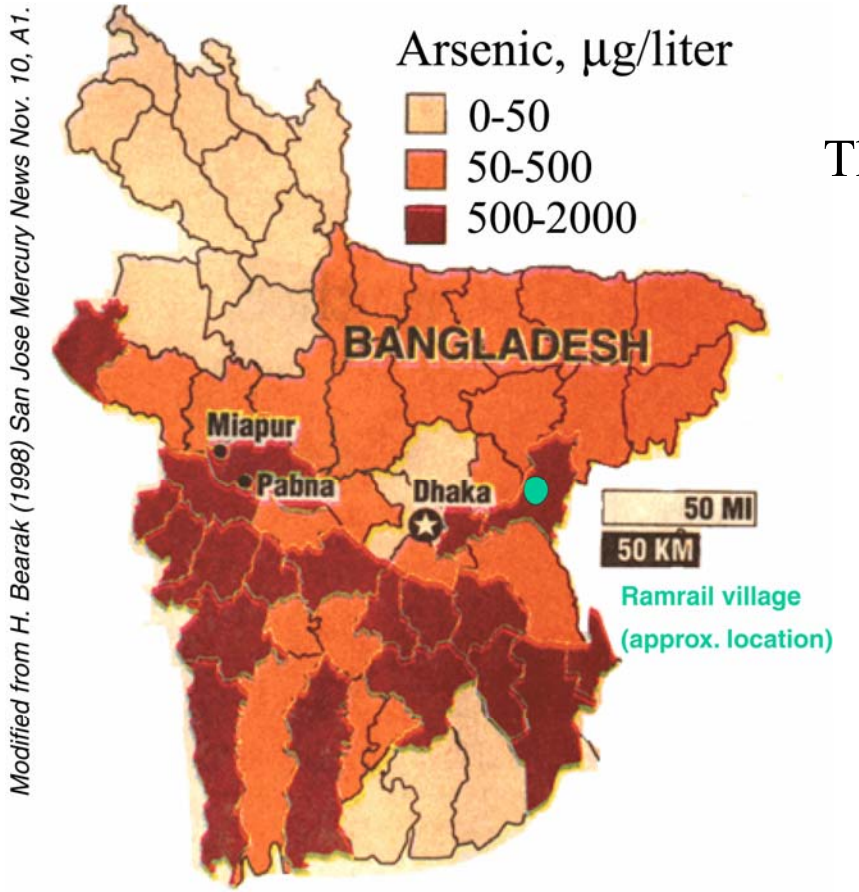

Modified from H. Bearak (1998) San Jose Mercury News Nov. 10, A1.

the southeastern part of the country (unaffected by As) is not shown in this graphic

The Problem: Widespread Contamination of Potable Water Supply

- Surface Water: contains pathogenic microorganisms, resulting in many deaths
- Groundwater: contains Arsenic (As)
- Endemic arsenicosis is common
- Estimated 25 million people drink water containing in excess of 50 µg/liter As (current U.S. EPA MCL is 10 µg/liter)
- World Health Organization standard: 10 µg/liter

USGS
science for a changing world

Generally Accepted Theories of Arsenic Cycling in Bangladesh

Erosion and Oxidation

$Fe(II)+As(0,III)+ O_2$

↓

FeOX-As(V)

Nepal River

Oxidation and Reduction during Deposition

FeOX-As(V)+Corg

↓↑

Fe(II)+As(III)

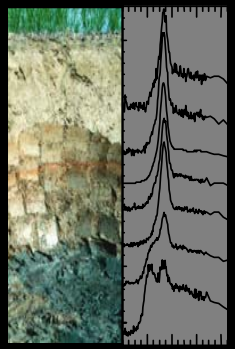

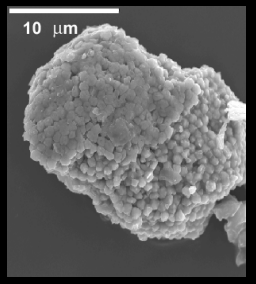

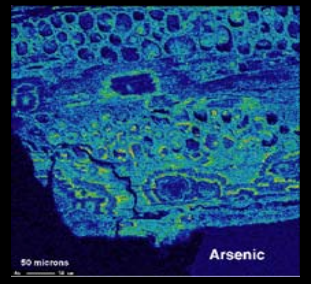

Sulfide formation near the sea

$Fe(II)+As(III)+S(II-)$

↓

$Fe(As)S_2$

Himalaya

Bangladesh
Deltaic Sediments

Indian Ocean

Disseminated FeOx

USGS

(Andrea Foster, USGS)

XANES Results: Bangladesh Soil Profile

A. Foster (USGS)

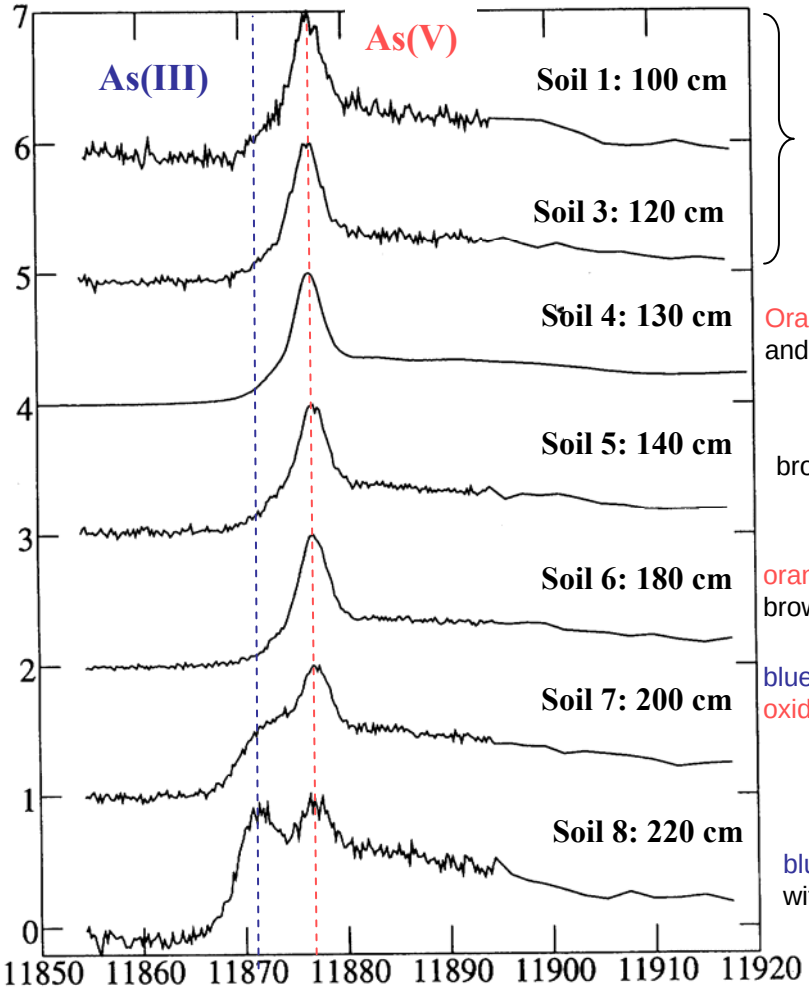

brown clayey silt

Orange Fe oxyhydroxide and brown clayey silt

brown clayey silt

orange brown coating on brown gray clayey silt

blue gray massive silty clay with iron oxide casts in burrows

blue-gray massive silty clay with some fine sand

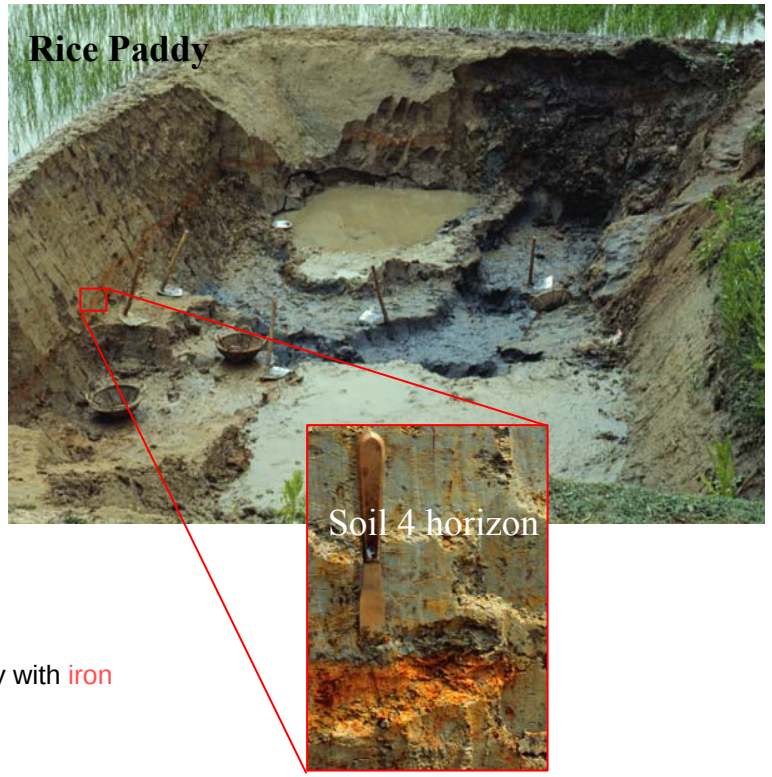

Surrounding soil layers have 4 ppm As
Fe-oxyhydroxide layer has 216 ppm As

XANES Spectra and Speciation of Bangladesh Aquifer Sediments

(Andrea Foster, USGS)

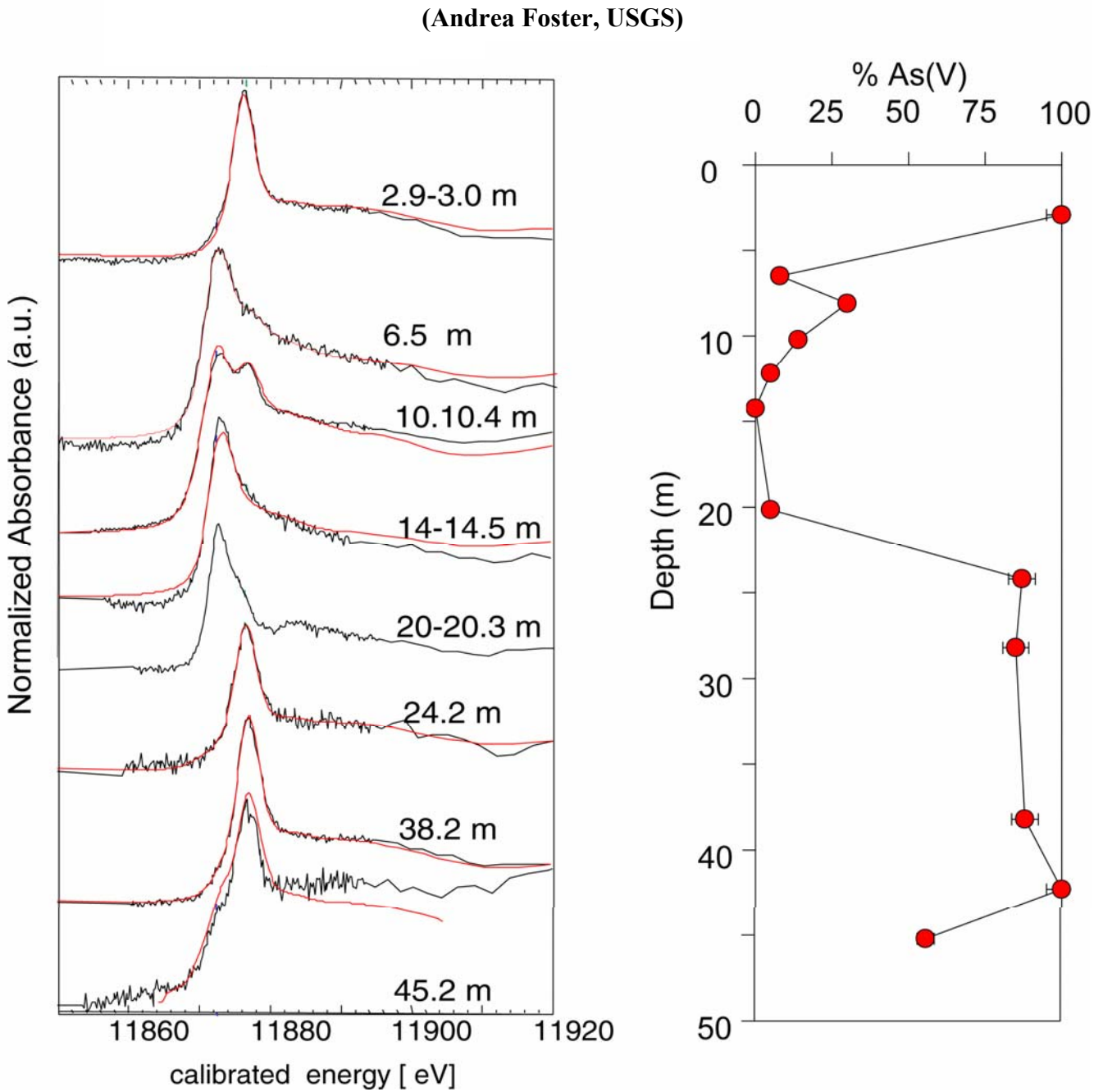

Selenium Contamination in the Central Valley of California: 1.5 Million Acres of Farmland at Stake

Article from the San Francisco Chronicle
Monday, February 21, 1994

Selenium Levels Rising At Kesterson Refuge

Poisons still found despite costly cleanup

By Lloyd Carter
Chronicle Correspondent

Los Banos, Merced County

More than five years after a costly cleanup of the Kesterson National Wildlife Refuge — where poisonous farm runoff killed thousands of migratory birds — potentially toxic levels of selenium are cropping up in coyotes, hawks and other species.

Annual monitoring tests ordered by the state as part of the $30 million cleanup show rising levels of selenium in a range of species, suggesting that the contaminant may be seeping back to the surface and entering the food chain.

"There is no indication that things are getting better at Kesterson," said Fish and Wildlife biologist Joe Skorupa, one of the agency's top selenium experts. "Are they just going to leave it the way it is and monitor it forever?"

According to the latest report, completed last month, half of the embryos collected last year from the nests of several bird species were dead, and hawks feeding at the fouled refuge showed selenium levels seven times higher than normal.

Although researchers found no deformities or other overt signs of selenium poisoning among the hawks, officials at the U.S. Fish and Wildlife Service say the latest data "seem to be indicating a

KESTERSON: Page A11 Col. 1

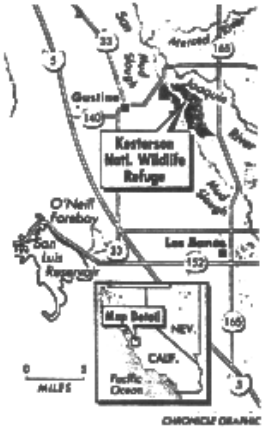

Eh-pH Diagram for Selenium

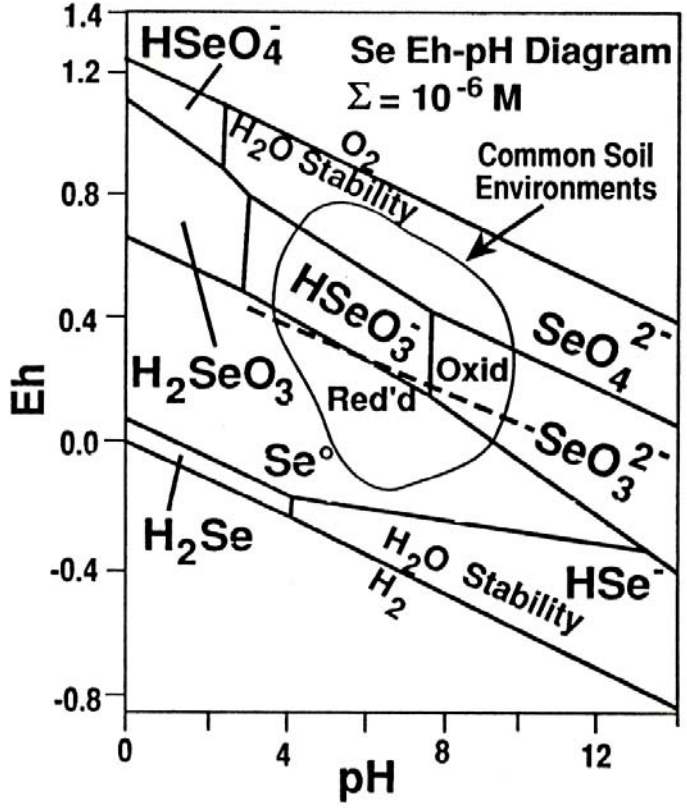

Selenium Speciation in Kesterson Reservoir Soil, CA

(Pickering, Brown, and Tokunaga, *Environ. Sci. Technol. 29*, 2456, 1995)

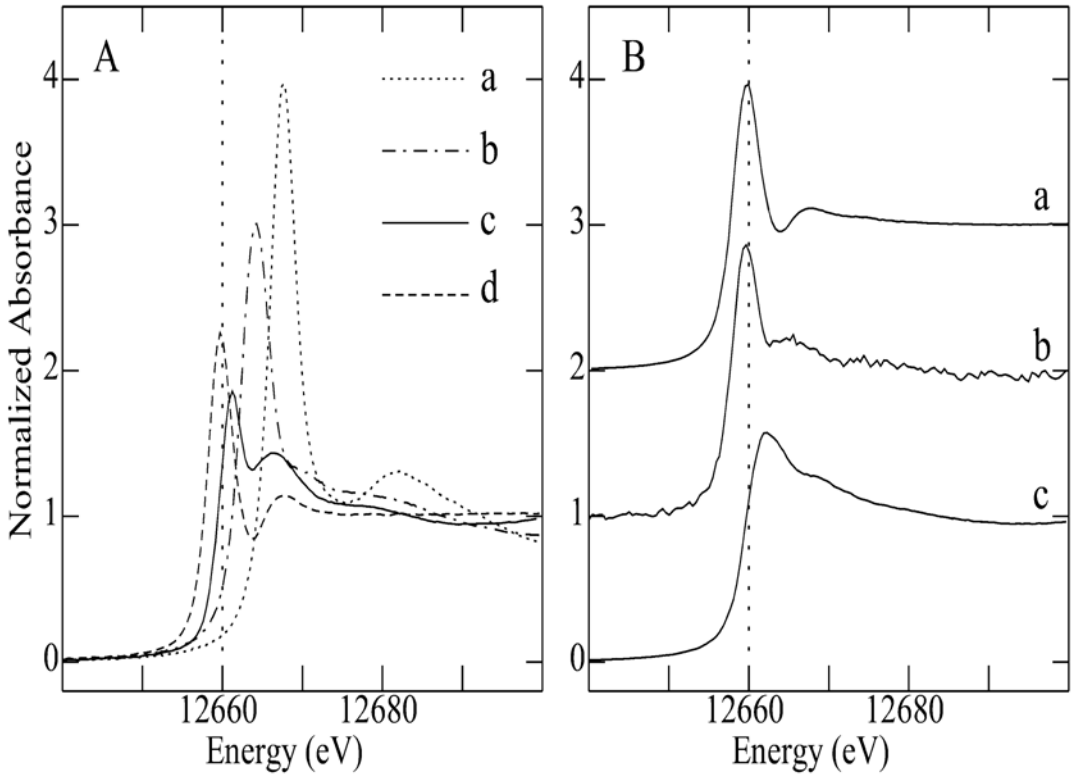

a: SeO_4^{2-} (aq)

b: SeO_3^{2-} (aq)

c: selenomethinine (aq)

d. elemental Se (red)

a. Se (340 ppm) in soil (0 to 0.5 m)

b. Se (40 ppm) in soil (0.05 to 0.15 m)

c. Se (500 ppm) in mushroom (*A. bernardii*)

Examples of Radionuclide Contamination in the United States

Tank Farms
Hanford Site, WA

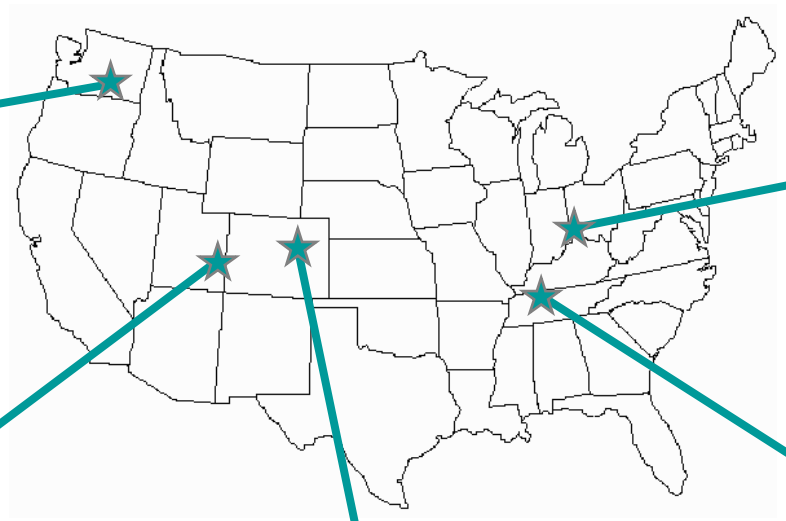

Waste Pits
Fernald, OH

Uranium Tailings Pile
near Moab, UT

Uranium Processing Facility
Rocky Flats, CO

Disposal Ponds
Oak Ridge, TN

Plutonium Contamination at Rocky Flats Environmental Technology Site, CO

- Between 1944 - 1988, the US produced approximately 100 metric tons Pu
- Sudden shutdown of plants stranded 26 tons of Pu in various intermediate steps of processing
- 2 decades of monitoring show that RFETS environment is contaminated with Pu from site operations

  - 903 pad oil leakage (5000 gl, 86g Pu)
  - 1957 glovebox/filter plenum fire
  - 1965 glovebox drain fire
  - 1969 foundry glovebox fire
  - 1974 control valve failure
  - process waste line leaks (14 mi)

  (Superfund National Priorities List)

- 90% of Pu contained in upper 10-12 cm of soil
- Local claims that large amounts of Pu migrates during spring rain events generated widespread public concern.

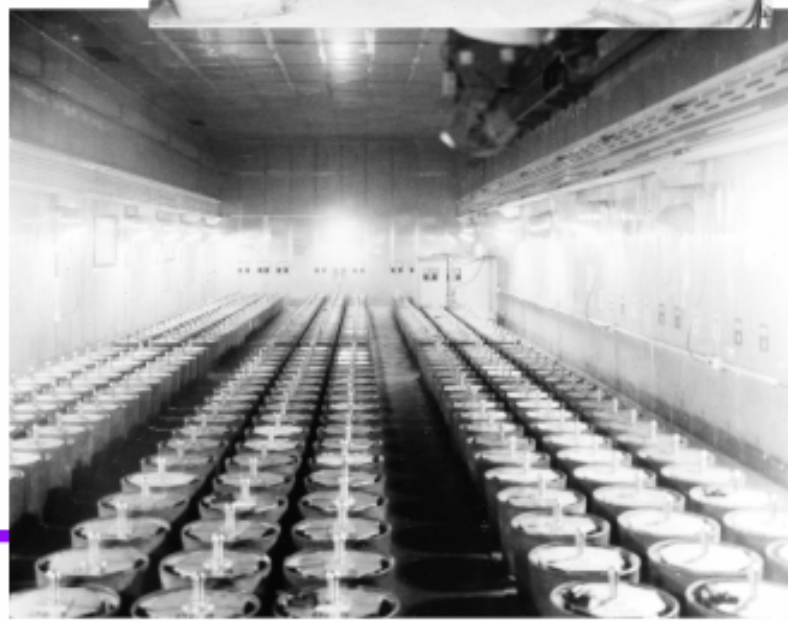

ITS
Los Alamos

Remediation of Pu-Contaminated Soils and Concrete at Rocky Flats Environmental Site, CO

(Neu *et al.* 1999)

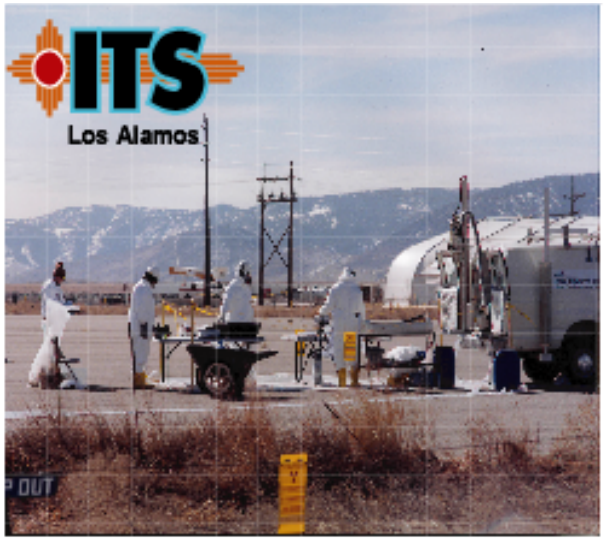

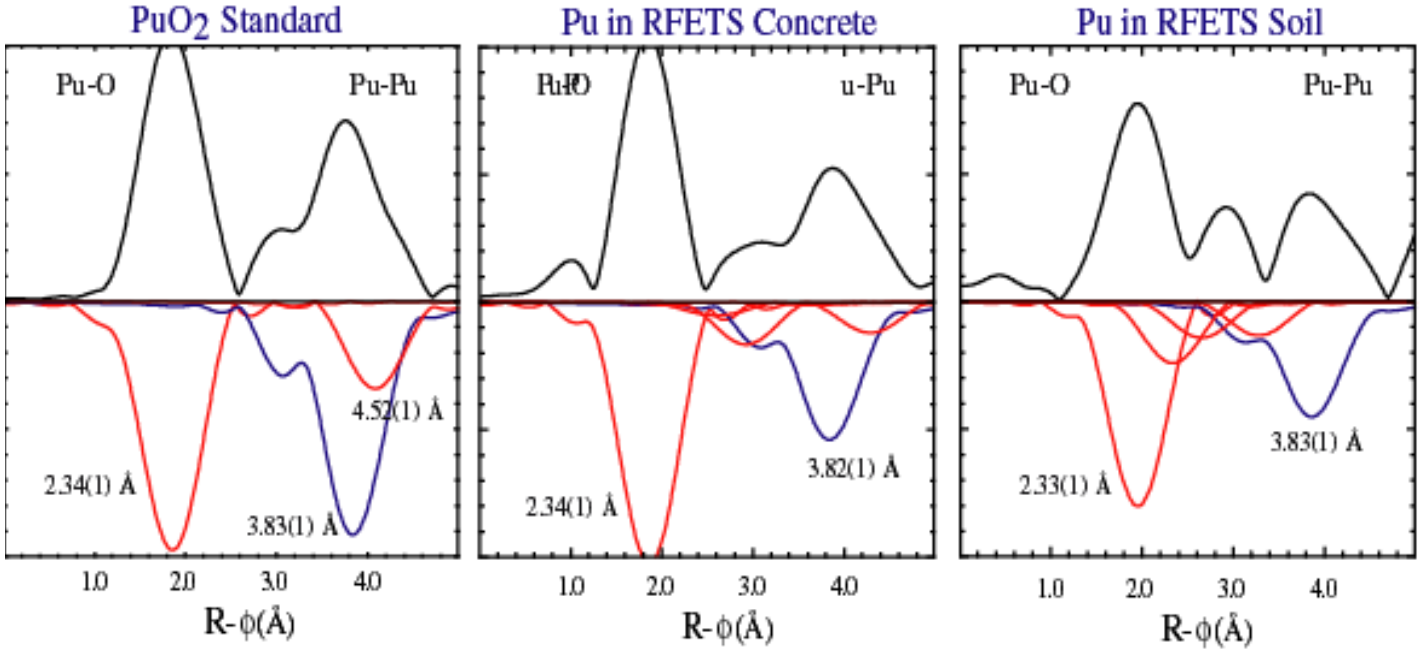

(SSRL)

Pu L_{III}-XANES Spectra of RFETS Soil and Concrete Compared with Model Compounds

(Conradson, *Appl. Spectros. 52*, 252A, 1998)

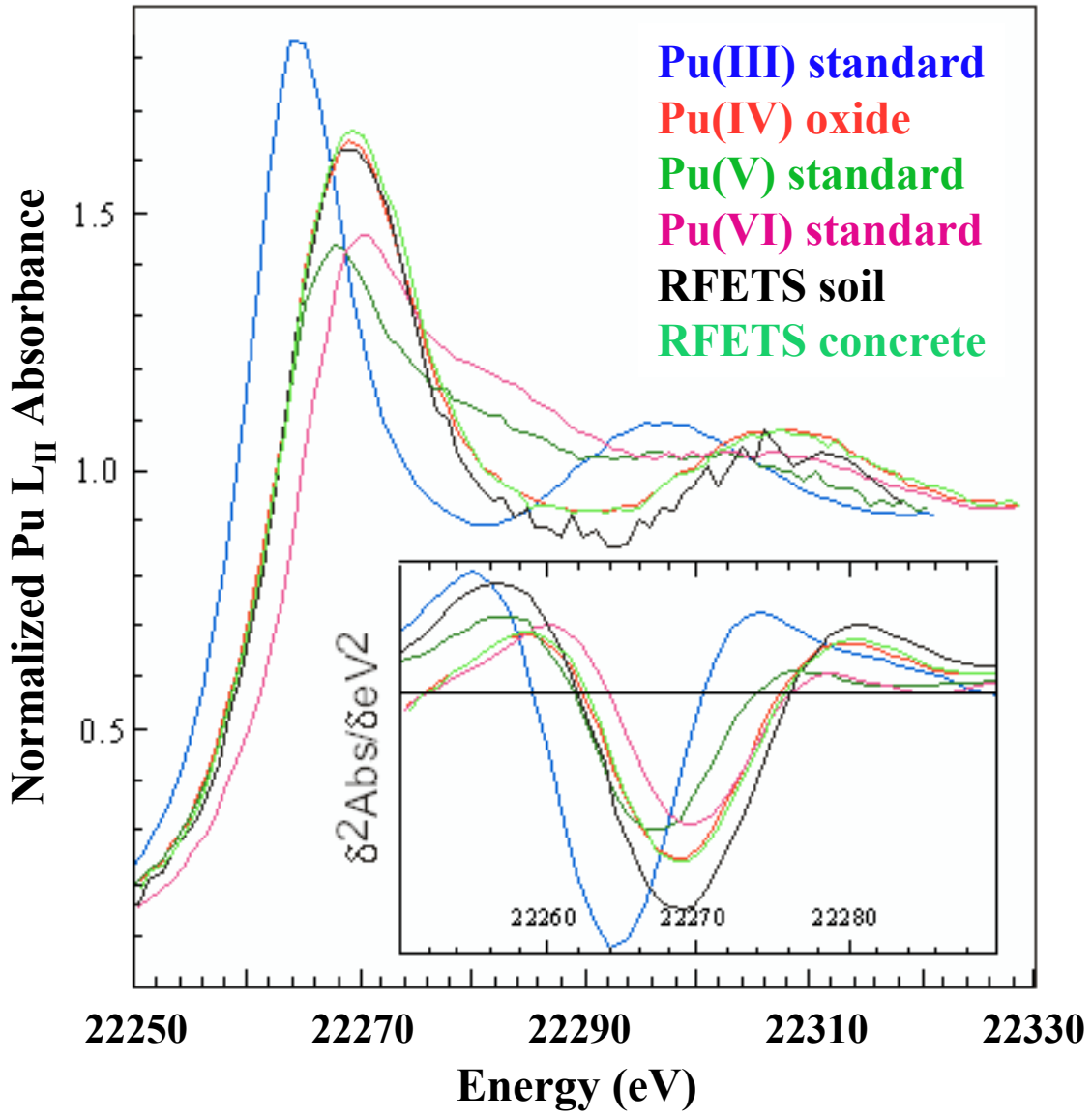

(SSRL)

The Hanford Site

- WW II and Cold War site of Pu production for nuclear weapons
- Reactors operated from 1944 to 1990

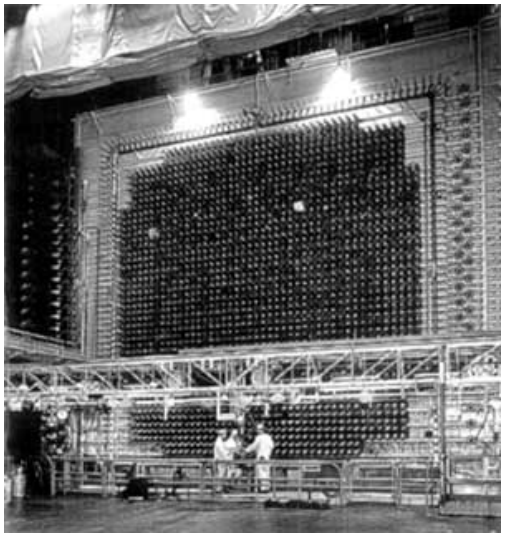

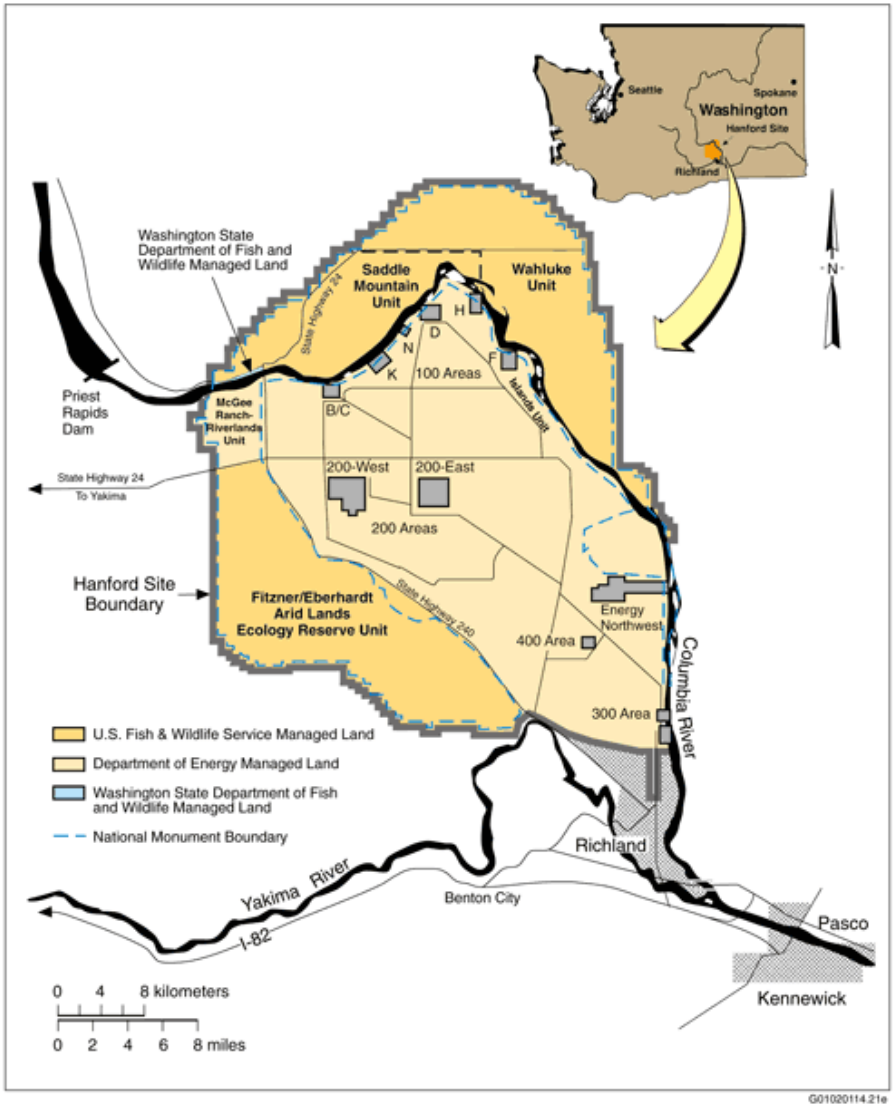

- Located on Columbia River
  - A source of cooling water

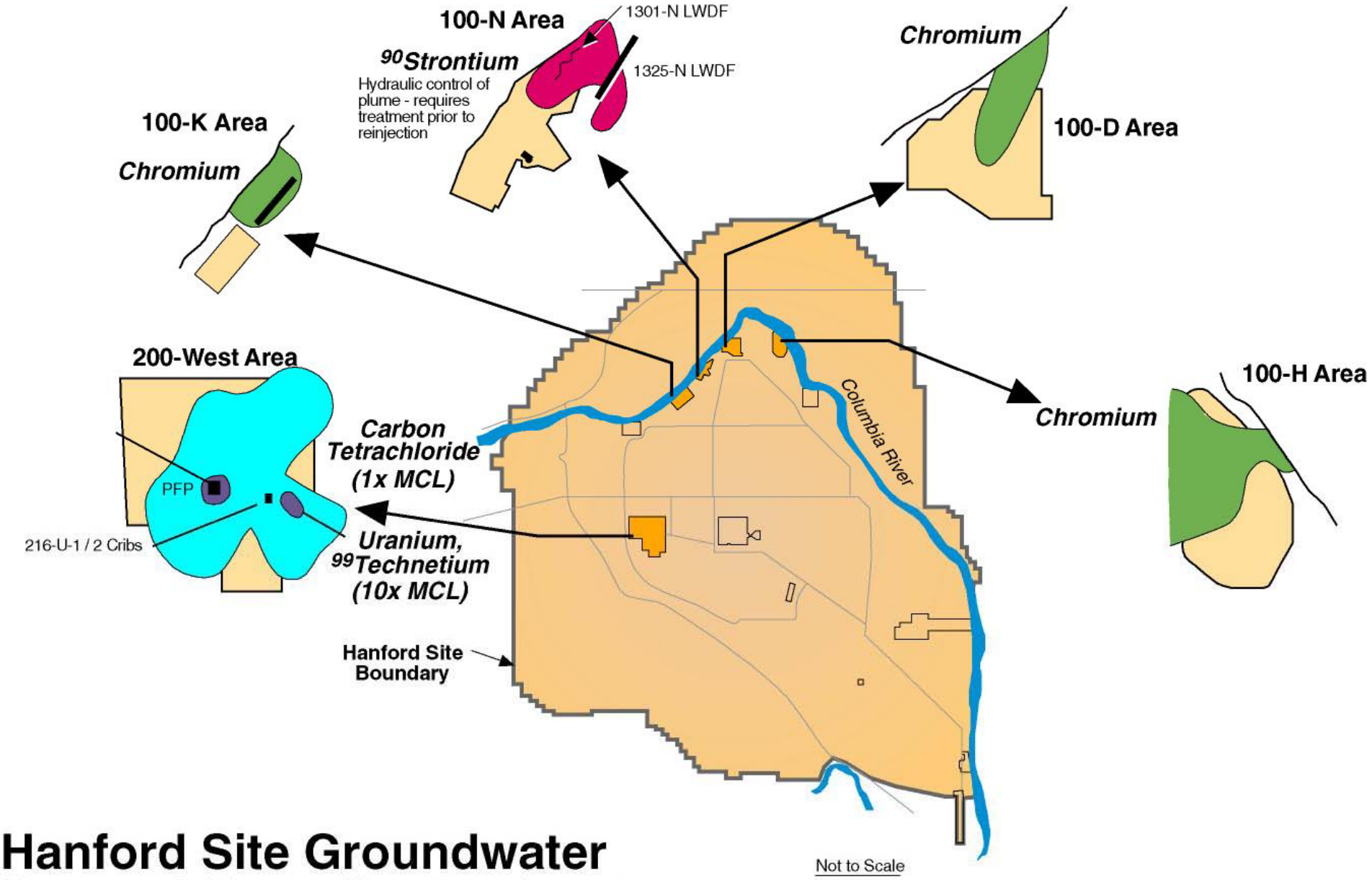

Hanford Site Groundwater Pump & Treat Contaminant Plumes

Hanford 200 Area Tank Farms

- Extraction of Pu required dissolution of the fuel rods followed by chemical precipitation of Pu phases
- Result was massive quantities of high-level nuclear waste
- 500,000 to 1,000,000 gal tanks were created to store the waste products.

Cr Speciation in the Hanford Tank Farm Vadose Zone

(Zachara *et al.*, *Geochim. Cosmochim. Acta* 68, 13, 2004)

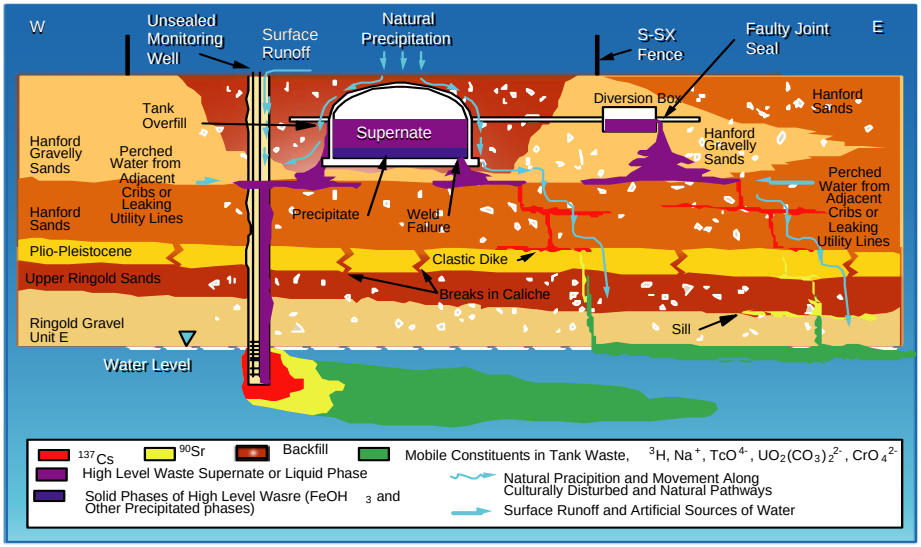

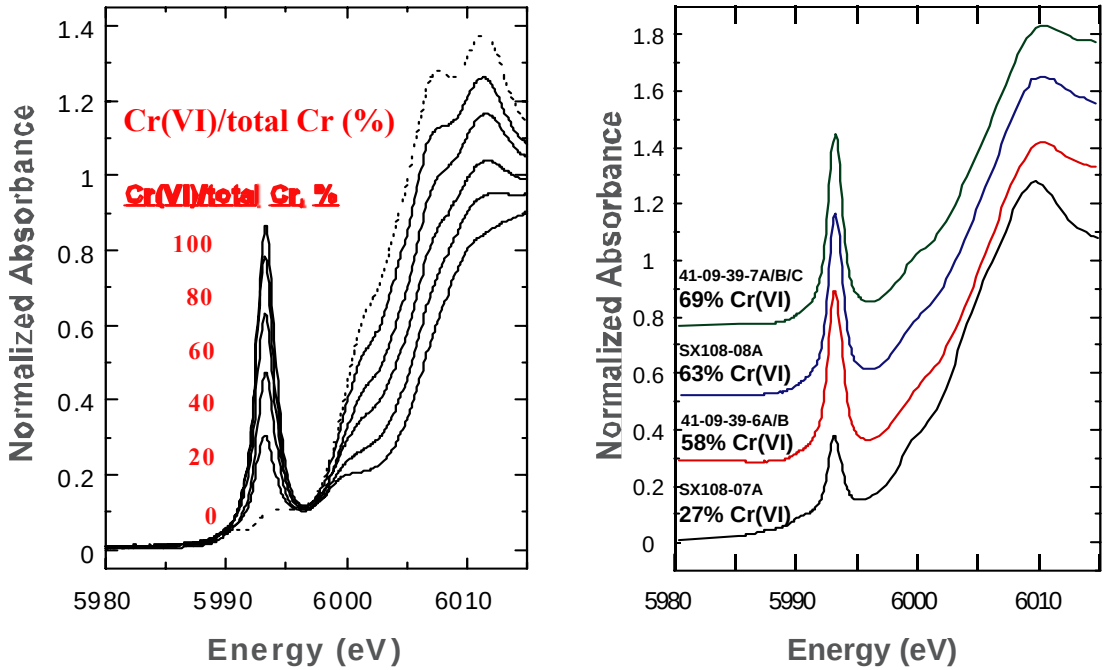

(SSRL)

Synchrotron-Based Studies of Uranium Speciation in Contaminated Sediments and Related Model System

Leakage at Tank BX-102

- **300,000 L of waste containing 7 to 8 metric tons of U spilled in 1951**
- **Waste composition**
  - **pH 10**
  - **0.5 M uranium**
  - **0.6 M carbonate**
  - **0.36 M phosphate**
  - **3.0 M sodium**
  - **Numerous fission products**
- **Extensive vadose zone plumes developed**

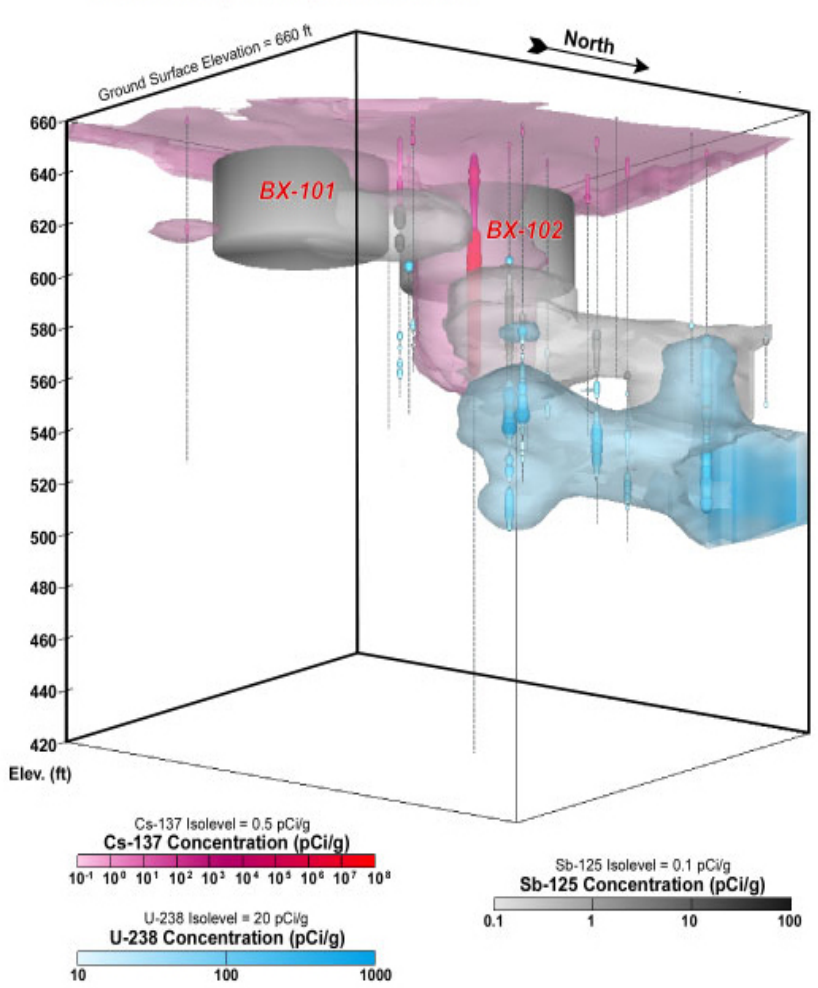

A.W. Pearsons (2000) *Hanford Tank Farms Vadose Zone Monitoring Project, BX Tank Farm Addendum.* U.S. Department of Energy GJO-98-40-TARA, GJO-HAN-19

What is the speciation of uranium in the Hanford Vadose zone?

Adsorbed to Mineral Surfaces

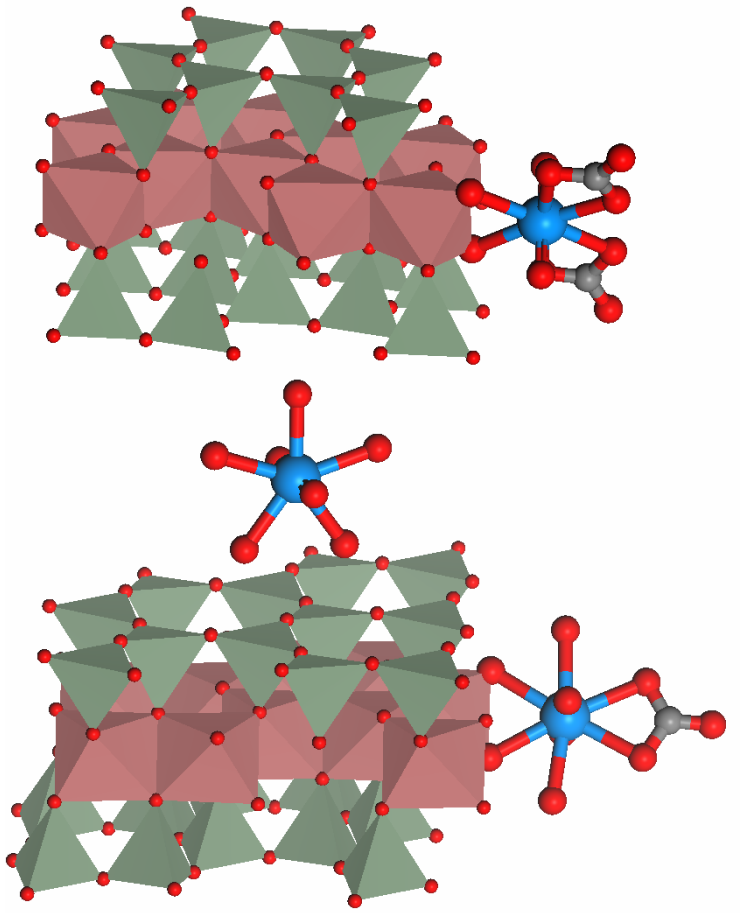

Uranyl and uranyl carbonate complexes sorbed to clay

Precipitated as a Solid Phase (if so, how insoluble?)

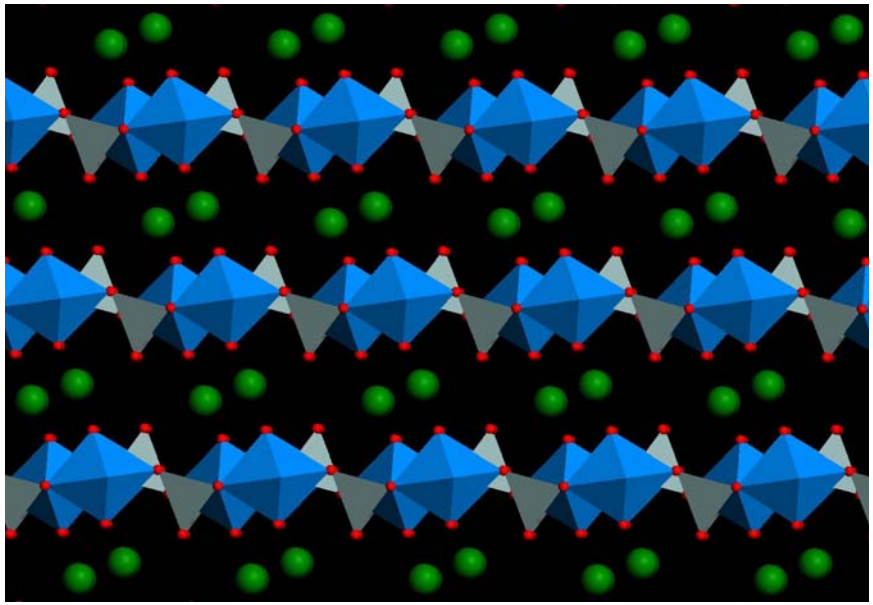

Na-Boltwoodite ($NaUO_2SiO_3OH \cdot 1.5H_2O$)

Comparison of the Raw EXAFS Spectra of BX-102 Slant Bore Hole Samples

(Catalano *et al.*, *Environ. Sci. Technol. 38*, 2822, 2004)

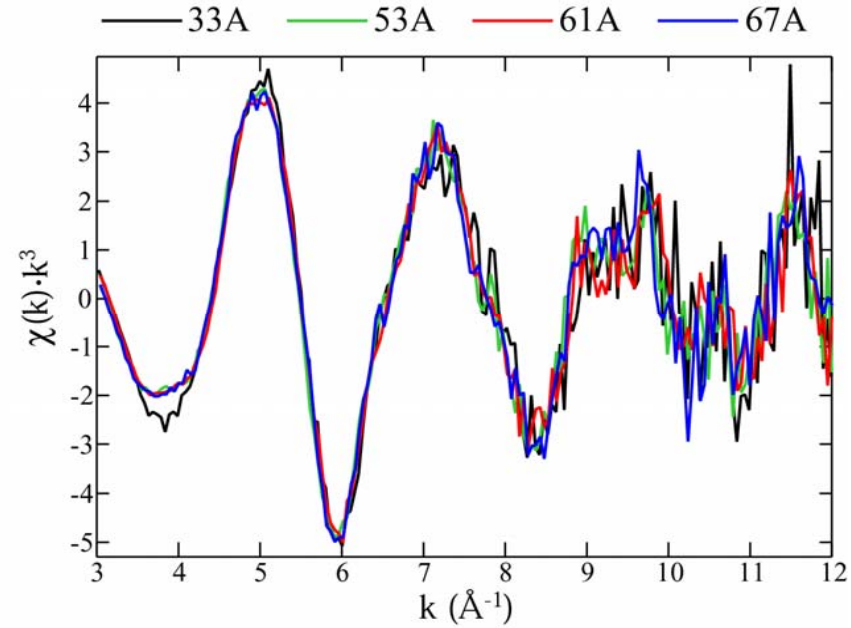

- The spectra are essentially identical
  - All major features present in all 4 spectra
- The striking similarity of spectra suggests there is only one primary phase present

(SSRL)

EXAFS as a Fingerprint of U(VI)-containing Phases

(Catalano *et al.*, *Environ. Sci. Technol. 38*, 2822, 2004)

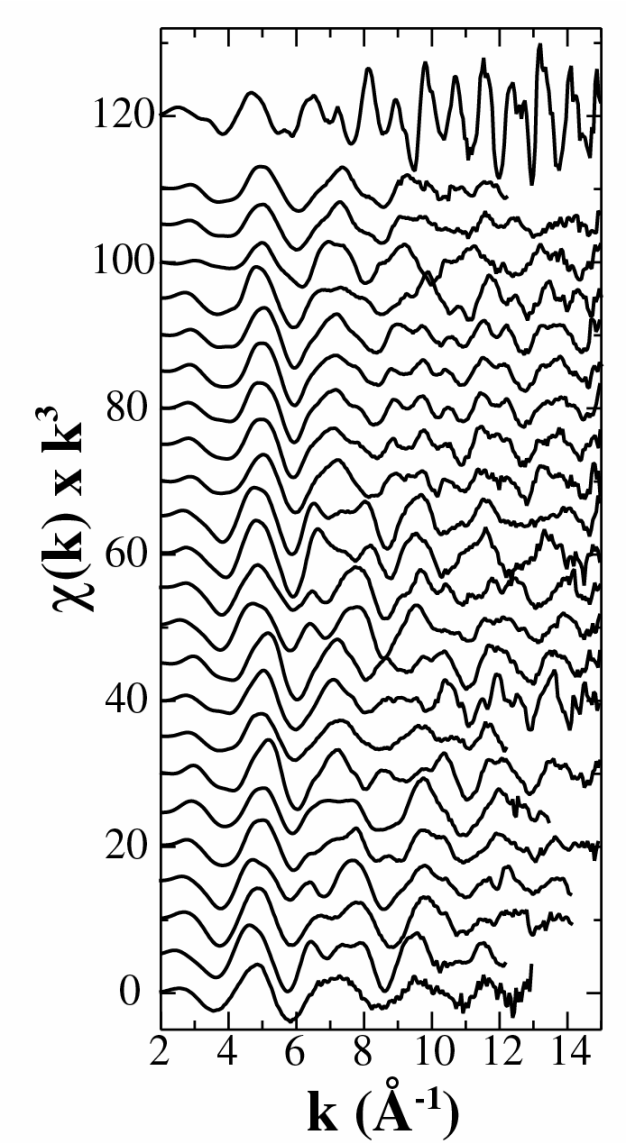

Name	Chemical Formula	
Uraninite	UO_{2+x}	
Schoepite, syn	$(UO_2)_8O_2(OH)_{12}\cdot 12H_2O$	U(VI)-hydroxides
Compreignacite	$K_2(UO_2)_6O_4(OH)\cdot 7H_2O$	
Clarkeite, syn	$Na_2U_2O_7\cdot xH_2O$	
Soddyite, syn	$(UO_2)_2SiO_4\cdot 2H_2O$	U(VI)- silicates
Uranophane	$Ca(UO_2)_2(SiO_3OH)_2\cdot 5H_2O$	
Boltwoodite, syn	$KUO_2SiO_3OH\cdot 1.5H_2O$	
Sklodowskite	$Mg(UO_2)_2(SiO_3OH)_2\cdot 5H_2O$	
Cuprosklodowskite	$Cu(UO_2)_2(SiO_3OH)_2\cdot 6H_2O$	
Kasolite	$PbUO_2SiO_4\cdot H_2O$	
Liebigite	$Ca_2UO_2(CO_3)_3\cdot 11H_2O$	U(VI)- carbonates
Sodium uranyl carbonate	$Na_4UO_2(CO_3)_3\cdot xH_2O$	
Rutherfordine	UO_2CO_3	
Zellerite	$CaUO_2(CO_3)_2\cdot 5H_2O$	
Saleeite	$Mg(UO_2)_2(PO_4)_2\cdot 8H_2O$	U(VI)- phosphates
Metaautunite	$Ca(UO_2)_2(PO_4)_2\cdot 6H_2O$	
Phosphuranylite	$KCa(H_3O)_3(UO_2)_7(PO_4)_4O_4\cdot 8H_2O$	
Metatorbernite	$Cu(UO_2)_2(PO_4)_2\cdot 6H_2O$	
Uranyl hydrogenphosphate	$UO_2HPO_4\cdot 2H_2O$	
Uranyl orthophosphate	$(UO_2)_3(PO_4)_2\cdot 4H_2O$	
Uranyl nitrate	$UO_2(NO_3)_2\cdot 6H_2O$	
Uranyl, aqueous	$UO_2^{2+}{}_{(aq)}$	
Uranyl-carbonato, aqueous	$UO_2(CO_3)_3^{4-}{}_{(aq)}$	
Uranyl adsorbed on smectite	S-UO_2^{2+} (Fe-UO_2CO_3 ?)	

(SSRL)

Linear Combination Fitting of EXAFS

(Catalano *et al.*, *Environ. Sci. Technol. 38*, 2822, 2004)

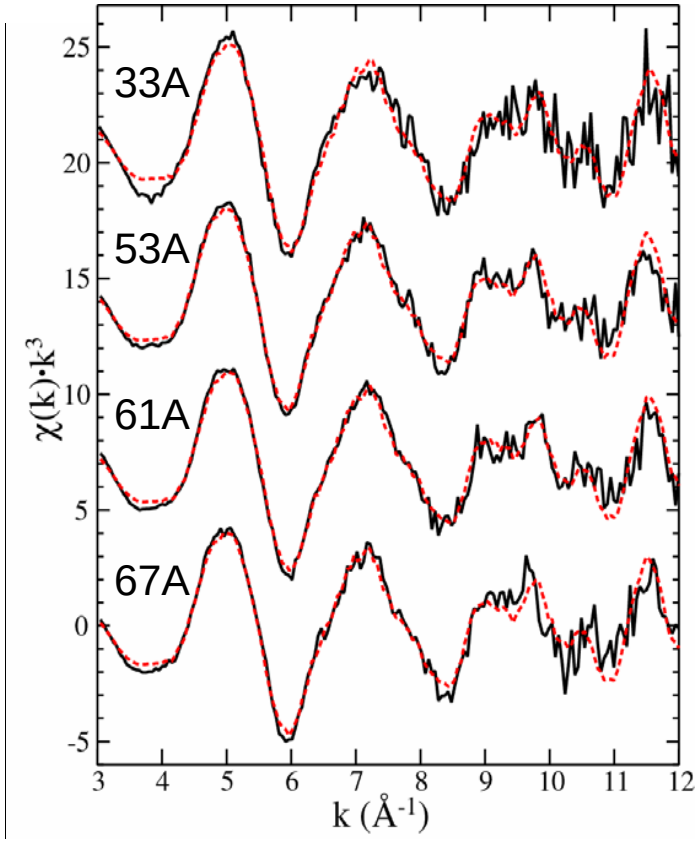

102% Uranophane
residual = 0.674

99% Uranophane
residual = 0.240

98% Uranophane
residual = 0.212

100% Uranophane
residual = 0.348

- **All samples appear to be ~100% Uranophane**

(SSRL)

Na-Boltwoodite vs. Uranophane

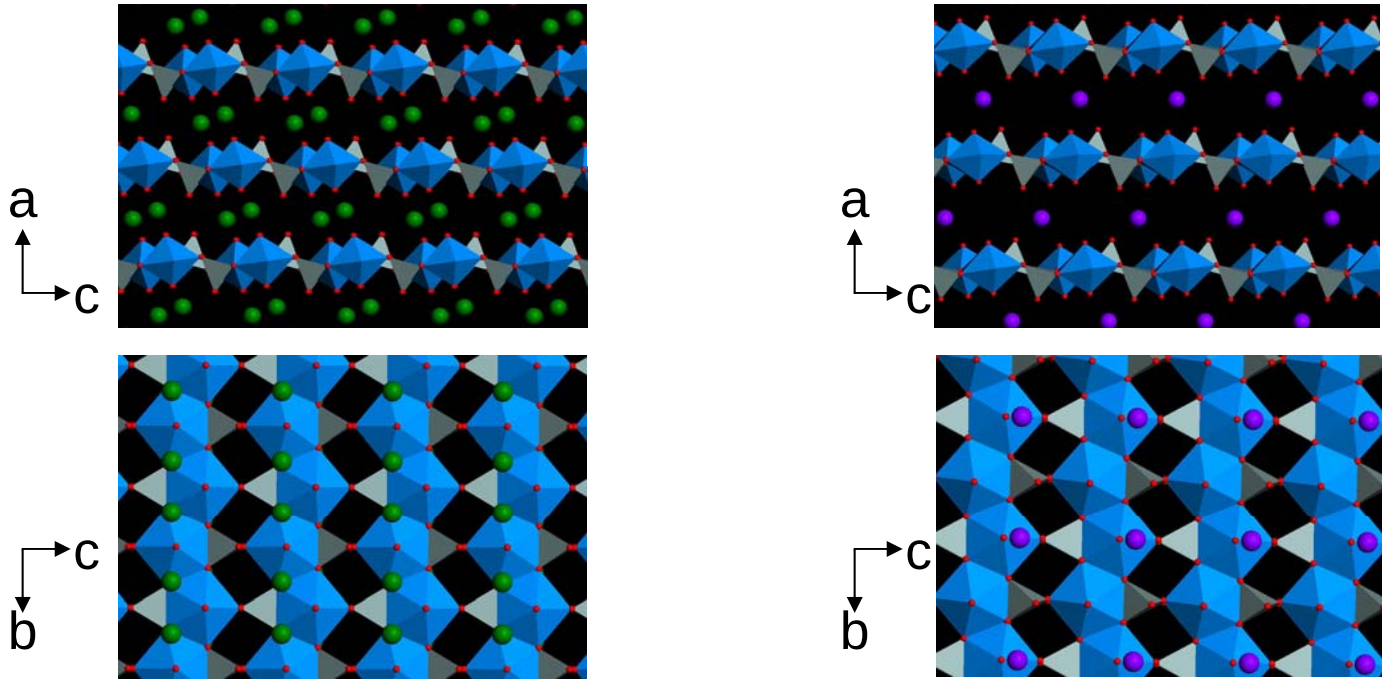

- **Waste stream and sediment chemistries suggest these are the most likely phases from the uranophane group**
- **Crystal structures only differ in the hydrated interlayer**
  - **While EXAFS spectra are identical, XRD patterns differ significantly because of difference in spacing along a axis**
- **Solubilities of uranophane and Na-boltwoodite differ substantially:**
  - **Uranophane up to 3 times more soluble than Na-boltwoodite in local Hanford porewater**
  - **Uranophane up to 1000 times more soluble than Na-boltwoodite in a Na-rich, Ca-pore solution**

U Precipitate Distribution and Morphology

(McKinley *et al*., 2004, unpublished)

- **U "hotspots" found using μSXRF**
- **Then analyzed by SEM and EPMA**
- **0.1 by 1 mm grains**
- **Acicular habit**
- **Form clusters in cracks in silicates**

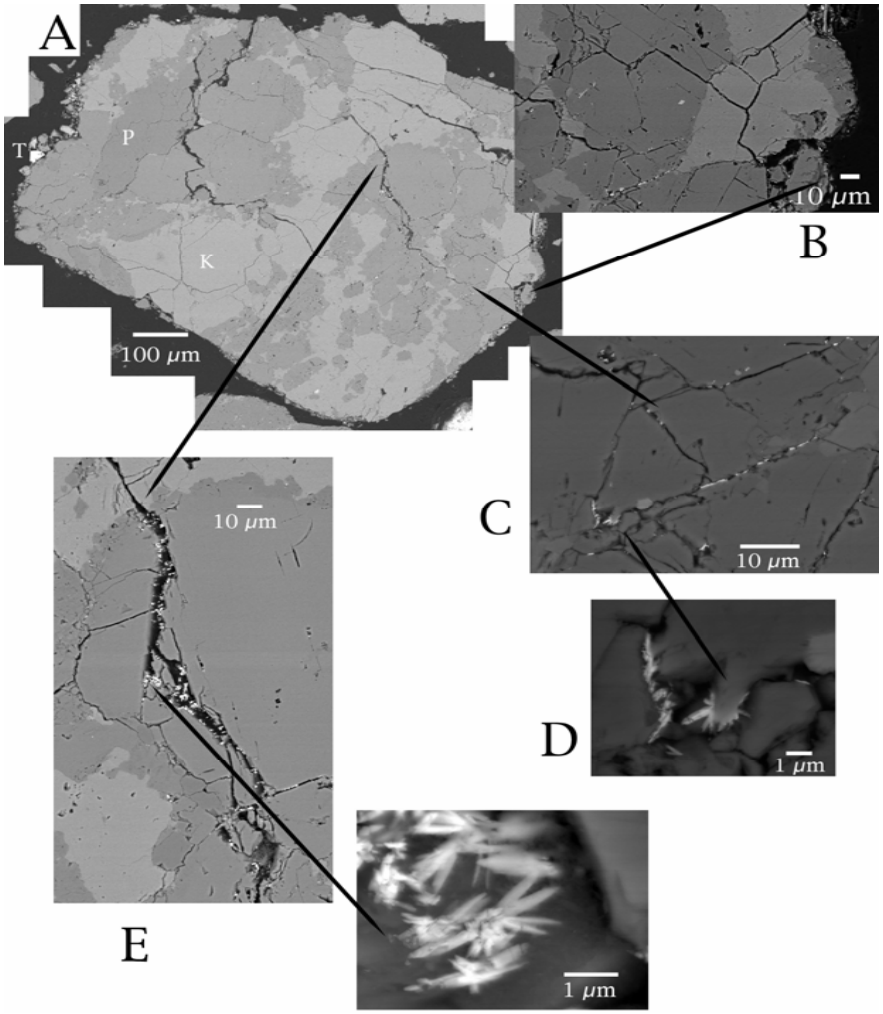

BSE images of U-silicate microprecipitates in cracks inside of a feldspar grain

μXRD Data Collection and Processing

(Catalano *et al.*, *Environ. Sci. Technol. 38*, 2822, 2004)

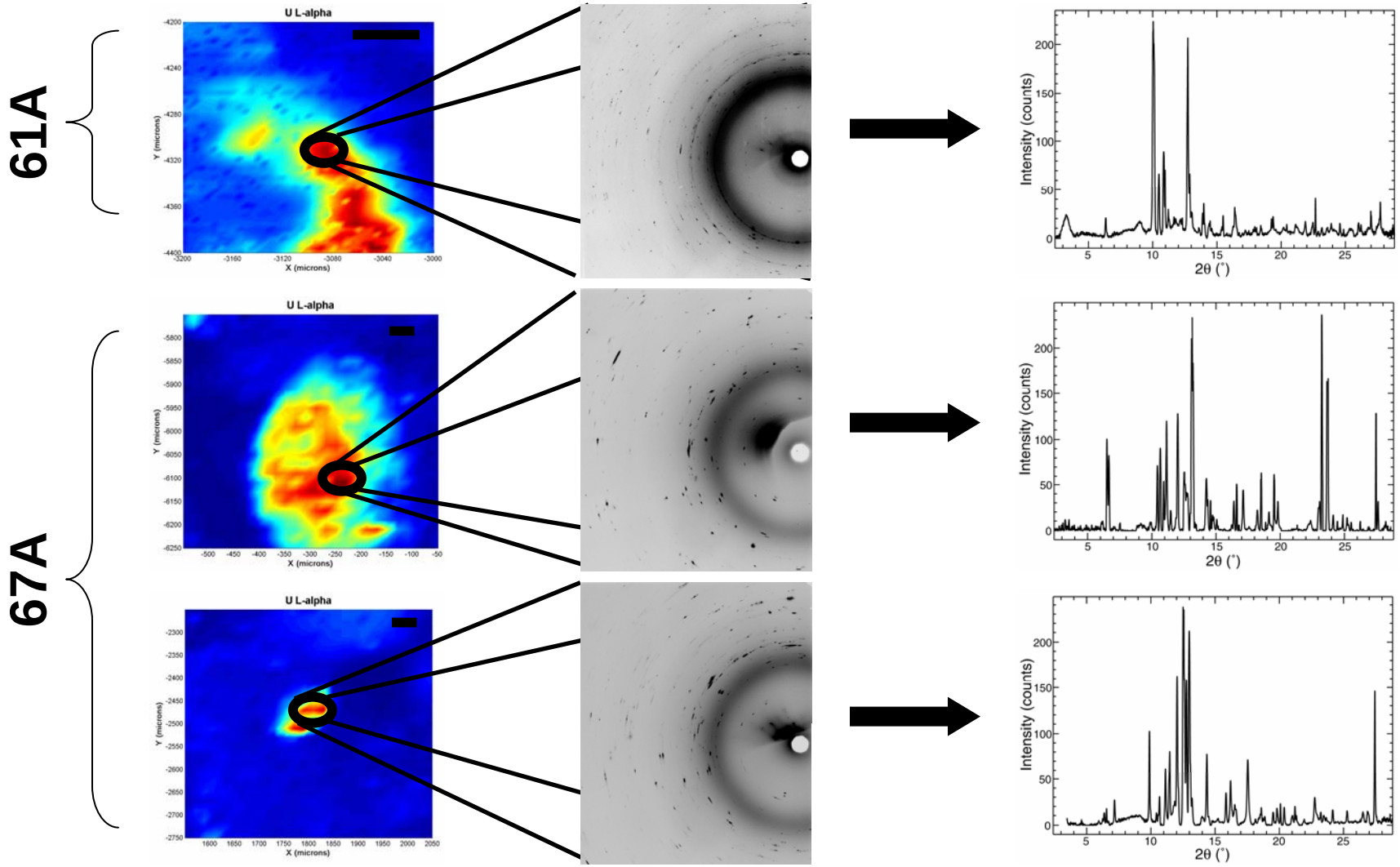

μSXRF map of U distribution using U L_a fluorescence

Raw μXRD pattern of 20 x 20 μm spot

Integrated, background-subtracted μXRD patterns

(APS)

Strongest Diffraction Lines of Uranophane Group

(Catalano *et al.*, *Environ. Sci. Technol. 38*, 2822, 2004)

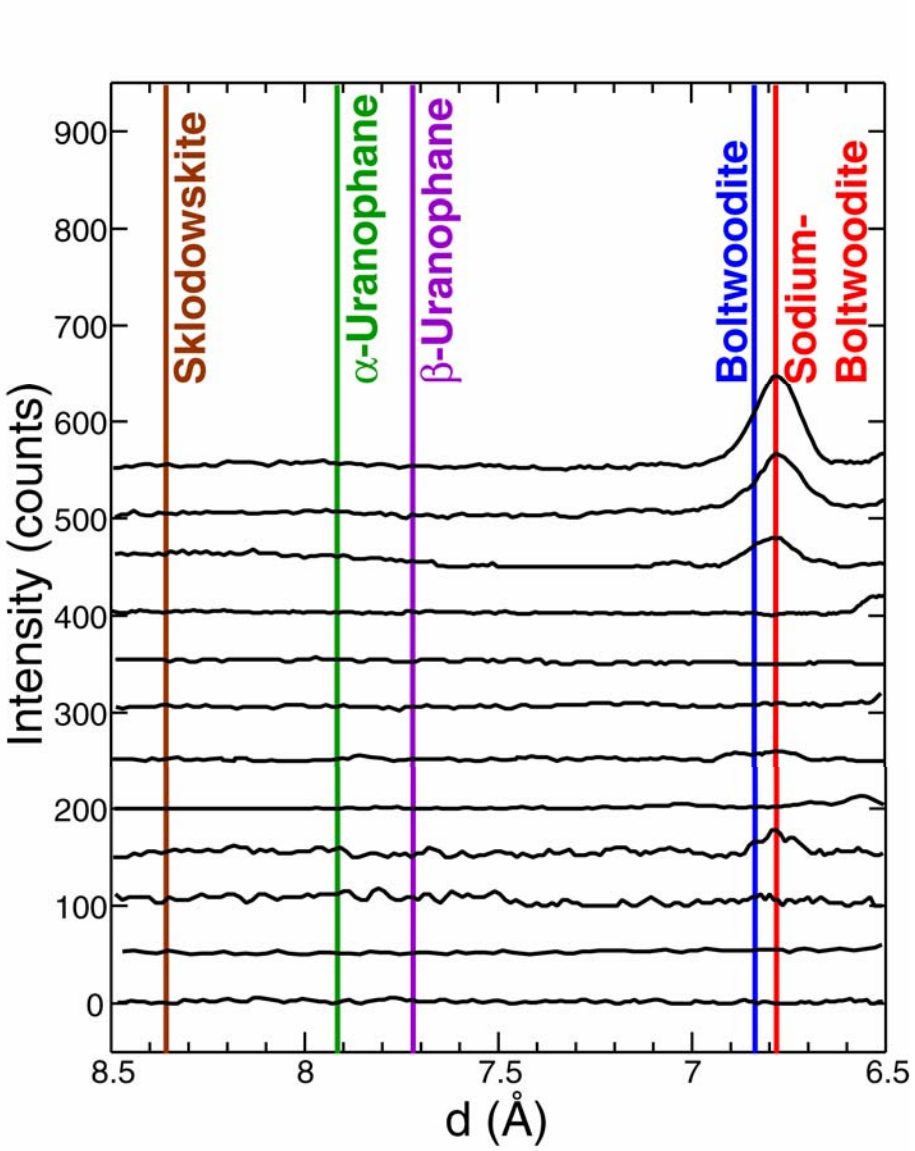

- **Reflections from Na-boltwoodite observed clearly in 4 patterns**
- **Reflections from other uranophane group minerals were not observed**

(APS)

U Speciation in Area 200 at Hanford: Conclusions

(Catalano *et al.*, *Environ. Sci. Technol. 38*, 2822, 2004)

- **The following speciation information was derived:**
  - **XANES demonstrated that uranium occurs in these samples in the form U(VI)**
  - **μSXRF and EPMA showed U-silicates have precipitated as small (~1 mm) acicular crystals in cracks in feldspar grains**
  - **EXAFS demonstrated that these precipitates are minerals from the uranophane group of uranyl silicate minerals**
  - **μXRD confirmed the presence of Na-boltwoodite; other uranophane group minerals were not observed**
- **Future dissolution of these precipitates may provide a continuous source of U to the local Hanford porewater**
- **By using multiple bulk and microbeam x-ray methods, we were able to identify the specific uranium phase present in these samples**

In-situ Reactive Barrier at Fry Canyon, UT

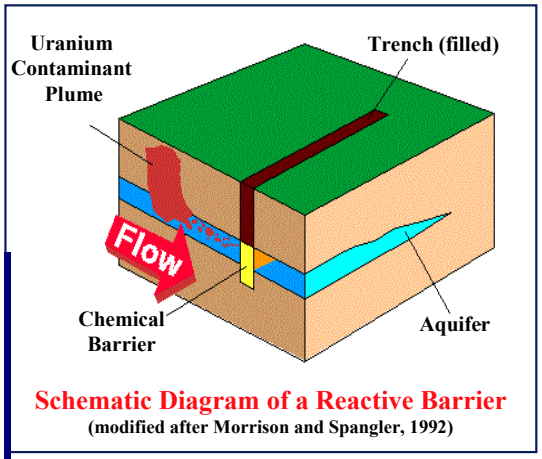

Schematic Diagram of a Reactive Barrier
(modified after Morrison and Spangler, 1992)

- U(VI)-contaminated groundwater
- Intercepted by reactive barrier
- Fill material (apatite) releases PO_4
- *Hypothesis: precipitation of U(VI)-phosphate (autunite) attenuates U(VI)*

Synchrotron-based XAFS and XRD

- XAFS: inconsistent with local structure in apatite and U(VI)-phosphate
- XRD: No U-containing crystalline phases; U solid solution in apatite not observed
- TEM & Filtration: no colloidal U-phases
- *U(VI) attenuated by chemisorption on apatite surfaces*

Installation of Fry Canyon Trench

SEM Images of Bone-Char Pellets

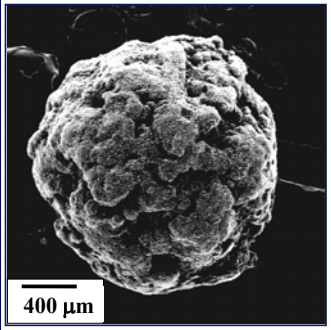

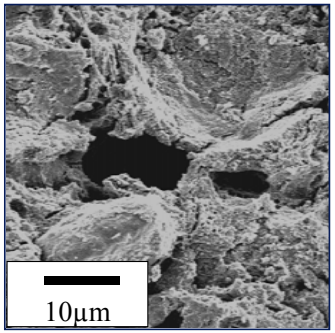

EXAFS-derived local structure of U(VI) on apatite

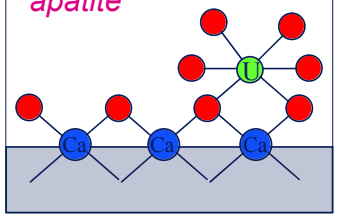

Impacts barrier design, cost, maintenance, life span

(Fuller *et al.*, *Environ. Sci. Technol. 36*, 158, 2002)

Future Synchrotron Radiation Developments and Their Potential Impact on Research in Low-T Geochemistry and Environmental Science

- **A number of 3rd-generation SR sources exists or will come on line over the next few years (*e.g.*, Diamond in the U.K., Soleil in France, the Canadian Light Source in Saskatoon, Boomerang in Melbourne, Australia)**

- **These high brightness light sources will result in new beam line stations devoted to μXAFS, μXRF, μXRD, STXM, and other X-ray microscopic and spectromicroscopy methods.**

- **Anticipated growth areas:**
  - ⇒ **Combined μXAFS and μXRD studies of complex multi-phase samples**
  - ⇒ **X-ray microscopy and spectromicroscopy studies of natural organics, biological samples, and nanoscale phases**
  - ⇒ **XSW and X-ray reflectivity studies of interfacial processes**
  - ⇒ **Soft X-ray/VUV photon in-photon out methods for *in situ* studies of "wet" samples**
  - ⇒ **SR-based IR spectroscopy studies of organics on mineral surfaces**

Future Synchrotron Radiation Developments and Their Potential Impact on Research in Environmental Science

- **4th-generation synchrotron light sources are now/will be available in the U.S. (SPPS and LCLS) and in Germany (TESLA) by 2009-2011**

- **These light sources will produce highly coherent, very short pulses (< 100 femtoseconds) containing on the order of 10^{13} photons**

- **Such pulses will allow studies of the mechanisms of chemical reactions at an unprecedented level of detail**

- **They will also allow diffraction patterns of single molecules to be collected using a single pulse of X-rays**

- **The challenge for the next generation of geochemists, microbiologists, soil scisntists, and environmental scientists is to think of new classes of problems to address using these new light sources**

Conclusions

1. **XAFS spectroscopy and other SR methods can be used to address some of the major issues in environmental science, including the complexity of environmental samples, the ubiquity of aqueous solutions, and molecular-level speciation, which controls contaminant toxicity and potential bioavailability.**

2. **Synchrotron radiation-based studies of environmental interfaces and of chemical reactions at such interfaces are revealing why some environmental materials are more reactive than others, explaining why certain sorbents are more effective at sequestering environmental contaminants than others.**

3. **XAFS studies of simplified model systems, particularly those involving solid/aqueous solution interfaces, are providing unique information on the reaction products of sorption reactions as well as the electrical double layer.**

4. **X-ray standing wave fluorescence-yield spectroscopy, in combination with grazing-incidence XAFS spectroscopy, can provide unique information about the effect of organic and microbial biofilm coatings on the reactivity of the substrate.**

5. **Soft X-ray imaging/microspectroscopy can provide unique information on biocolloids, the microenvironments surrounding bacteria, and C-functional groups present in bacteria. Hard X-ray imaging/microspectroscopy can provide information on speciation, spatial distribution, and phase association of environmental contaminants in complex environmental samples.**